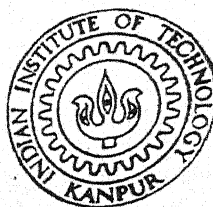# COMPUTER SIMULATION OF NUCLEAR DETECTORS
FOR DIGITAL SIGNAL PROCESSING

by

VISHAL SAXENA

DEPARTMENT OF ELECTRICAL ENGINEERING

INDIAN INSTITUTE OF TECHNOLOGY KANPUR

JULY, 1990

COMPUTER SIMULATION OF NUCLEAR DETECTORS FOR DIGITAL SIGNAL PROCESSING

A Thesis Submitted
in Partial Fulfilment of the Requirements
for the Degree of
MASTER OF TECHNOLOGY

by

VISHAL SAXENA

to the
DEPARTMENT OF ELECTRICAL ENGINEERING
INDIAN INSTITUTE OF TECHNOLOGY KANPUR
JULY, 1990

CERTIFICATE

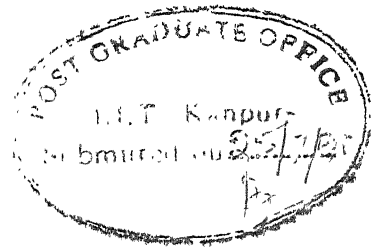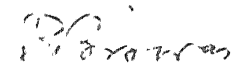This is to certify that the thesis entitled "Computer Simulation of Nuclear Detector For Digital Signal Processing", by Mr.Vishal Saxena (Roll No.8510463), is a record of work carried out under our supervision and has not been submitted elsewhere for a degree.

R.N.BISWAS
Professor
Department of Electrical Engg.
Indian Institute of Technology
Kanpur-208016

ANIL MAHANTA
Assistant Professor
Department of Electrical Engg.
Indian Institute of Technology
Kanpur-208016

July, 1990

DEDICATED

with humility to the
infinite forbearance of
my thesis supervisors

ACKNOWLEDGEMENTS

ABSTRACT

Electrical Circuit Modelling of nuclear detector behaviour under various electronic instrumentation environments for nuclear experimentation has been undertaken. The insight gained has been utilized to develop a software simulation package for nuclear detector response. A specific electronic instrumentation environment has been adopted for determining the impact of simulation on spectral distributions of energy of radiation as a test-case. Factors affecting resolution in pulse height spectra have been studied with a view to evolve simulation tools for testing the efficiency of digital signal processing algorithms.

CONTENTS

1. INTRODUCTION

Nuclear physics is an extensive study of the properties of atomic nuclei involving investigations into the basic interactions among the various constituents of the nuclei and the structure of the bound nucleus. The field also includes considerations of interaction of nuclear radiations with matter as well as evolving techniques for the practical applications of its results in the shape of technology.

Like other branches of physics, nuclear physics covers both theoretical and experimental areas of research. While the theoretical physicist seeks to develop models of the nucleus and nuclear interactions using basic principles and mathematical description of the observed nuclear phenomena, the experimental nuclear physicist conducts experiments to test various aspects of these models as well as gather data from observations that may eventually unravel new ideas towards a better understanding of the nuclear phenomena. The principal activity of an experimental nuclear physicist is to perform nuclear spectroscopic analyses.

1.1 NUCLEAR SPECTROSCOPY

Nuclear spectroscopy is concerned with studies of various ways by which nuclei absorb and emit energy. The main aim of these studies is the determination of the quantum mechanical properties of nuclear energy levels, such as energy, parity and angular momentum. In practice, this information is derived by observing particles or radiations emitted by nuclei either occurring as excited states or formed as a result of nuclear decay or nuclear reaction.

In certain nuclear reactions, particles emerging as a result of inelastic scattering from the nucleus possess specific properties which are uniquely related to their angular distributions and energies. Analysis of such properties reveals information about the energy levels of the target nuclide(i.e. the nuclear species with characterstic numbers of protons and neutrons).

The experimental study of nuclear structure and interactions is mainly a matter of recognizing or identifying and counting fragments released by atomic nuclei to rid themselves of excess energy. This, in turn, strongly depends on the capacity of the apparatus to detect and identify various nuclear radiations using specific transducers, called detectors alongwith ancilliary electronic instrumentation to provide qualitative and quantitative information.

Experiments in nuclear physics fall into two major categories:

(1) Energy Spectroscopy : Here the objective is to obtain information about the energy of a byproduct of a nuclear event.

(2) Time Spectroscopy : Experiments, in this case, involve monitoring whether or not there is the coincident (simultaneous) occurrence of two or more nuclear events in the time domain and the determination of interval of temporal separation of selected events.

1.2 EXPERIMENTAL CONFIGURATIONS

The experimental arrangement in each of the two classes is implemented with an appropriate configuration of a definite set of electronic instrumentation modules which form the basic building blocks of the measurement apparatus. These configurations are shown in Fig.1.1(a) and Fig.1.1(b). It will be noticed that certain functional blocks are common to both types of measurements. In fact, in some experiments both energy spectroscopy and time spectroscopy are required in combination for a useful investigation of certain nuclear phenomena and then the instrumentation adopted is the one that is strategically appropriate.

4

a. ENERGY SPECTROSCOPY SYSTEM

b. TIME SPECTROSCOPY SYSTEM
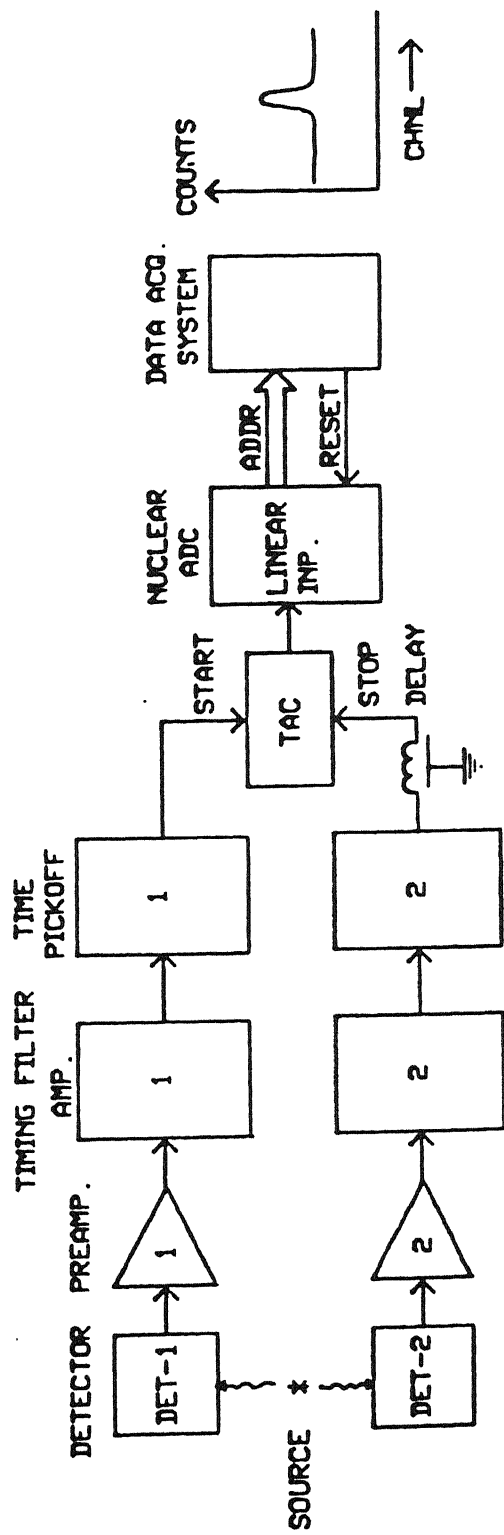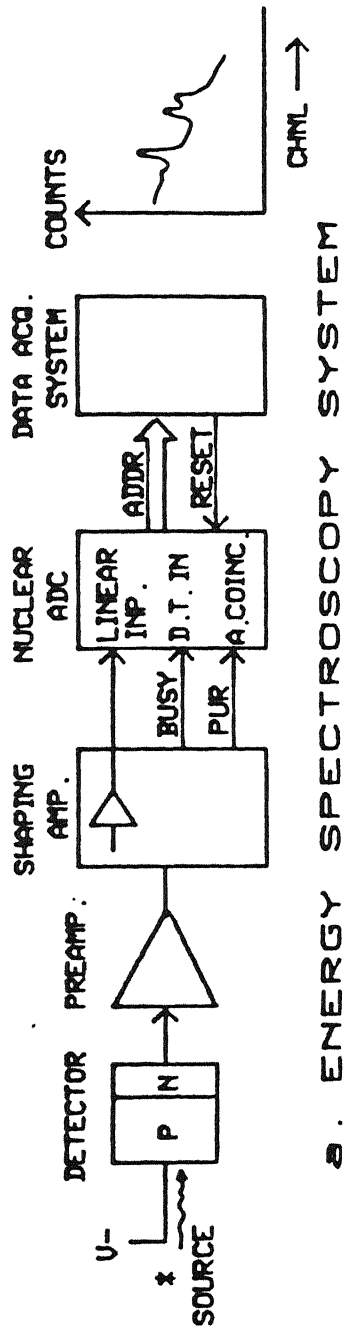
FIG.1.1 TYPICAL NUCLEAR SPECTROMETERS

The most important element in these apparatus is the transducer situated at front-end called nuclear detector which is immediately followed by a companion element, the preamplifier. The detector-preamplifier combination transduces the incident radiation into a suitable electrical signal which conveys information regarding energy and/or time of occurrence of the nuclear event.

Actually, the desired information is encoded into the temporal profile or waveform of the detector response. This signal is logged eventually into the data acquisition and analysis system which is designed to extract the information and present it suitably to the experimenter. In order to facilitate this decoding process, the raw detector response signal is first put through an intermediate stage of electronic circuits, known as waveshaping amplifier, to accentuate certain aspects of the waveform and suppress others enabling the data aquisition system to receive a properly tailored profile with an optimum signal-to noise ratio. On receipt of input, the data acquisition system known as a Multichannel Analyzer (MCA) logs the data and routes it into the appropriate slot or bin known as channel, (one for each energy or time value), in order to cumulatively build up a histogram-type of counts or frequency of occurrence versus energy of each valid event. This representation corresponds to the distribution of energies of the incident radiation.

According to the uncertainty principle in quantum mechanics, a single observation or measurement excercise on a submicroscopic physical system yields at best a grossly approximate picture of the system. Therefore, for obtaining a precise description of a nuclear phenomenon, it becomes necessary to record a large number of observations and to infer conclusions on the basis of a statistical analysis of large amount of data. Moreover, the associated errors of statistics have to be estimated because it is not possible to speak of a true value of a parameter; rather we should refer to a true mean value which, however, cannot be determined in a finite series of measurements but can only be approached by increasing the number of observations. The Multichannel Analyser provides the necessary means for meeting this requirement since it possesses the attributes of discriminating each energy or time interval value, increment its count and hold it in its internal memory storage. The MCA can also provide a scanned readout of its contents of counts versus channel number for visual display of spectrum or subsequent processing on computers. The channel axis, on proper calibration, would be corresponding to energy values or any other parameter like time, depending upon the experimental context.

1.3 DESIRABLE ATTRIBUTES OF MEASUREMENT SYSTEMS

The calibre of any particular system of spectrometry is evaluated by its abilities to distinguish or resolve incident radiation particles having nearly the same energy, and to recognise as indeed two separate events when two particles are

In the case of energy spectroscopy, energy resolution capability is primarily determined by the width of the peak shown in the spectrum. In time spectroscopy, for assessment of the time resolution capability, the obvious figure of merit is the smallest time interval which can occur between pulses that are successfully recognized and recorded as separate events.

1.4 FACTORS AFFECTING RESOLUTION

Although the capabilities of detectors can be fully realized only if the ancilliary electronic equipment is designed to match their characterstics, yet there exist some unavoidable factors which cause a loss of resolution to a certain extent and consequent degradation of accuracy of data. These factors are:

(1) Detector characterstics such as efficiency and speed of charge collection.

(2) Statistical fluctuations in the ionization effects of incident radiation.

(3) Transient response behaviour and frequency dependent electronic noise characterstics of preamplifier and waveshaping circuits in intermediate stage.

(4) Pile-up effects: When incident radiation particles arrive too rapidly in succession so as not to allow the detector to complete its response to each single quantum of

radiation and recover before the next incidence, there occurs interfering superposition of response signals on the tails of the response to the preceding stimuli. This causes serious waveshape distortion resulting in loss of useful information content as well as overloading drive to electronic circuits following the detector. The slow recovery of baseline following pulses severely load the amplifier system and produce excursions that are much longer than the pulse time width for an individual event.

(5) Pick-up of spurious and extraneous radiation in background.

(6) Sampling, linearity and quantizing noise(errors) in the Analog-to-Digital Convertor (ADC) interfacing the conditioned signal with the multichannel analyser. The ADC measures the incoming pulse height and encodes it into a digital code which defines the channel number corresponding to the energy or time parameter applicable to the incident radiation event. This channel number specifies the address of the location wherein the count stored is incremented by one for each fresh occurrence of the event. However, any erroneous or noisy digital code will mean a count in the wrong channel number would be incremented.

These factors can adversely affect the accuracy of data for analysis and inference thereafter. All sources of undesired contributions need to be tackled and reduced.

1.5 OVERVIEW OF NOISE SUPPRESSION TECHNIQUES

Accordingly, a common problem for nuclear spectroscopy practice in fundamental research and in commercial applications is the optimization of the signal-to-noise ratio of the composite detector and waveshaping amplifier system.

Noise refers to any extraneous or undesired signal that can distort the temporal profile(waveshape) of the desired signal during the measurement time which can be as long as several microseconds. (Such long times are necessitated by the slow response speed of the detector). Noise arises most typically from two principal sources:

(1) "electronic" noise arising within the waveshaping amplifier circuits, and

(2) detector signals from unwanted radiation which contribute to ionization current during the measurement interval.

The usual practice of noise suppression techniques involves the use of electronic filters which specifically shape the frequency response of the system. The post-detector system response is tailored to match the time response of the detector so that those frequency components which correspond to the detector response are enhanced. On the basis of this notion, the optimum solution has been found to be a filter which exhibits a semi- gaussian response in combination with a nonlinear element to insure baseline restoration i.e.rapid return of the response to the normal zero "baseline" level. Because this entails a price to be paid in that the baseline restoration circuit itself injects noise into the system, the

semi-gaussian filter must be carefully adjusted to obtain the optimum result. This is achieved when the semi-gaussian filter is carefully matched to the detector rise response for best resolution. The resulting disadvantage is a severe constraint on the acceptable rate of data taking, because spectral distortions due to pile up occur at high data rates and must be limited to a few tens of thousands of events per second. Furthermore, even if one ensures a low data rate from a specific source, the unavoidable presence of any spurious background radiation at high count rate makes it impossible to obtain a spectrum of reasonable quality.

In yet another approach, a technique known as Gated integration has been adopted and is an example of time-variant filtering. Basically it decouples the noise filtering function and the system time response. It is effectively a band pass filter coupled to an integration circuit. The integration circuit recovers the slow component of the detector response which would otherwise be rejected by the band pass filter. The disadvantage, however, is that it rejects the piled-up events which occur within the integration time. Consequently, the 'thoughtput' or efficiency of the scheme is intolerably low because valuble information is lost in the process.

Chrien and Sutter[1] have suggested techniques of incorporating digital signal processing (DSP) for correction of pulse distortion due to electronic noise and pile-up. In their scheme the main components of the system are pulse amplifier, time trigger, transient waveform recorder and a computer. When the detector develops its response signal, it is amplified, and

passed on to the transient waveform recorder. Here the scheme is to digitize the entire temporal profile of the detector pulse waveform so as to produce a sequence of numbers which represent the complete time history of the event. This representation consists of three regions: the interval prior to, an interval subsequent to the region of significant detector current and the main middle part itself. The digitized form of storage enables a set of appropriately designed processing alogorithms to be applied to examine and correct the event for noise and pile-up distortion. A corrected time integral of the current pulse can then be computed to measure the total charge collected by the detector and hence the energy of the photon(or particle) detected.

Use of DSP also offers scope for flexibility of incorporating different algorithms in an endeavour to continually improve the performance including innovative adaptation of proven solutions from other related areas or analogous problems. Furthermore, it seems promising to consider adapting this approach to an on-line real time processing of detector signals using special processors available from industry which have been optimized for digital signal processing and other high-speed numeric processing applications. Examples of such single-clip processors are ADSP-2100(Analog devices), TMS‡32010 (Texas Instruments) μPD77230(NEC) and a host of others from an ever expanding product line in this area[2].

A specifically designed instrumentation module incorporating a selected DSP processor and its support chips alongwith a set of proven and tested algorithms resident as firmware in the on-board

read only memories (ROMS) could be interposed between the detector-cum-amplifier combination, and the routine multichannel analyser or relevant data acquisition system and thereby enable improved thoughput of high resolution spectra. This constitutes an important step towards implementation of an on-line analysis capability which is understood to mean as the concurrent processing of recently acquired data in microseconds to milliseconds as opposed to off-line processing using seconds to minutes of machine time and which may be either local or remote requiring bulk storage and a communication link to a computer system elsewhere. A measurement system for nuclear data signals offers considerable advantage if it incorporates an on-line analysis capability such as the one that could result from the suggestions given above. Generally, the design objectives of an experiment are fast set up of the instrument configuration, self- test feature, high-speed data acquisition, rapid access to experimental data for monitoring purposes and at least an off- line data analysis capability. But incorporating an on-line analysis facility provides a significant reduction in experiment time by minimizing data storage requirements, preprocessing the data required to monitor key experimental parameters, and minimizing the time and effort required for any off-line analysis if found necessary. By analysing data on-line during acquisition, varying experimental parameters can be detected, monitored and modified. Without this capability such changes might go unnoticed and result in loss of instrument, computer and experimentalist's time.

Naturally, therefore, such a scheme points towards the practical need for developing a resource of efficient DSP algorithms for use in such environments which cater to different experimental requirements and situations.

1.6 ALGORITHM EVALUATION BY SIMULATED INPUTS

It is necessary to have means of testing these algorithms on a dry-run basis prior to incorporating them in real -life experimental apparatus. But the test and evaluation can be objectively fair only if the real-life experimental situations can be artificially created wherein these algorithms are run and be freely modifiable with strong human interaction on a closed-loop feedback basis. This notion suggests the need to be able to simulate a nuclear detector response signal and/or the amplifier output signal due to various waveshaping circuits as well as the random noise components associated with the detector and the amplifier circuits. Such an artificially created waveform is then presented as a stimulus to the relevant DSP algorithm under development, much as would be the case when the same DSP algorithm would operate on an actually acquired nuclear signal stored in a transient waveform recorder.

Consequently efforts were undertaken to develop a computer simulation model for a nuclear detector and the associated ancillary equipment. Inputs of nuclear events and their associated statistical fluctuations were generated using specially created random process simulation programs which were

also used to simulate the noise behaviour of various electronic circuits needed in real-life experiments. Since all perturbations due to noise can in any analysis be referred to the primary input and the main system then visualized as a noise-free system, the noise models, after proper mathematical treatment, were reduced to expressions that govern the injection of these perturbations right at the input to the detector model. Thus various statistical fluctuations were combined for the purpose of being used as a single-point injection along with the nuclear event to trigger the detector+amplifier response. Monoenergetic particle radiation incidence simulation was adopted. Successive radiation inputs were also duplicated as successive runs of the simulation program, each with a different input within statistical limits defined by the user.

In effect, the approach in these efforts has been to develop a model in software for each piece of instrument hardware and the flow of program corresponds to the cascade of various functional blocks. Further peak sensing routines and a software package for multichannel analyzer with histogram plotting graphics feature to provide a visual indication of temporal profiles and spectra were also created. Experimental set-up in a laboratory is translated into a main program setup, with each instrument block being activated as subroutine or a software module.

1.7 THESIS ORGANIZATION

The thesis consists of five chapters. Following the introductory material presented here, Chapter 2 discusses the physical processes of radiation. It also covers topics on the nature of radiation energy and its various types and how it interacts with the matter it passes through besides the phenomena of ionization effects of charged particle radiation. It thereafter presents a unified treatment of different types of detectors. Development of a circuit model for the detector is presented in Chapter 3, which also considers the role of preamplifiers, waveshaping amplifiers and noise, as also the factors affecting resolution of spectra. This treatment provides the basis for Chapter 4 to cover software development for a simulation model of the detector and the necessary programme modules associated with it. Finally the thesis ends with Chapter 5 presenting conclusions and discussions.

2. DETECTION OF RADIATION

2.1 PHYSICS OF RADIATION DETECTION

Detector being a sensor of radiation, forms virtually the eyes and ears for the experimentalist in his research work to provide information on the type, energy and multiplicity of the radiations emitted in a nuclear reaction. Radiation is sensed (i.e. 'detected') when it gets intercepted by the detector placed in the path of its propagation in space. This encounter results in an interaction of energy transfer between radiation and the matter of the detector, forcing the device to be stimulated into a change of state. The change in device behaviour so induced is utilized as a response to the stimulus. This response is generally in the form of pulse-like electrical signals obtained under suitable conditions for operation of the detector. By means of proper instruments, this signal can be carefully analyzed to obtain valuable information about the incident radiation. The basic requirement for any detector is a high detection efficiency and a good energy resolution.

The principles governing nuclear radiation detection depend upon the nature of different types of radiation and how they interact in characteristic ways with the physical material of the detector used. These aspects give rise to the existence of a variety of detector types, each with a different sensitivity characteristic for the different type of radiation.

Development of a suitable model of detector behaviour (which is explicitly undertaken in the next chapter), requires an understanding of various radiation types alongwith the mechanisms of their interaction with matter and loss of energy therein.

2.2 TYPES OF RADIATION AND THEIR INTERACTIONS WITH MATTER

For the purpose of experimental and theoretical study, nuclear radiations are classified into four classes falling under two major categories:

1)Charged Particulate Radiation consisting of

(a)Heavy Charged Particles, of mass comparable with nuclear mass, e.g., alpha particles,

(b)Light Charged Particles. e.g. electrons and positrons.

2)Uncharged Radiation (Particulate /Non-particulate) consisting of

a)Electromagnetic Radiation e.g. Gamma Rays, X-Rays.

b)Neutrons.

Charged Particulate radiations continuously experience a Coloumb force interaction with electrons present in any medium. The uncharged radiations are ,however, not subject to Coloumb force and, therefore, undergo 'catastrophic' interaction in a single encounter which radically alters their properties. The striking difference in the absorption of these types of radiation is that only charged particles have a

range. In traversing a certain amount of matter, a mono-energetic beam of heavy charged particles loses energy without changing the number of particles in the beam. After having crossed practically equal thickness of the absorber, all the beam particles are ultimately stopped. The minimum thickness of the absorber necessary to fully arrest or stop the particles is known as the Range of the particle. Range, therefore, represents the farthest distance beyond which no particles can penetrate. Now as the particles travel through the medium, they lose energy . The energy lost per unit path length $S(=-dE/dx)$ is known as the Specific Energy Loss and its average value is referred to as the Stopping Power of the absorbing substance. The collision processes along the path of penetration of the incident particle are statistical in nature so that different member particles of the beam of incident radiation undergo energy losses differently. Accordingly they are stopped within distances which are unequal. This small variation in ranges is referred to as Straggling. The stopping process is of great importance for understanding all types of nuclear detectors as well as for choosing the thickness of targets and shielding materials.

When an alpha particle, a proton, or any other heavy charged particle moves through matter it either ionizes or excites those atoms of absorber to which it comes sufficiently close. Coloumb forces give a sharp impulse to an electron as the particle moves swiftly by. The energy transferred to the electrons represents a loss of kinetic energy of the moving particle. The energy transfer to the positive heavy ions

released in ionization is negligible. Towards the end of the particle's path, its energy and speed will have been reduced. Then the phenomenon of the transfer of energy from this moving charged particle to the electrons of the surrounding medium becomes more significant because the slowed down speed makes the incident particle spend more time in the vicinity of the absorber's electrons and, therefore have a greater degree of probability of interaction and thus transfer energy more fully.

The energy loss of light charged particles like electrons is a much more complicated phenomenon than the energy loss by ionization of heavy ions. There are four important differences:

(1) The smaller mass of the electron causes it to undergo large angular deflections when colliding with the atomic electrons of the absorber. Consequently, the path of an electron is very irregular and not at all as straight as the path of heavy charged particles.

(2) Nuclear electrons have a continuous distribution of initial energy whereas the alpha particles are mono-energetic.

(3) Due to the identical character of the two colliding particles, exhange phenomenon, are involved which are to be theoretically investigated.

(4) High-speed of the Beta-particle makes it necessary to employ a relativistic treatment of the collision mechanism.

There are several processes which contribute to the dissipation of the energy of electrons passing through matter. At large velocities a process other than ionization plays an important role in the slowing down of electrons. This is the energy loss of radiation (called Brehmsstrahlung) due to the deceleration it experiences in the field of the nucleus or of the electons.

The interaction of Gamma-Rays with matter is markedly different from that of charged particles such as Alpha- or Beta-particles. One point of difference is the greater penetrating power of Gamma-rays and the other is that a different absorption law governs this type of radiation. Gamma-Rays and X-Rays which are both electromagnetic radiations have no definite range. Unlike charged particles, a well collimated beam of Gamma-Rays shows a truly exponential absorption in matter. This is because photons are absorbed or scattered in a single event. Because they have no charge, neutrons cannot ionize atoms directly. They can, nevertheless, be made to induce ionizing radiations by indirect processes, such as by producing recoil protons or by causing fission when captured by nuclei. It is not always easy to make these processes efficient because the probability of collisions is not high.

2.3 PRINCIPLES OF DETECTION

Detection of either particle or photon radiation occurs whenever the interaction of this radiation with the medium of its passage results in an observable effect such as one of the following actions:

(1) Ionization either by incident radiation or by secondary radiation particles produced through interaction of the primary incident radiation with the medium.

(2) Fluorescence of selected materials from the decay of short-lived metastable states excited in certain molecules on interaction with the incident radiation or its secondary progeny.

(3) Production of developable grains in photgraphic emulsions.

The above three phenomenona are the most pronounced effects though other effects are occasionally employed in special cases, such as the metallic photoelectric emission for ultraviolet photons and the Cerenkov radiation for relativistic charged particles.

The most practical method suitable for instrumentation and capable of yielding quantitative information utilizes the ionization effect of interaction of charged particles (primarily incident or secondarily produced) with the detector material. Here two parametric aspects of interaction emerge as important factors governing the choice of material and design of the geometry of the detectors because they determine the quantitative information relating to the type (particle identification), energy(Mev) and number (counts or count rate).

These factors are:

(i) Specific Rate of Energy loss(-dE/dx)

(ii) Range (cm. or mg/cm^2)

2.4 IONIZATION PRODUCTION BY CHARGED PARTICLE RADIATION

As the moving electric fields associated with swift charged particles can impart sufficiently strong impulses to the electrons of the atoms of the medium so as to overcome their binding energy, ionization occurs producing a succession of oppositely charged ion-pairs of the medium substance along the path of the moving particle. These ions can be prevented from mutually recombining and instead be collected by migration under an externally applied electric field to yield a current pulse of detectable magnitude.

The specific rate of energy loss is given by the following equations.

(i) For heavy charged particle radiation:

$$- \frac{dE}{dx} = (4\pi e^4) \ (z^2/(m_o v^2)) \ (NZ) \ [\ \ln \ ((2m_o v^2)/I)$$
$$- \ln \ (1-\beta^2) \ - \ \beta^2] \qquad \ldots (2.1)$$

(ii) For light charged particle radiation e.g. electons:

$$- \frac{dE}{dx} = (2\pi e^4) \ (1/(m_o v^2)) \ (NZ) \ [\ \ln \ ((m_o c^2)/I^2)^2 \ +$$
$$\ln\{(\beta^2\gamma^4)(\gamma-1)/(4(2\gamma-1))\}+(1/\gamma^2)] \qquad \ldots (2.2)$$

where m_o = electronic rest mass

   z = atomic number of absorber medium atoms.

   e = electronic charge

  ze = charge carried by incident radiation particle (in units of electronic charge)

   v = velocity of the incident radiation particle

   c = velocity of light

  NZ = concentration of electrons as number per unit volume of absorber medium

   I = Mean ionization potential for atoms of the medium.

      Its approximate value for a medium of atomic number Z is given by

   I = 13.5 electron volts

   β = (v/c) = $(\gamma^2-1)^{1/2}/\gamma$

   γ = $E/(mc^2)$

   E = $T + mc^2$

Where T=electron kinetic energy

   These expressions for dE/dx are valid provided the speed of the moving incident radiation particle exceeds considerably the speed of the orbital electrons of the atoms of the medium.

   The quantitative nature of radiation interaction with matter is explicitly conveyed in each of the above equations. In either expression for (-dE/dx), the right hand side can be observed to be a product of four bracketed terms. The first factor contains universal constants. The second factor $(z^2/(m_o v^2))$, including the case of z=1 for electrons, involves the characteristics of the incident radiation particle, namely the identity type (via the charge of z units and mass m_o) and

initial incident energy (via the velocity v). The third factor refers to the absorber medium in terms of its parameters, N and Z. The fourth and last factor carries both incident particle energy information and the ionization characteristics of the medium., but the logarithmic dependence makes these contributions relatively constant. Therefore the pronounced contributions come from the second and third factors.

A related parameter of significance for detector operation of an absorbing medium is the total range R of an incident particle of a particular type of radiation for that material. The range is the length of flight path within the medium before it comes to rest and is given by the relation.

$$R = \int_{x=0}^{x=R} dx = \int_{0}^{E_o} \left(- \frac{dE}{dx} \right)^{-1} dE \qquad \ldots (2.3)$$

Use of Eq 2.1 for integration as required in Eq 2.3 with the the precaution to integrate only over the length x for which the equation is valid and addition of an empirical term for the rest of the range to account for loss of energy by a modified interaction mechanism (towards the concluding seqment of transit under lowered velocities) has been carried out in literature [3]. The main result relevant to the present context is that the range of an incident radiation particle of mass m and charge z is given by

$$R(v) = (m_o/z^2) \, F(v_o) \qquad\qquad \ldots(2.4)$$

Where $F(v_o)$ represents a unique function of the particle's, initial velocity v_o which is related to the incident energy E_o. Since range of a particle is a function of the density of the absorber medium, the direct comparision of ranges in different media is difficult. However this handicap is overcome by measuring the range in terms of equivalent thickness, according to the following definition:

Equivalent thickness (mg/cm2)

= actual thickness (cm) X density (g/cm^3) X 1000

The foregoing remarks bring forth certain conclusions which are of significance for selection of detector material and geometry and the design of certain experiments which in turn have an impact on the design and performance of electronic circuits of the ancilliary instrumentation following the detector. These conclusions are:

(i) Range of a given radiation type (m,z) within a particular absorber material increases as the initial energy of incidence increases. The relationship is not simply linear or parabolic but is empirically of the form $R=aE_o^b$ where a and b are constants for the material of the absorber. These relations can be given as curves for different particle types and absorber medium. One important application of these curves is the determination of dimensions for a detector made from a certain absorber material. This is because any detector

intended to measure the full incident energy of a charged particle must have an active thickness which is adequately greater than the range of that particle in the detector material so that it can be fully brought to rest for reliable registration of its occurrence. Accommodation has also to be made for the fact that charged particles are also subject to range straggling, defined as the fluctuation in path length for individual particles of the same initial energy. The same stochastic factors that lead to energy straggling at a given penetration distance also result in slightly different total path lengths for each particle.

(ii) When comparing different charged particles of the same velocity or energy at incidence, particles with the greatest charge (ze) undergo the largest specific energy loss (stopping power) and the lowest range, since $(-dE/dx) \alpha z^2$ and $R \alpha 1/z^2$. For example, alpha particles will lose energy at a rate faster than protons of the same velocity but less than that of more highly charged particles.

(iii) In comparison of different materials as absorbers, the linear dependence of $(-dE/dx)$ on NZ (which is outside the logarithmic term) suggests that high atomic number, high-density materials yield the greatest linear stopping power. This feature provides the rationale for preferring condensed media as solid state detector materials because very small dimensions (few millimeters) will be adequate for arresting charged particles of moderate energy range.

2.4.1 Range Formulae

Certain empirical relations cited below for illustration give a clue to the factors determining the size of active width in detectors:

For Alpha-particles in air, Geiger discovered range R_α to be

$$R_\alpha = 0.00318 E^{3/2} \text{ meters} \qquad \qquad ....(2.5)$$
$$\text{where E is in Mev.}$$

For protons, a corresponding range-energy relation due to Brobeck and Wilson [3] is

$$R = (E/9.3)^{1.5} \qquad \text{for } E < 2 \text{ Mev} \qquad ....(2.6a)$$

$$R = (E/9.3)^{1.8} \qquad \text{for } 2\text{Mev} < E < 200 \text{ Mev} \qquad ....(2.6b)$$

If the range in air is known, we can obtain the range in another material using the empirical relation :

$$R/R_{air} = 0.151 \, A \, (z+10)^{1/2} /(\rho \, z) \qquad ...(2.7)$$

where A = mass number of absorber material

z = atomic number of absorber material

ρ = density of absorber material.

In case of light charged particles such as nuclear beta particles, the corresponding empirically obtained range-energy relations in aluminium is as follows:

$$R = 412 \, E_o^{(1.265 - 0.094 \ln E_o)} \quad \text{for } E_o < 2.5 \text{ Mev} \qquad ...(2.8)$$

and

$$R = 530 \, E_o - 106 \qquad \text{for } E_o > 2.5 \text{ Mev} \qquad ...(2.9)$$

where the units of range is (mg/cm^2) and that for energy E_o is Mev.

2.4.2. Stopping Time [4]

The time required to stop a charged particle in an absorber can be calculated from range and average velocity. The expression for estimating the stopping time is approximately given by

$$T = 1.2 \times 10-7 \ R \ (m_A/E)^{1/2} \qquad \ldots\ldots(2.10)$$

where T is in seconds, R in meters, m_A is in atomic mass units and E in Mev. and is reasonably accurate for heavy charged particles (protons, alpha etc.) over much of the energy range of interest and is not valid for relativistic particles such as fast electrons. For typical range values, stopping times according to this equation for charged particles are of the order of a few picoseconds in solids or liquids, and a few nanoseconds in gases.

2.5 DETECTION OF γ-RAYS / X-RAYS [3,4,5]

The interaction of γ-Rays with matter follows a different mechanism than those that occur for the case of charged particles. Although the interaction is mainly with the atomic electrons, the γ-Ray can also lose a large fraction of its energy or all of it in a single encounter. There is, therefore, no quantity corresponding to range. There is also no definite value for the specific ionization of a single γ-Ray. When a γ-ray enters a detector, it must produce a recoil electron by one of the following processes before it is recorded as an event:

1) Photoelectric Effect
2) Compton Effect
3) Pair Production

2.6 TYPES OF DETECTORS

A wide variety of detectors are available in practice. They all exploit the phenomena of interaction of radiation with matter to produce an observable effect[6]. Since ionization and excitation are the two principal effects of such interaction, the detectors are broadly classified into two main categories; one, based on collection of ions produced by ionization; other, based on consequences of excitation effect. This classification is shown in Table 2.1

In the group of detectors, based on the ionization effect, the electric charge of the ion-pairs (positive and negative) formed through radiation interaction is collected and electronically amplified, or processed. These detectors are called Ionization detectors. On the other hand, for the type of detectors which utilize the excitation effect the detector material can be an inorganic or an organic substance. The passage of radiation through certain organic materials produces excited atomic states, whereas in certain inorganic materials, the molecular vibrational states undergo excitation. In both cases, when deexcitation or relaxation occurs, light photons are emitted which are collected and converted into electric pulses which are sent onwards to the measuring system. The group of detectors based on this principle are known as Scintillation detectors.

In the case of saturation collection, the signal thus obtained is due to the charge collected on detector electrodes only due to all the ion-pairs that can possibly be generated by radiation. As stated earlier, in ionization detectors, an
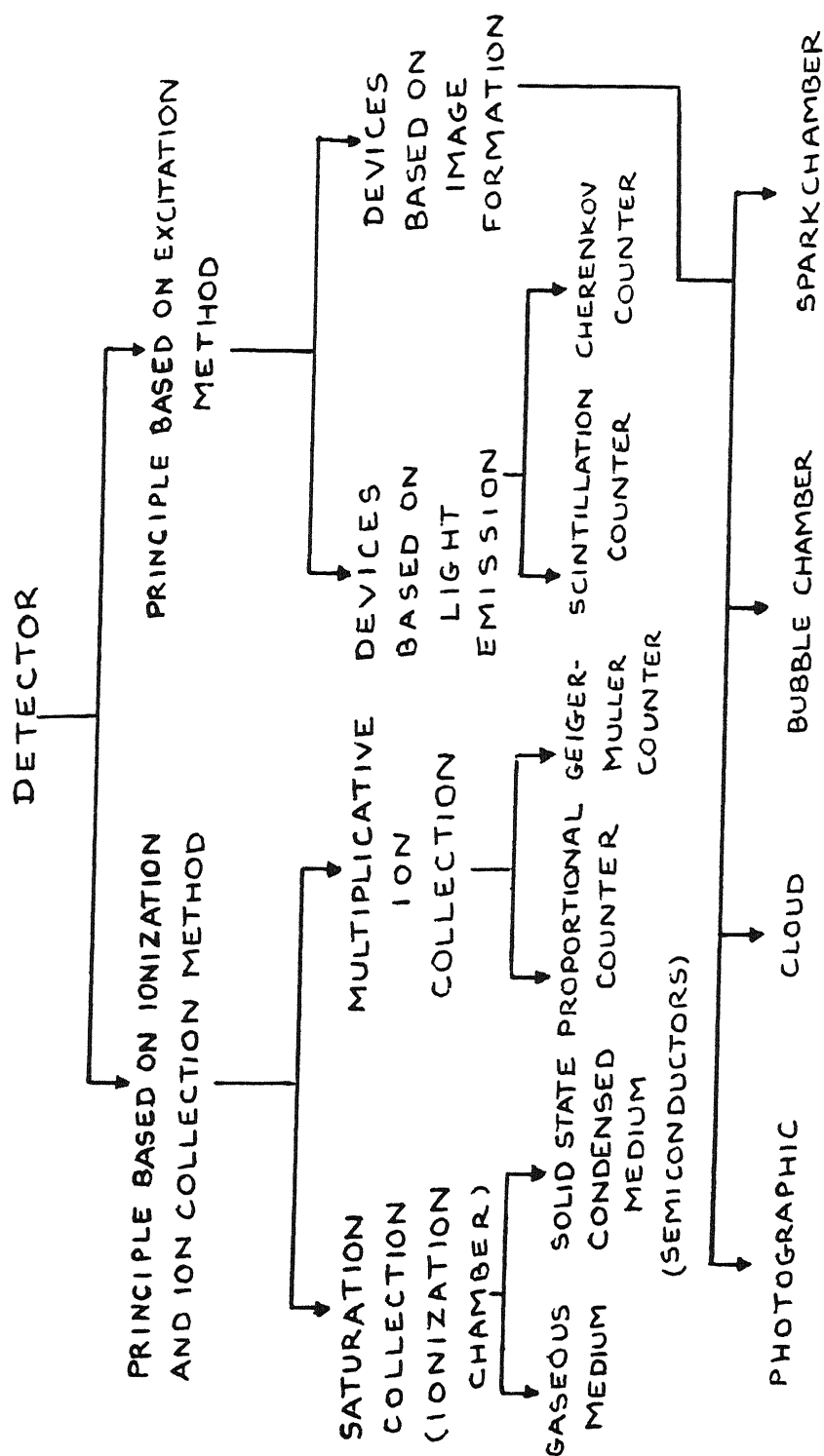
TABLE 2.1 CLASSIFICATION OF DETECTORS

externally applied electric field forces a migration of the ion pairs produced by radiation towards the terminal electrodes to collect them. This collection is manifested as a current pulse or a charge step signal at the external terminals of the detector connected to the electronics in a measurement system.

If during the course of migration, the ion carriers undergo no collisions of secondary ionization with the other detector atoms, then the maximum signal amplitude is due only to all the ion-pairs that can possibly be generated by radiation and no more. This process of development of detector signal is termed as saturation collection. The signal strength is extremely feeble and in order to be properly discriminated from noise data acquisition system(e.g. MCA) needs an indispensable amplification and signal conditioning in the intervening stages.

On the other hand, multiplicative ion collection refers to the process wherein the primary ion pairs produced by radiation are not allowed to be the sole contributor to signal strength, but are instead utilized by intense electric fields to start off a secondary ionization of creating new ion-pairs within the detector. This causes an avalanche-type of charge carrier generation which effectively increases the population of charge carriers and thereby yields a stronger output signal pulse whose amplitude is proportional to the number of primary ion-pairs and the avalanche-type multiplication factor.

Scintillation based detectors (often called scintillation counters) also use the charge carrier multiplication in increasing the number of electrons for contributing to the signal strength. There is an effective internal amplication in the multiplicative ion collection type and scintillation detectors.

A brief summary of some commonly used types are given below:

Gas-filled counters are detectors in which the incident radiation of charged particle ionizes a volume of gas enclosed in an envelope containing two electrodes across which a high voltage is applied. The occurrence of the ionizing event is manifested as an electrical signal for measurement purposes. Depending upon the electric field gradient and gas pressure, the gas-filled counter is an ionization chamber[7], a proportional counter, or a Geiger-Muller counter. Voltage pulses produced by gas counters have rise times of the order of 10^{-6} sec. Randomly timed radiation particles arriving at an average rate of up to 105 per second can be counted by a carefully designed proportional counter.

However, the Geiger-Muller counter, after producing its output pulse requires upto 200 microseconds to restore itself to its original undischarged condition and cannot be used for counting rates much greater than 1000 per second.

Semiconductor detectors[8-13] function qualitatively in the same way as an ionization chamber except that the medium between the high-voltage electrodes is a solid state crystal instead of gas. The high density of this medium implies a high stopping power and very small range for incident charged particle radiation. This results in advantageously small dimensions for the detector. The primary difference between gas and semiconductor detectors is the nature of oppositely charged ion-pairs produced in radiation induced ionization. Whereas in gas filled detectors, the positively-charged ions are ionized gas molecules, and negatively-charged ions are free electrons, in a semiconductor detector, the negatively charged ions are again free electrons, but the positively-charged particles are holes. For all the various members of this family, the detection mechanism is the same: when radiation is incident on a semiconductor crystal, electron-hole pairs are created and they separately migrate to their respective terminals. This produces an electrical pulse which is approximately proportional to the energy of the incident particle.

The development of semiconductor detectors and their adoption in spectrometers represent the emergence of an important new technique in experimental physics which is now very widespread in usage. These detectors are the solid-state analogue of the gaseous ionization chamber and possess many advantages over other types of radiation detectors.

The most significant features of merit are:

    (i) linear response over a large energy range,

    (ii) fast pulse-rise time from most detectors,

    (iii) relative simplicity and convenient size

    (iv) the facility of making special configurations,

    (v) high density of detector material enabling them to stop energetic particles.

The detectors were first applied to the study of heavy charged particles and their use has led to many advances in the field particularly in studies of nuclear reactions. Basically two types of semiconductor detectors are in use:Silicon (Si) and Germanium (Ge). Though their construction and operations are essentially identical, each has unique characteristics, peculiar to its material properties, which are best suited for specific situations. Continuous research into the physics and technology of semiconductor materials has led to improvement in design and performance of detectors especially concerning efficency (sensitivity), speed of collection, noise and resolution of energy. In semiconductor detector, the basic principles of operation are analogous to the operation of ionization chambers. i.e., an incident ionizing particle produces several electron-hole pairs which are collected by an applied electric field across the device, resulting in an electrical pulse which is proportional to the energy lost by the incident radiation particle. For good spectrometer characteristics, it is

important that the detector collect all the charge produced. Though, the collection of charge is more complicated in the semiconductor detector than in the ionization chamber, yet this solid-state detector has many advantages. The energy required to produce an ion pair is much lower and hence the spread in values of peak in spectrum due to statistical fluctuations is smaller. The density is much greater than that of gases, and so the detectors can be made smaller and can absorb higher energy particles. They also usually have shorter pulse rise-times. Certain physical properties of detector are of great relevance to the measurement process. A presentation of these properties is postponed until after the detector model has been developed in the following chapter.

3 NUCLEAR DETECTOR MODEL EVOLUTION

Derivation of an electric equivalent circuit model for a nuclear detector is demonstrated in this chapter. Such a model is needed as an important artifice in the development of a suitable mathematical model of the composite detector and the measuring system for purposes of computer simulation. Also, this detector circuit model provides a useful way of understanding the nature of electric circuit interaction between the detector and the preamplifier, as well as the amplifier(waveshaping) electronics which invariably follow it, in terms of transient behaviour and noise performance.

The excercise, here, proceeds by first using physical considerations of detection mechanism to formulate a suitable detector model in an intutive way. Next the issues involved in experimentally derived spectra such as peak shapes, accuracy, count losses, dead-time pile-up and baseline restoration are analysed in order to examine how detector performance affect these factors favourably and adversely. This helps in further refining the model to conform to a more realistic behaviour and thereby help improve the computer simulation model for the integral assembly of detector and electronics.

3.1 SIMPLIFIED DETECTOR MODEL

It is true in general that, for any type of detector to respond at all, each particle or photon in the incident stream must undergo interaction through one of the mechanisms outlined in the preceeding chapter and during the course of this

in the preceeding chapter and during the course of this interaction it deposits its initial energy within a certain distance equal to its range and within a certain time interval equal to its stopping time. In most practical situations, these times are so short(typically a few nanoseconds in gases and a few picoseconds in solids) that the interaction by a single particle or quantum of radiation can be assumed to a first approximation, to be an instantaneous action with energy deposition in zero distance and zero time and immediate ionization of the detector material atoms at the point of interaction. The net effect of this interaction is the sudden appearance of certain number of oppositely charged ion-pairs, within the active volume, equivalent to a burst of charge of either polarity of a definite amount. (Active volume is a term which refers to the particular region within the detector bulk where interaction produces the most effective ionization). This amount of charge is linearly related to the energy of the radiation particle.

Now in pursuit of formulation of the model, and assuming that only incidence of a single particle or quantum of radiation is considered, suppose there occurs at time t=0, an irradiation of such a particle or quantum. As a result, at the same instant t=0, oppositely charged ion-pairs of value, say Q of either type, appear upon ionization of the detector atoms. Next, this amount of charge of either type must be arranged to be collected to develop the transduced signal. This is achieved by application of an electric field across the active region of the detector via

electrodes which are the external terminals both for this bias and for the signal. As the d.c. voltage applied between the electrodes produces an electric field across the active region within the detector, the oppositely charged ions experience electric forces in opposite directions which make them move apart further and further and travel towards the opposite electrodes. The electrons, being negatively charged go towards the anode and positively charged ions(as in ionization chamber) or holes (as in semiconductor detector) approach the cathode as destination. The migration of these ions towards the respective electrode constitutes the collection process which is considered complete when all the generated ions or charge carriers have been collected by the electrodes. As the ions traverse the active region, this transit takes some nonzero time because of the finite velocities of the ions, eventhough the distances to be covered are small. The total time duration for such a collection process to be fully over is called collection time and ranges from a few milliseconds in an ion chamber, to a few nanoseconds in semiconductor detectors. These collection time values reflect the mobility of charge carriers within the detector active volume and the average distance which must be travelled before reaching the collection electrodes. While in transit, even before they have been fully collected, these ions induce charge on the electrodes due to the migrating ions.

Therefore, it may be concluded from such heuristic considerations of the transduction process in nuclear detectors that while the measurand is the physical quantity, as the energy of incident radiation or quantum, the output signal is developed as current pulse having a time width due to the finite collection time $(=t_c)$, howsoever small, involved in collecting the charge burst. But it is the actual charge (due to either ion polarity) produced by ionization which is directly and linearly proportional to the input measurand(energy). This magnitude of charge is indeed delivered totally to the electrodes (assuming no loss of migrating ions on the way due to recombination or trapping) but only as a current pulse would more approximately reflect the magnitude of charge developed in that specific interaction and hence the energy(measurand). This is indicated mathematically as

$$\int_0^{t_c} i(t)\ dt = Q \qquad \ldots 3.1$$

where $i(t)$ is the time-dependent current flowing in the detector and referred t_o as current pulse above; and t_c is the collection time for the migrating ion-pairs. Fig.3.1 illustrates this point. It is to be noted that whereas Q is the strength of the impulse function for charge burst created instantaneously, the current is a finite function of time which must be spread over a duration t_c to deliver effectively a charge of equivalent value at the electrodes.
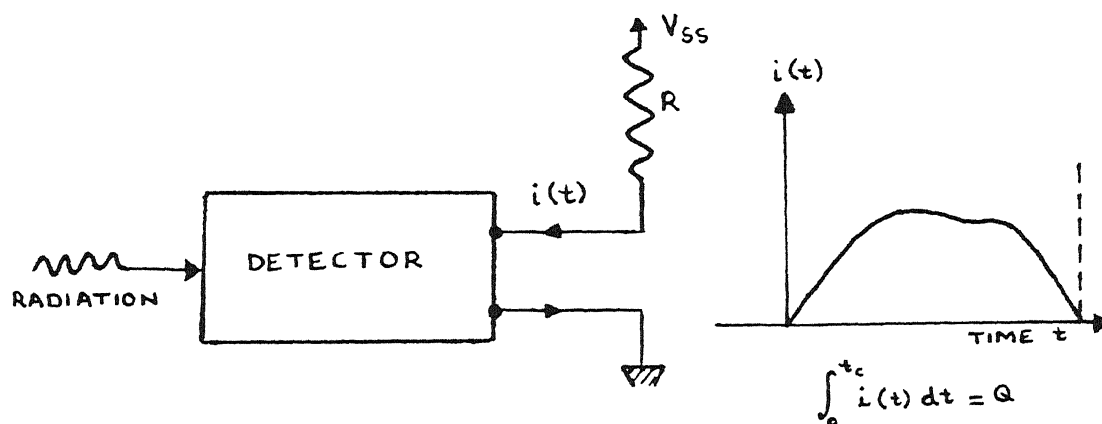
FIG. 3.1 OUTPUT CURRENT PULSE OF A PROTOTYPE DETECTOR MODEL

$$\int_0^{t_c} i(t)\,dt = Q$$
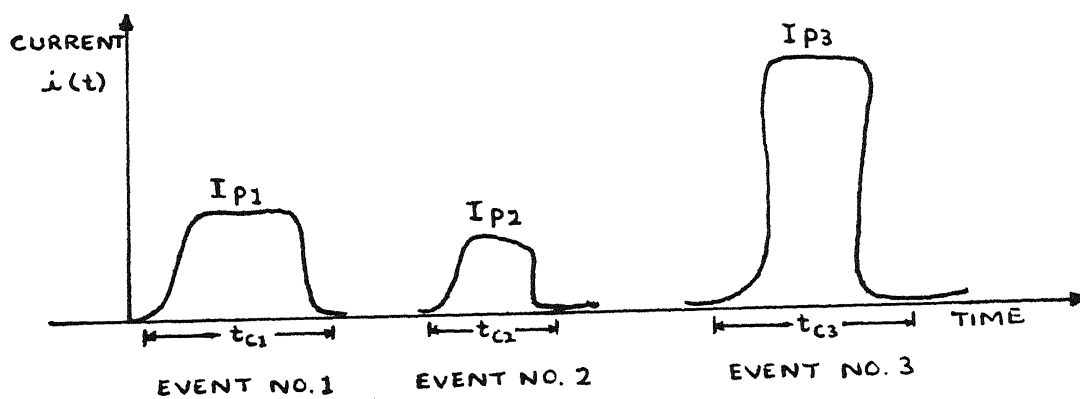
FIG. 3.2 UNIQUE DETECTOR RESPONSE FOR SEPARATE RADIATION QUANTA

In any real situation, there will be occurring a stream of many particles or quanta of radiation over an interval of time. The detector is expected to respond to each one nuclear event, separately and independently of the others in order to distinguish among them, especially since each incidence may represent a different event of interaction, each of which must be measured uniquely. Now if the irradiation rate is high, as can often happen in practice, situations arise in which a detector is just going through its response to one radiation event and is suddenly stimulated to an irradiation by a new incidence causing it to be stimulated once again; whereupon its net effect will cause the detector current to flow under the influences of two or more almost simultaneous interactions making resolution among the successive radiation events difficult.

Therefore, another simplifying assumption made, is that radiation rate is low enough (or the events are spaced in time sufficiently apart) so that each singular radiation event gives rise to a current pulse which is distinguishable from that due to all others. Variations in energy of different particles or photons yield current pulses of correspondingly different amplitudes. This is sketched in Fig.3.2. The situation of responses almost overlapping due to very rapid irradiation is considered as a suitable modification of the assumption here of one event-one response.

3.1.1. Modes of Detector operation

Detectors can operate in two modes:

(i)Continuous mode: In this application the detectors are allowed to respond to incident radiation without maintaining distinction among different incident particles or radiation quanta, because one is interested in only measuring the average current flowing in the detector, averaged over many interactions. Accordingly the measuring instrument is chosen an average responding meter of known response time T which functions as ratemeter and is used in radiation dosimetry and nuclear reactor power monitoring. Fig.3.3 shows the graphic relation between instantaneous current i(t) and time-dependent ammeter current which can be mathematically stated as

$$I(t) = \frac{1}{T} \int_{t-T}^{t} i(t')dt' \qquad \ldots (3.2)$$

since the response time T is typically a fraction of a second or greater, the result is to average out many of the fluctuations in the intervals between individual radiation interactions, so that the average current I(t) reported depends on the local rate of irradiation and the average charge per interaction.

(ii) Pulse Mode: Here the viewpoint adopted is that it is important to recognize the discrete particulate nature of incident radiation as a succession of distinct events, each of which must be transduced by the detector without overlap to provide uniquely measured values. Thus the
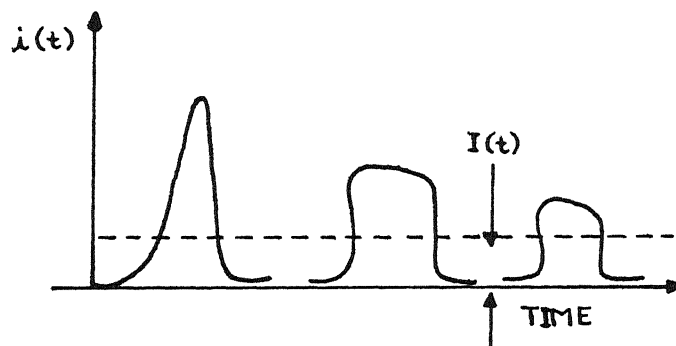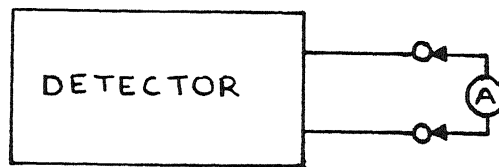
FIG. 3.3   AVERAGING ACTION ON OUTPUT CURRENT
PULSES FOR RAPID SUCCESSION OF
RADIATION QUANTA.

detector response is on an event-by-event basis as a series of discrete current pulses. This mode enables each event to be measured for energy or time of occurrence, both of which are important in nuclear spectroscopy.

Although it has been established here that the general nature of output signal is a current pulse in its fundamental form in the transduction process of the detector, the actual nature of the signal pulse produced from a single event depends on the input characteristics of the circuit to which it is connected. It is almost always followed by a preamplifier whose role is to match the output characteristics of the detector with the input characteristics of the waveshaping amplifier stage.

In principle, it is possible to exploit the current pulse as such or obtain a suitably derived voltage pulse of the detector. Actually, two basic types of information can be obtained at the output of the detector. One is the energy released by the incident radiation inside the detector material; the other is the time of occurrence of the interaction. In case of high resolution spectrometry, energy information is extremely important and therefore, it is desirable to integrate the primary current waveform over collection time to derive the charge and hence the energy information. In its most primitive form, this integration is carried out by the internal detector capacitance associated with the very nature of its operation for applying electric field across medium to collect

ion pairs. On the other hand, the naturally produced current pulse has the fastest rise time due to the very basic action of ion collection with very short transit times. These considerations raise issue as to whether detector is to be operated in a current mode or in a voltage mode. The issue is examined in detail below.

In normal detector operation, a d.c. voltage source alongwith a very high resistance are connected in series to form a closed loop so that the resulting voltage at the detector provides electric field across the active region of the detector (Fig.3.4).

Circuit analysis considerations evidently suggest the existence of an effective capacitance between the detector terminals which sustains this electrostatic field and the associated charges on the electrodes. Thus the equivalent circuit model (Fig.3.5) would consist of a current source (representing the current pulse due to charges being collected and responsible for signal in parallel with detector capacitance. But the biasing resistor R_s is also to be included since it is the bias that provides the the electric field and thereby validates the current source equivalence of charge migration and collection. Also R_s accounts for the effect of leakage of charge (Capacitance discharge) that would inevitably occur in actual circuit. Bias supply is replaced by a short circuit in the incremental signal equivalent circuit model.
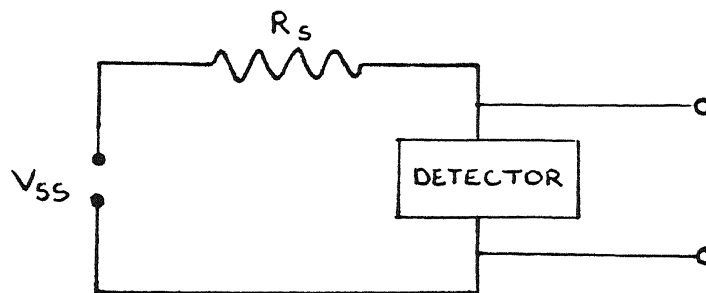
FIG. 3.4   CIRCUIT FOR APPLICATION OF BIAS
               TO DETECTOR
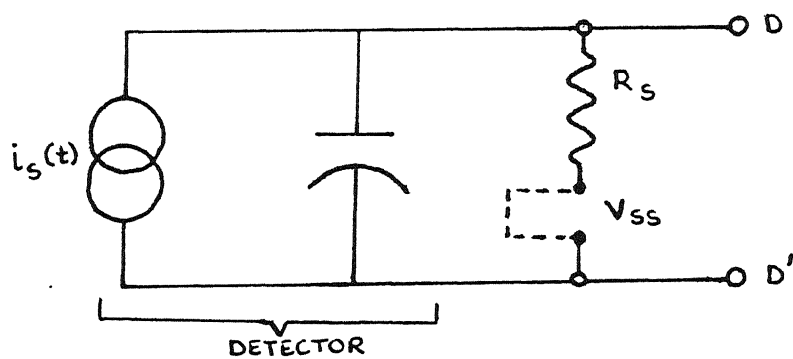
FIG. 3.5 EQUIVALENT CIRCUIT OF A SIMPLIFIED
                    DETECTOR.

The detector signal in any form always requires amplification of its extremely feeble strength to be recordable in a data acquisition system. This amplification is traditionally done in two stages:first in the preamplifier and then in the main amplifier.

The signal conditioning and impedance matching functions of the preamplifier are so important that this unit is an indispensable complement to the detector transducer. Consequently the parametric values of its input characteristics at the interface with the detector will also govern as to whether the detector will operate in current mode or voltage mode.

Representing the passive input driving point impedance of the preamplifier as a resistance R_p in parallel with input capacitance C_p, the resultant equivalent circuit model of the detector-preamplifier cascade combination at the interface nodes will be as in Fig.3.6. The parallel combination of resistances R_s and R_p into a single effective resistance R and the similar combination of capacitances into a single effective capacitance C appear in shunt with the detector signal current source $i_s(t)$.To determine the voltage v(t) response function, the differential equation applicable to the equivalent circuit thus obtained is solved for a given current $i_s(t)$ forcing function.

The differential equation by Kirchoff's current law at node D is

$$\frac{v(t)}{R} + C\frac{dv(t)}{dt} = i_s(t) \qquad \qquad ...3.3$$
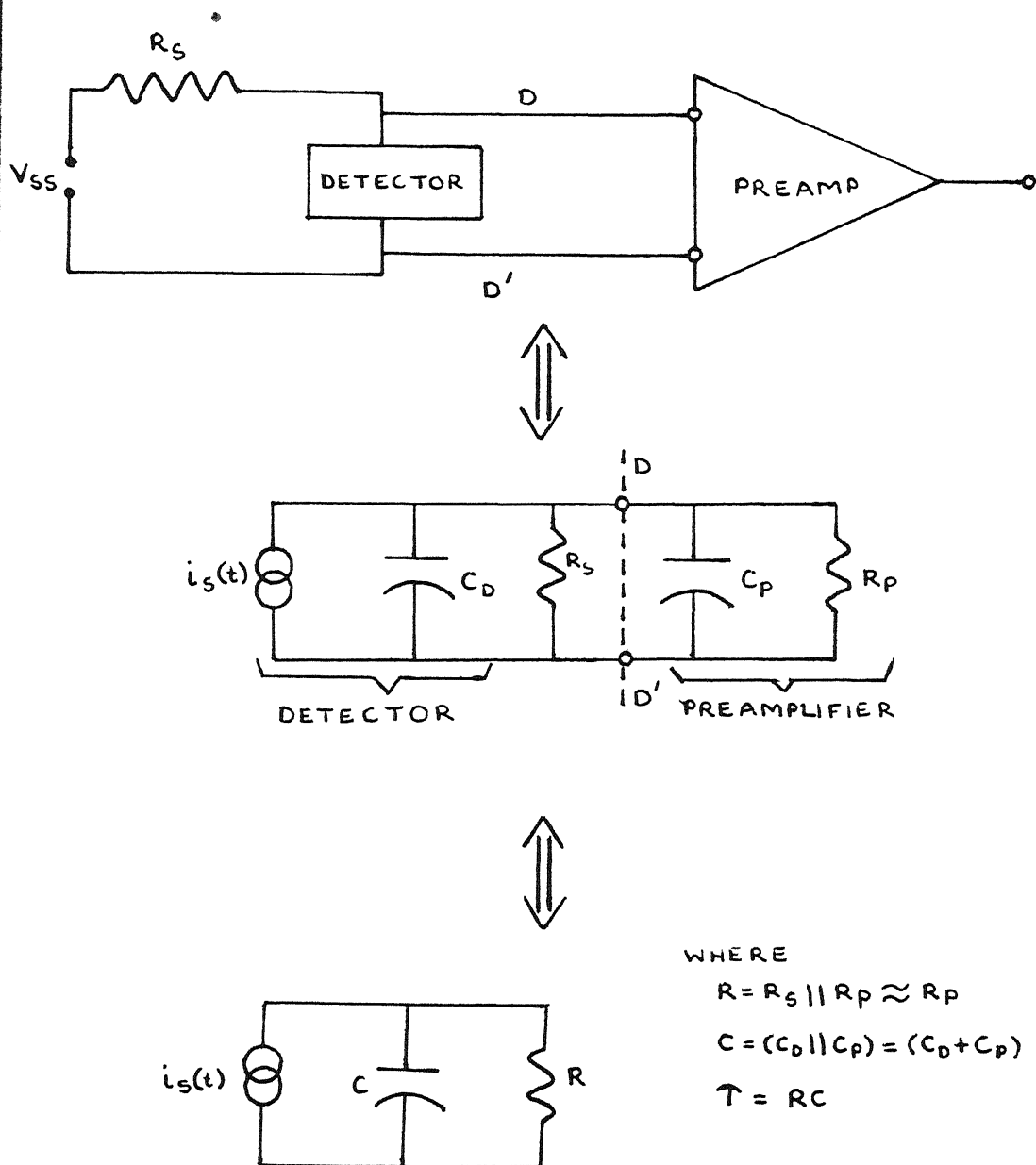
FIG.3.6 EQUIVALENT CIRCUIT OF DETECTOR –
PREAMPLIFIER INTERFACE

Now let it be assumed for the sake of simplicity that current pulse $i_s(t)$ is a rectangular current pulse of peak amplitude I_p and of duration t_c as graphically shown in Fig.3.7a. It follows that I_p and t_c are related to the charge of ion-pairs generated by the equation:

$$Q = \int_0^{t_c} i(t)dt = \int_0^{t_c} I_p dt = I_p t_c \qquad \ldots 3.4$$

where Q is the magnitude of charge burst created at $t=0$

and
$$\left.\begin{array}{ll} i(t)=I_p & \text{for} \quad 0 < t < t_c \\ =0 & \text{for} \quad t \geq t_c \end{array}\right\} \qquad \ldots 3.5$$

$$I_p = Q/t_c \qquad \ldots 3.6$$

and $i_s(t) = I_p [u(t)-u(t-t_c)]$ \qquad $\ldots 3.7$

where $u(t)$ is a unit step function beginning at $t=0$

The differential equation for output voltage response $v(t)$ due to the current pulse given above is now (for $\tau = RC$) given by

$$\frac{v}{\tau} + \frac{dv}{dt} = \frac{1}{C} i_s(t) = \frac{1}{C} I_p [u(t)-u(t-t_c)] \qquad \ldots 3.8$$

The solution of this differential equation in terms of voltage $v(t)$ is

$$v(t) = I_p R \ [(1-e^{-t/\tau})u(t)-(1- e^{-(t-t_c)/\tau})u(t-t_c)] \qquad \ldots 3.9$$

Plot of this waveform is shown in Fig.3.7b.

$i_s(t)$

I_p

t_c

t
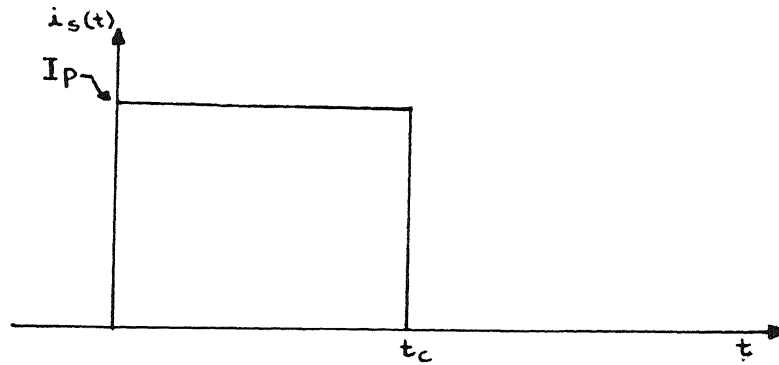
FIG. 3.7(a) IDEALIZED CURRENT PULSE THROUGH DETECTOR

$V(t)$

V_{max}

t_c
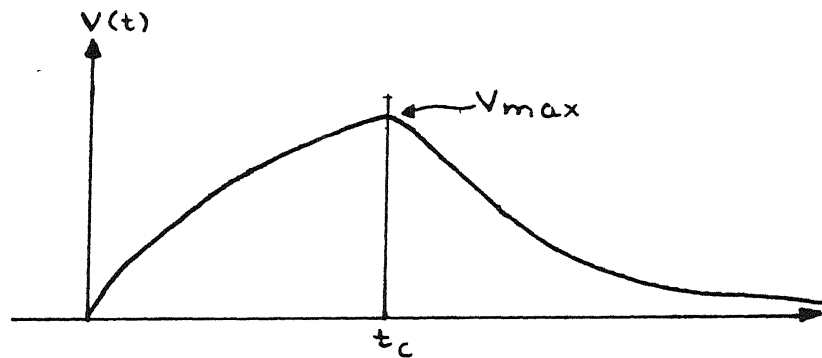
FIG. 3.7(b) OUTPUT VOLTAGE OF DETECTOR

$V(t)$

CURRENT MODE V_{max} $= I_p R$

VOLTAGE MODE V_{max} $= (Q/C)$

$RC \ll t_c$

$RC \gg t_c$

TIME t
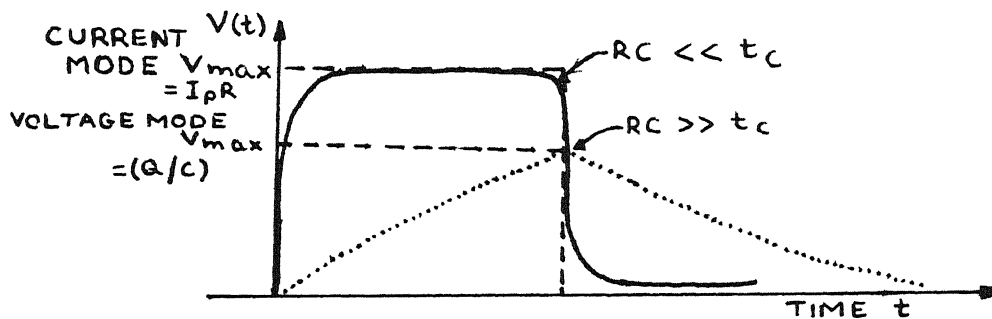
FIG. 3.7 (c) OUTPUT VOLTAGE OF DETECTOR
IN VOLTAGE MODE : ······
IN CURRENT MODE: ——

The maximum or peak value of v(t) occurs at $t=t_c$. Let it be denoted by v_{max}

$$v(t) \Big]_{t=t_c} = v_{max} = I_p R [1-e^{-t_c/\tau}] \qquad \ldots 3.10$$

Two cases arise; case (1): $t_c \gg \tau$,

case (2): $t_c \ll \tau$.

For case 1 and case 2, denote the corresponding value of v_{max} as v_{max1}, v_{max2} respectively. Then,

For case (1) : $t_c \gg \tau$,

$$e^{-t_c/\tau} \cong 0, \qquad \text{and}$$

$$v_{max1} = I_p R = (Q/t_c) R \qquad \ldots 3.11$$

for case (2) : $t_c \ll \tau$,

$$-e^{-t_c/\tau} = 1-(1-t_c/\tau + 0.5 (t_c/\tau)^2+\ldots]$$

$$\cong t_c/\tau$$

and $\qquad V_{max2} = I_p R(t_c/\tau) = (I_p R t_c)/RC = (I_p t_c)/C$

or, $\qquad V_{max2} = Q/C \qquad \ldots 3.12$

Case (1): $t_c \gg \tau = RC$;

$$V_{max1} = QR/t_c$$

In this extreme situation the time constant of the equivalent circuit is very much smaller than the charge

collection time. In terms of circuit behaviour it means that
the capacitance of the detector, preamplifier and stray
elements will discharge faster than the charge is induced on
it by collection process. The current into the input of the
preamplifier is then almost equal to the signal current source
due to the movement of charge carriers in the detector; thus
this corresponds to current mode and the peak value transmitted
onward to the data measurement system is $V_{max1} = QR/t_c$
(Fig.3.7c). It is evident that whereas the measurand quantity
(energy) does appear in this expression as charge Q, the presence
of t_c indicates that the voltage peak value will depend on
the collection time associated with each event. Then for
incidence of monoeneregetic radiation, even when all events
should be registered uniformly as having the same energy per
event, due to the statistical fluctuation of the point of
incidence of particle within the detector, there will be
corresponding fluctuations in charge collection time from event
to event, which are reflected in peak value fluctuations for
the signal voltage. As a result, the energy measurement in
spectrum suffers in resolution, as pecularities in the
detector characteristic also enter the quantity being recorded
alongside rather than only the quantity being measured.

Case (2) $t_c \ll \tau = RC$,

and $V_{max2} = Q/C$.

In this case, the capacitance is not able to discharge faster than the charge deposited on it, because the much shorter duration of collection process is able to ensure its full completion and very little current flows into the input of preamplifier. Therefore the induced charge remains on the capacitance and transformed to a voltage v_{max2} = Q/C. This corresponds to the voltage mode. The peak voltage expression depends primarily on the incident parameter as charge Q but not on its collection time t_c and its vagaries. This voltage mode is thus better suited for energy measurements in spectroscopy, provided the capacitance C is kept fairly constant, because a recorded distribution of pulse amplitudes properly reflects the corresponding distribution in energy of the incident radiation.

Assuming the time separation between successive nuclear events to be sufficiently large, in the voltage mode the capacitance will discharge through the shunt resistance (and hence through the bias resistance and input resistance of preamplifier), returning the signal voltage to zero, at a falling time constant =RC. The corresponding voltage profile is shown in Fig 3.7d.

Some important implications of the consideration of voltage mode and current mode of detector operation arise as follows:
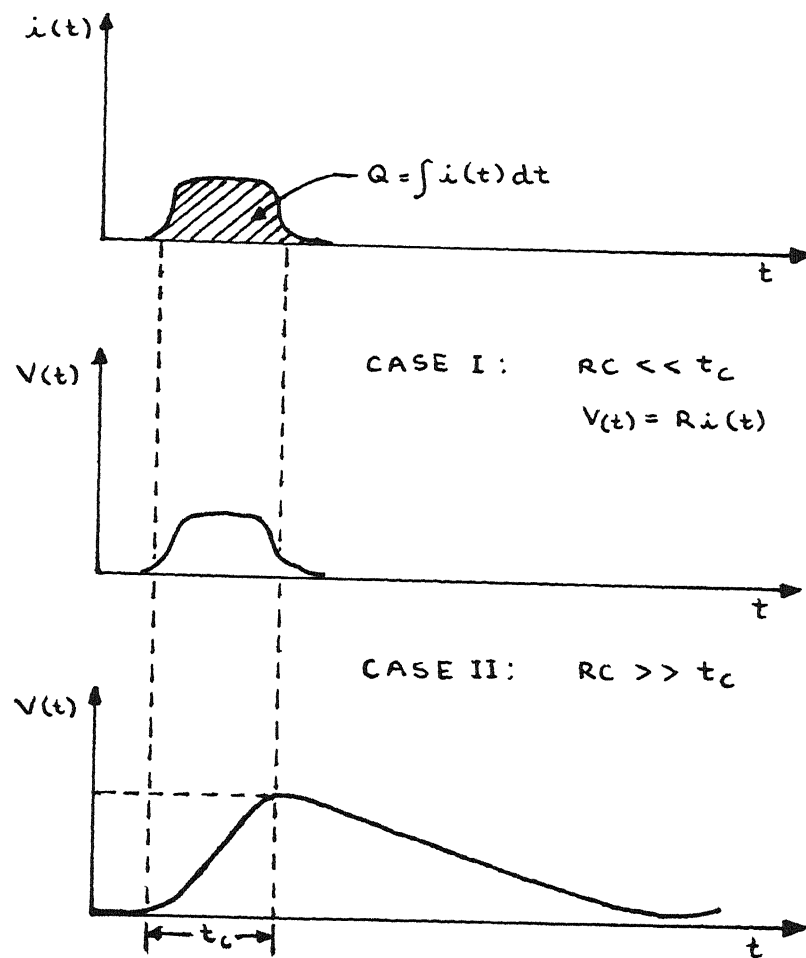
FIG. 3.7 (d)   DETECTOR SIGNAL VOLTAGES FOR
        TWO EXTREME TIME CONSTANTS

(1) In the current mode ($RC \ll t_c$), the shape of the signal voltage is very nearly identical to the temporal profile of the current produced within the detector. This is illustrated in Figs.3.7c and 3.7d. This mode of usage might be adopted especially when timing information is at a premium, because current pulses appear virtually instantaneous.

But its applications in actual circuit operations imply certain impractical requirements. The collection time in such detectors is extremely small, being the order of nanoseconds or less (as low as 500 ps for 50 μm depletion depth for example). The input time constant (RC) for current mode ($RC \ll t_c$) would, therefore, have to be of the order of 100 ps. For a detector with capacitance of typical value of 100 p_f, the input resistance of the preamplifier and bias resistance must then be one ohm or less in the gigahertz range. Higher capacitance detectors are in common use and would need even lower values of input resistance. At the present day levels of technology, it is impossible to meet this requirement of such low values of input resistance at high frequencies (corresponding to very low collection time values). Therefore, in a system employing them and high capacity detectors, current mode operation is just not practised at all. However, in the voltage mode, ($RC \gg t_c$), the time required for the signal voltage to attain its maximum value is determined only by the charge collection time within the detector, as the voltage pulse is formed by integrating the detector current pulse on the detector capacitance. Its rise time, then equals the time width

of the current pulse which is the collection time tc. This rise time is not influenced by the external circuit properties.

But the decay profile of this signal pulse, and hence the time required to restore the signal voltage to zero is indeed determined by the time constant (RC) which is due mainly to the external circuit parameters.

Thus in voltage-mode, the leading-edge of signal pulse is detector-dependent and the trailing-edge is circuit-dependent. (ii) Since a common analytical practice is to record a distribution of signal amplitudes from which some information can be inferred about incident radiation, it is important to have a linear dependence of signal amplitude on the energy associated with each individual nuclear event of radiation incidence. The voltage mode (RC $\gg$ t_c) affords this opportunity in that in responding to a string of discrete signal pulses, the amplitude of each individual pulse reflects the amount of charge Q generated uniquely due to each individual interaction, as is evident from equation (3.2).

3.2 CHARGE PREAMPLIFIER

The linear proportionality between peak voltage v_{max} and collected charge Q holds only if the capacitance C remains fixed in its mathematical role as a constant of proportionality. Generally, in most detectors this assumption of constancy   is upheld as the intrinsic detector capacitance is determined by size and shape of its geometry. But in semiconductor detectors,

particularly the reverse-biased junction diode types, the capacitance is a function of the applied voltage ($C \propto V^{-1/2}$ or $C \propto V^{-1/3}$). Any variations in normal operating parameters cause changes in the capacitance. In such cases, events with the same Q may produce voltage pulses of different amplitude, distorting the basic information carried by the magnitude of Q into the spectrum being recorded. This danger is remedied to a great extent by the introduction of charge sensitive preamplifier. Its shematic is shown in Fig.3.8. The introduction of very high gain amplifier (-A) using a capacitance to close the path of negative feed-back loop, introduces a Miller effect capacitance of effective value $C_f(1+A)$ in shunt with C of the detector to present a total capacitance $C_T = C + C_f(1+A)$ to the detector signal current source and as the new proportionality constant for voltage mode, so that at detector terminals with charge amplifier and Miller effect

$$v_{max} = Q/C_T = Q/(C+C_f(1+A)) \qquad \ldots 3.13$$

instead of

$$v_{max} = Q/C \qquad \ldots 3.12$$

in the previous case of an ordinary voltage amplifier.

The waveform is similar to that of the voltage mode with the leading edge being a relatively straighter ramp like but the decay is with a much larger time constant resembling a flat top (Fig. 3.7c.).
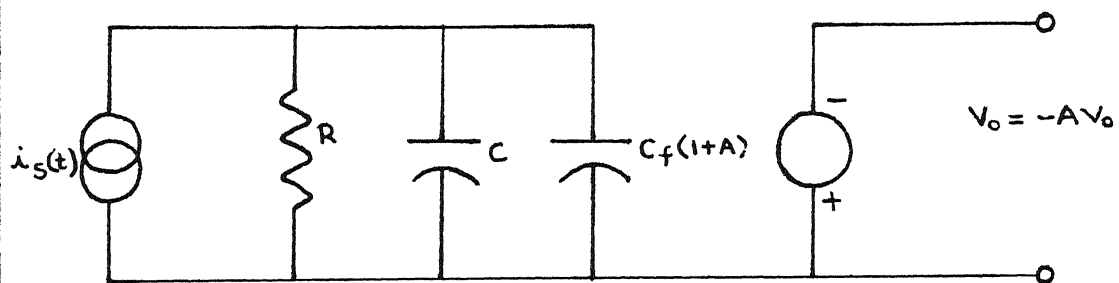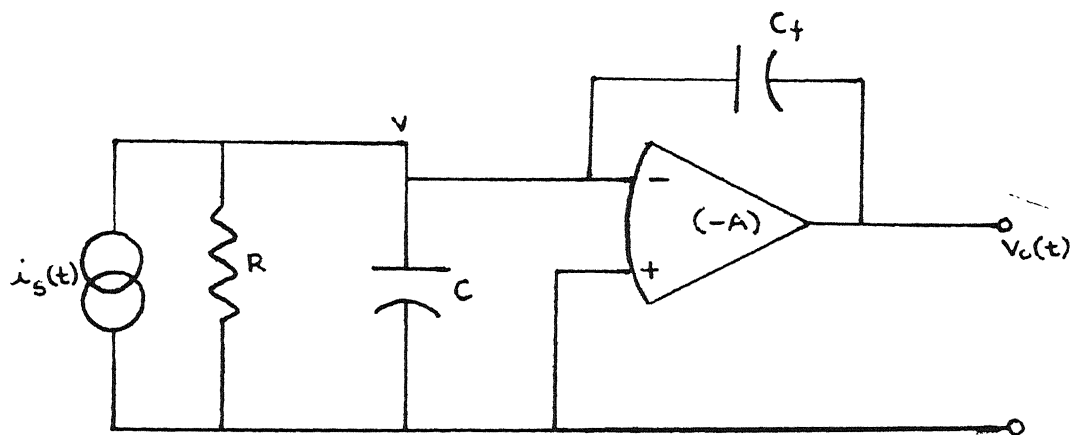
FIG. 3.8 EQUIVALENT CIRCUIT OF DETECTOR—
CHARGE PREAMPLIFIER INTERFACE

The maximum output voltage of the charge preamplifier is

$$v_{omax} = -Av_{max} = -AQ/(C+C_f(1+A)) \qquad \ldots 3.14$$

This charge preamplifier output signal is used in place of a simple voltage preamplifier signal output for purposes of subsequent electronics. The importance of linearity due to the charge preamplifier is demonstrated by a comparison of the parametric sensitivity function for the two cases of charge preamplifier and voltage preamplifier for changes in the detector capacitance as the parameter variation. Sensitivity function measures the ratio of fractional change in a function to the fractional change in a parameter of the function.

Case (1) Charge preamplifier:

$$v_{omax} = -Av_{max} = - AQ/(C+C_f(1+A))$$

Sensitivity function is:-

$$S_o = \left| \frac{\partial v_{omax}/v_o}{\partial C/C} \right| = \left| \frac{\partial \ln v_{omax})}{\partial \ln (C)} \right| = \frac{C}{C+C_f(1+A)} \qquad \ldots 3.15$$

For large A, $A+1 \cong A$ and $C_f(1+A) >> C$. So

$$S_o \cong C/(C_f A) \qquad \ldots 3.16$$

and $A \longrightarrow \alpha \quad S_o \longrightarrow 0$

Case 2. Voltage preamplifier :

This occurs for $C_f = 0$ (i.e. no feed back path)

$$v_{omax} = - Av_{max}$$
$$= -AQ/C \qquad \ldots 3.17$$

Sensitivity function is

$$S_o = \left| \frac{\partial \, v_{omax} \, / \, v_{omax}}{\partial C/C} \right| = \left| \frac{\partial \, \ln v_{omax})}{\partial \, \ln (C)} \right| = 1 \qquad \ldots 3.18$$

Therefore, adoption of the charge ampliflier approach accomplishes a very strong immunization of output signal amplitudes against detector capacitance changes by swamping out its effect by the Miller effect. This benefit passes on as a significant improvement in linearity of energy or charge in signal voltage output.

3.3 NATURE OF PULSE HEIGHT SPECTRA

In this section, starting from an examination of the kind of data analysis generally adopted, an evaluation of how imperfections in detector performance introduce errors in measurement is undertaken. Motivation for this exercise comes from the need for a basis for designing appropriate perturbations in the simulation model of the detector.

It has been recognized that pulse amplitude distribution (alternatively called Pulse Height Analysis) is an important way to analyze detector outputs in response to incident radiation and thereby deduce information about the incident radiation or detector performance itself. It forms the basic technique of spectroscopy.

When the detector responds in pulse mode, to convey the charge generated by irradiation, it is possible to examine a large number of these pulses, each corresponding to the individual quantum of radiation and study variations in their amplitudes. These variations can be attributed to differences in incident energy of the various constituents of radiation or to fluctuations arising in the inherent response of the detector to monoenergetic radiation. While the variations of the first kind are generally sought to be studied in research, the variations of the second kind, due to imperfections in the detection process, represent sources of error in measurement. It is important to be able to distinguish between the two kinds of variations.

The graphical representation of pulse amplitude distribution (typically as shown in Fig.3.9 is a two-dimensional plot of a discrete multichannel analyzer spectrum. In such plots, when visually displayed in its most elementary form, the x-axis or abcissa corresponds to the measurand values represented by pulse amplitude values as actually measured in experiments, and the y-axis or ordinate axis is the counts or number of occurrences of each pulse height. Actually
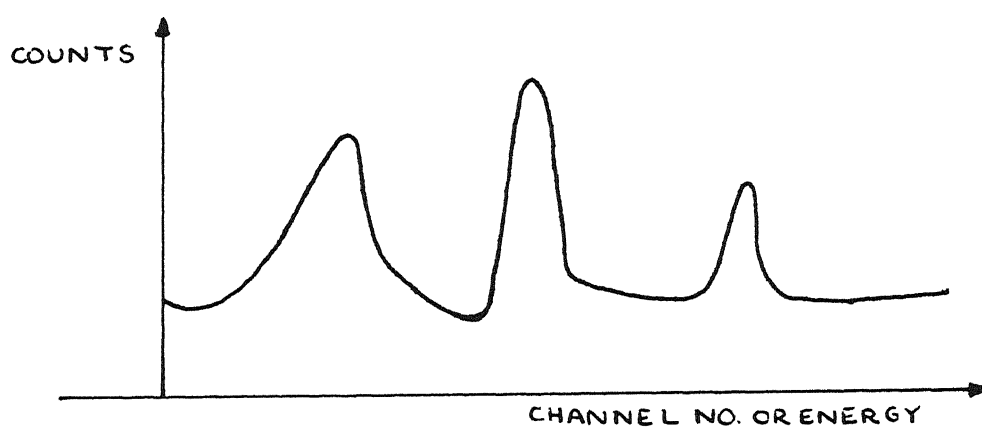
FIG. 3.9   SPECTRAL DISTRIBUTION OF ENERGIES

the pulse heights are represented uniquely by numbers called channels which are derived from the analog-to-digital converter and treated as address locations of the memory holding the spectrum. The vertically high points are spectral peaks which represent concentrations of radiation of a particular energy indicated by the channel number on the abcissa.

In spectroscopic measurements, with pulse height analyzers, the detector is required to respond properly to a wide range of energies of incident radiation particles or quanta. In order to estimate the degree of accuracy in data, it is necessary to be able to judge the inherent quality of detector performance. This evaluation is generally accomplished by subjecting the detector to an incidence of radiation from a known or calibrated source of monoenergetic flux and analyzing the pulse height spectrum of the detector response obtained thereby. Monoenergetic source provides a means of studying the detector under controlled conditions. Irradiation of a detector by any monoenergetic source should, in principle, produce signal pulses of a fixed height to the pulse height analyzer causing counts to accumulate in only one channel corresponding to the energy of the source. But, in practice the detector signal amplitudes under these conditions exhibit a fluctuation in size causing the ideal vertical line to be broadened into a rather bell-shaped gaussian curve so that counts appear in an inteval of channels around the mean value and his erroneously attributes different energies to the ioenergetic source. The implication of this broadening
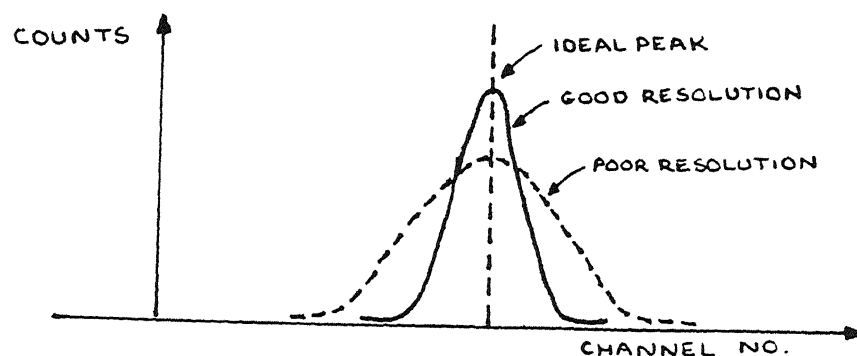
FIG. 3.10 (a) DIFFERENT DEGREES OF RESOLUTION
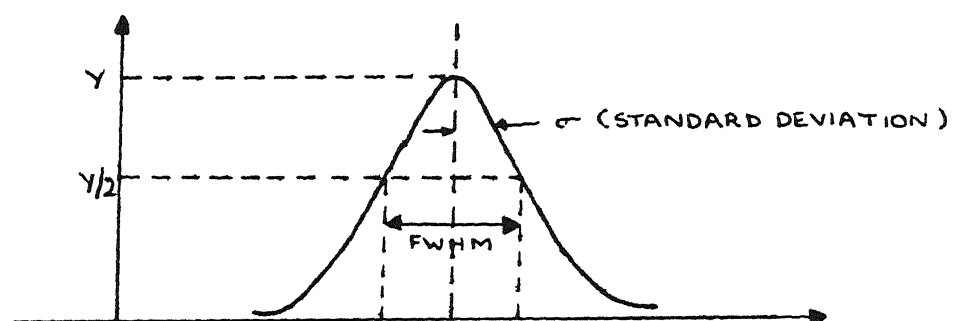
FIG. 3.10 (b) DEFINITION OF FWHM
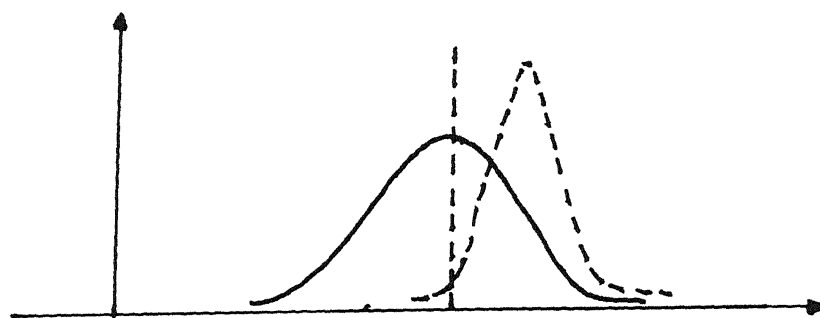
FIG. 3.10 (c) OVERLAP OF NEIGHBOURING PEAKS

(2) Random noise in detector. This noise arises from fluctuations in the detector leakage current and Johnson noise in the resistance in the leads to the detector and input circuit of the preamplifier.

(3) Noise in the electronics of the preamplifier, dependence of this noise on the capacitance of detector and input capacitance of detector.

(4) Effectiveness of noise filtering action of waveshaping amplifier

(5) Ballistic deficiency : This refers to the combined effects of inefficiency in charge collection and fluctuations in it. If all the ion-pairs or charge carriers generated as charge burst Q by the incident radiation are collected then such an efficient collection yields a signal in the external circuit proportional to the energy of the incident particle. However, incomplete charge collection due to loss by recombination or trapping results in smaller signals. Moreover, recombination and trapping are themselves random phenomena i.e. they vary from event to event, therefore are causes of variation in the collection efficiency, leading to loss in energy resolution.

(6) **Statistical Effects** :.This noise fluctuation feature arises because the charge Q generated by interaction with detector material of each quantum of radiation is not a continuous variable but rather a discrete number of charge carriers. This ionization is subject to random fluctuation from event to event even though energy deposited is the same for each event.

Treatment in literature [3,12] of the statistics of the ionization assumes a Poisson process for the formation of each charge carrier. A specific case of semiconductor is considered for illustration of this contention.

When radiation energy is incident on a detector (e.g. Semiconductor material) its deposition occurs by two competing processes of conversion: the ionizing process and the process of the vibrational excitation(phonon generation) of the lattice atoms. This means that energy loss is shared between these processes random means and the resultant signal output charge, which is produced by the ionization component, is intrinsically subject to random fluctuations. Since the collisions for ionization are very rare compared to phonon collisions, the variance, or the root mean square fluctuation, in the number of electron-hole pairs generated obeys Poisson statistics.If E is the absorbed energy (eV) due to incident radiation to be measured and ω is the average energy to produce a single hole-

electron pair(eV/hole-electron pair) then the number N of electron-hole pairs is

$$N = E/\omega \qquad \qquad ...3.19$$

Because this obeys Poisson statistics, standard deviation σ_N in N is given as

$$\sigma_N = N^{1/2} = (E/\omega)^{1/2} \qquad \qquad ...3.20$$

The charge Q due to N electron-hole pairs and hence due to incident energy E is

$$Q = qN = (qE)/\omega \qquad \qquad ...3.21$$

where q = electronic charge = 1.6X10-19 Coloumbs.

Since ω represents the average energy of absorption to produce an electron-hole pair for the particular detector material, the variations in N and also in charge Q can be translated back into terms of energy to reflect the uncertainity in the measurand, namely, the energy E.

A measure of the uncertainity in E is the standard deviation σ_E is given as

$$\sigma_E = \sigma_N/\omega = (E\omega)^{1/2} \qquad \qquad ...3.22$$

To conform to the standard practice of expressing this uncertainity in terms of full width half maximum of energy, we write

$$(FWHM)_E = (2.35)\sigma_E \qquad \qquad ...3.23$$

electron pair(eV/hole-electron pair) then the number N of electron-hole pairs is

$$N = E/\omega \qquad \qquad ...3.19$$

Because this obeys Poisson statistics, standard deviation σ_N in N is given as

$$\sigma_N = N^{1/2} = (E/\omega)^{1/2} \qquad \qquad ...3.20$$

The charge Q due to N electron-hole pairs and hence due to incident energy E is

$$Q = qN = (qE)/\omega \qquad \qquad ...3.21$$

where q = electronic charge = 1.6X10-19 Coloumbs.

Since ω represents the average energy of absorption to produce an electron-hole pair for the particular detector material, the variations in N and also in charge Q can be translated back into terms of energy to reflect the uncertainity in the measurand, namely, the energy E.

A measure of the uncertainity in E is the standard deviation σ_E is given as

$$\sigma_E = \sigma_N/\omega = (E\omega)^{1/2} \qquad \qquad ...3.22$$

To conform to the standard practice of expressing this uncertainity in terms of full width half maximum of energy, we write

$$(FWHM)_E = (2.35)\sigma_E \qquad \qquad ...3.23$$

In practice, the assumption about the rarity of ionizing collisions relative to phonon vibrations has been empirically studied and a correction factor due to FANO needs to be introduced into the standard deviation of N, the number of ion-pairs generated. The modified expression is

$$\sigma_N = (FN)^{1/2} \qquad \ldots 3.24a$$

and therefore
$$\sigma_E = (FN)^{1/2}\omega = (FE\omega)^{1/2} \qquad \ldots 3.24b$$

and thus
$$(FWHM)_E = 2.35 (FE\omega)^{1/2} . \qquad \ldots 3.24c$$

where F is the Fano factor which is specific to material of the detector being approximately 0.12 for Silicon and Germanium.

An important implication arises from the foregoing consideration of statistical effects in detector response. The basic origin of statistical fluctuations is in the ionization process and manifests as a variation in N, the number of hole-electron pairs, for a given energy measurand E assuming ω, the energy of absorption per ion-pair generation, to be constant. Yet it is more meaningful to refer this variation back to the input side of the detector transducer and substitute it with an equivalent variation which is associated with the measurand E, while the detector is imagined to be now fluctuation-free. By this artifice, the actual detector response is better judged in terms of the equivalent uncertainity in measurand necessary to produce a

known or observed fluctuation in output. At the same time, the basic nature of variation in N goes onward to actually reflect as variation σ_Q in charge burst Q and equivalently as a variation σ_v in the pulse height V_p, where

$$V_p = Q/C$$

Therefore $\sigma_Q = \sigma_N \, q$ and $\sigma_v = \sigma_Q/C = (q\sigma_N)/C$

Hence, using eq 3.20

$$\sigma_v = (q/C)(\sigma_E/\omega) \qquad \qquad ... \; 3.25a$$

$$\sigma_E = (C\in\sigma_v)/q \qquad \qquad ... \; 3.25b$$

From the practical standpoint, pulse heights are actually the quantities that are reported by instrumentation electronics and recieved for recording in the multichannel analyzer or other data recording equipment. Therefore, fluctuations in N will be noted as fluctuations in pulse heights and corresponding variations in channel numbers causing the observed broadening of ideal vertical lines into bell shaped curves.

But from the physical standpoint channel numbers are also associated with energy values as the measurand of interest and therefore the actually observed variations in pulse heights and channel numbers need to be translated for reference at detector input so that they be perceived more meaningfully in terms of equivalent energy uncertainity interval around the measurand energy E. Equation 3.25b translates the fluctuation in observed pulse heights to uncertainities in energy. Since q is constant and W is fixed for a definite detector

material, the detector capacitance is a dominant factor in determining the magnitude of amplification of the observed pulse height error into the energy uncertanity and hence the FWHM.Now there can be other sources of fluctuation in the signal chain such as noise of detector, preamplifier and amplifier electronics, as well as drift which will all be observed as resultant fluctuations in pulse height but could be more properly evaluated if these numbers are referred to input and seen as pseudo-fluctuations in energy and corresponding standard deviations.If the source of these fluctuations is independant then the overall effective standard deviation in energy is the quadrature sum of the standard deviation values for each individual contributing source. Thus

$$(\sigma_E)^2_{over\ all} = (\sigma_E)^2_{statistical} + (\sigma_E)^2_{noise} + (\sigma_E)^2_{drift} + \ldots\ldots$$

$$\ldots 3.26a$$

or equivalently,

$$(FWHM)^2_{over\ all} = (FWHM)^2_{statistical} + (FWHM)^2_{noise} + (FWHM)^2_{drift} + \ldots$$

$$\ldots 3.26b$$

The statistical fluctuations in ionization and hence the associated FWHM for energy is the smallest or limiting resolution in energy and is a characteristic of the detector as an intrinsic resolution. Typical intrinsic energy resolution for silicon and Germanium detectors as a function of energy is given in Table 3.1.

Table 3.1

	Incident Energy	$(FWHM)_E = 2.35 \ (FEW)^{1/2}$ electron volts
1 KeV	50	44
2	70	62
5	111	99
10	157	140
20	222	198
50	351	313
100	496	442
200	701	626
500	1109	990
1 Mev	1568	1401
2	2217	1980
5	3506	3132
10	4960	4420
20	7010	6260
50	11090	9900
100	15680	14010
200	22170	19800
500	35060	31320

3.4 DETECTOR PULSE SHAPE

Signal from the detector contains two important items of information. One is the energy deposited by the incident radiation inside the material. The other is the time of

occurrence of the event of irradiation. Both these are related to the charge collection process. The peak value of the transient charge signal corresponds to the energy,and therefore, for high resolution, collection of charges generated must be fully completed by the time information is recorded in the multichannel analyzer. The time of occurrence is obtained by determininig the instant when the rising edge of the detector signal profile exceeds a fixed threshold level. To reduce the timing uncertainity, slope of the signal must be maximized, or equivalently charge collection time be minimized. These issues can be handled best if the temporal profile of the detector signal, i.e. detector pulse shape, is known. The strategy adopted in the derivation of pulse shape profile is to consider a simple detector, the gaseous ionization chamber, as canonical basis for analyzing the charge collection process. The structures and operation of detectors of different types are described in literature [4,7,14]. The salient features pertaining to charge collection process process are considered here. In the simplified diagram, in planar form of Fig. 3.14 is shown a pair of electrodes, bounding a volume of region in which gas is filled, connected to a high d.c.voltage source v_o in series with a resistance. This provides an electric field necessary to sweep away the charges of ion pairs formed by incident radiation. Certain simplifying assumptions and definitions are made to assist in the derivation of the pulse
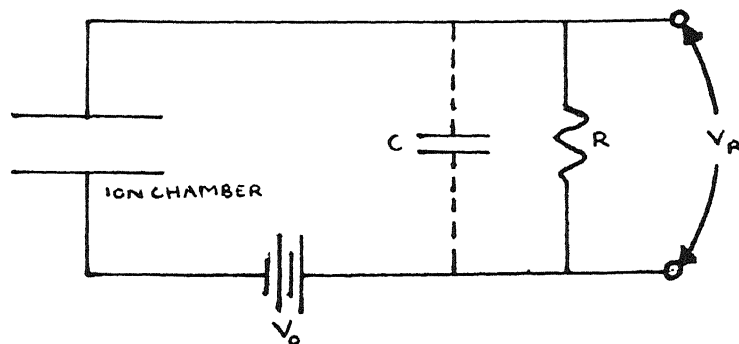
FIG. 3.14a EQUIVALENT CIRCUIT OF AN ION CHAMBER OPERATED IN PULSE MODE
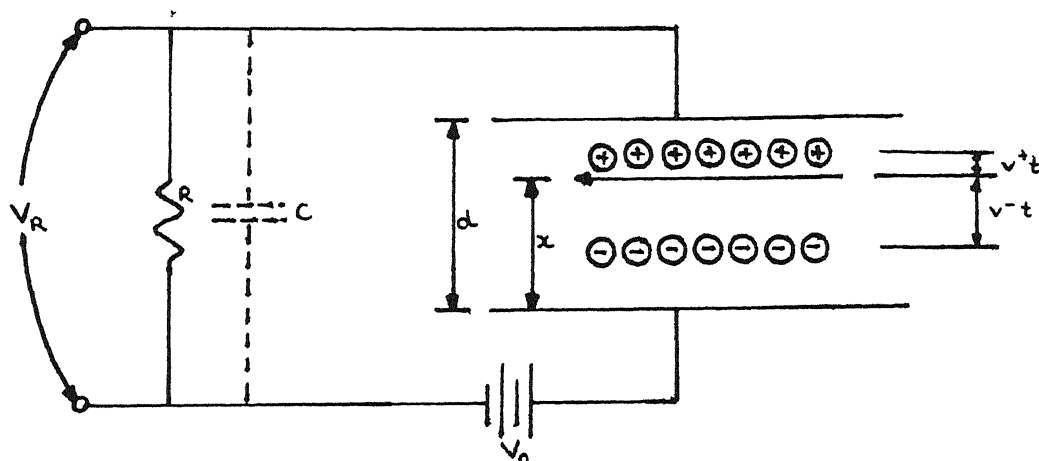
FIG. 3.14b DERIVATION OF THE PULSE SHAPE $V_R(t)$ FOR THE SIGNAL FROM AN ION CHAMBER
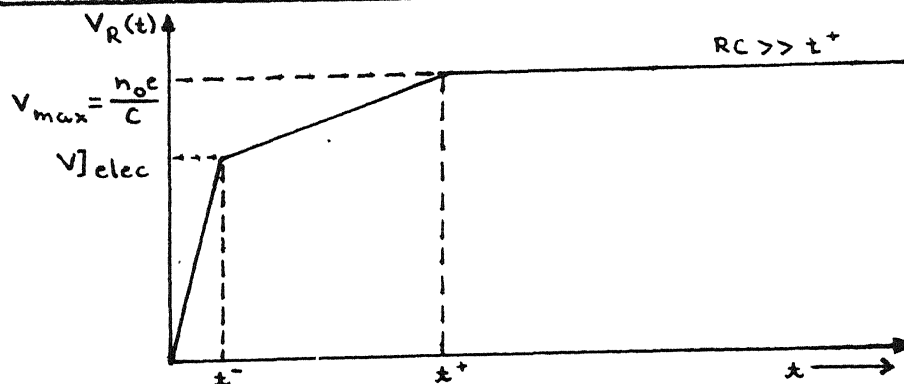
FIG. 3.14c OUTPUT PULSE SHAPE $V_R(t)$.

shape. These are:

(1) The detector has a planar geometry.

(2) d = spacing between electrodes

V=potential difference across electrodes

(3) Resulting electric field   is   assumed   to   be   uniform
throughout   the   interelectrode   region.   Then ϵ = V/d
Under   quiescient   conditions   no   current   flows   from   the
source   and   a   potential difference   V   across   the
electrodes equals the d.c. source   equals V_o.   However,
when current flows V will not be equal to V_o

(4) Let x_o be the distance of   any   point   with   respect   to
the anode (x= 0)   at   which   the   incident   radiation
strikes and produces ion   pairs all at the   same   point.
Electric potential at this point is ϵx_o.

(5) Drift   velocities   of   ion   pairs   are   uniform. v_p=Drift
velocity of each positive ions. v_n =Drift   velocity   of
electron. At time t=0,   an   irradiation   of   energy   E
produces n_o ion pairs of charge Q   =n_oe where e is   the
electronic charge.

Due   to the prevailing electric field ϵ,   charge   collection
process   starts   off immediately causing ions   to   separate   with
electrons moving towards anode with velocity v_n and positive ions
towards cathode with velocity v_p. During   an elapsed time dt, the
positive ions have drifted a distance vpdt towards cathode   which
corresponds   to   a   potential change of dV = ϵ dx = ϵ v_p dt   and

work done on them by electric field

$$dW_p = (charge)\ dV$$

$$= (n_o\ e)\ (\ \in\ v_p dt) \qquad \qquad ...\ 3.27$$

Likewise the work done on movement of electrons is

$$dW_n = (n_o e)\ (\in v_p dt) \qquad \qquad ...\ 3.28$$

Total work done on movement through differential distances of these ion pairs corresponds to appearance of a differential induced charge dq on electrodes (-dq on cathode and dq on anode) under the potential difference V across the electodes which is the source of work. By conservation of energy principle equating the workdone by external d.c. source to the work done by electric field.

$$dW_n + dW_p = V\ dq \qquad \qquad ...\ 3.29$$

$$n_o e \in v_n dt + n_o e \in v_p dt = V\ dq$$

$$dq/dt = (n_o e)\ (v_n + v_p\ )\ (\in/V_o)$$

using $\in = V/d$

$$dq/dt = (n_o e/d)\ (v_n + v_p) \qquad \qquad ...\ 3.30$$

This represents the current flow into the detector and contains contributions from the positive ions and electrons migrating separately.

Integrating to obtain the charge profile and noting that at t=0, charge induced is zero, we obtain :

$$q(t) = n_o e/d \ (v_n + v_p) \ t \qquad \ldots \ 3.31$$

Now this expression indicates a ramp-like linear rise of the leading edge with slope $(n_o e/d) (v_n + v_p)$. But as it involves the motion of electrons and positve ions, it may be noted that:

    (a) Destination of electrons being anode, distance covered for collection is x_o in time $t_n = x_o/v_n$

    (b) Destination of positive ions is cathode, and distance covered for collection is $(d-x_o)$ in time $t_p = (d-x_o)/v_p$.

Due to their unequal velocities they arrive at their respective destinations electrodes at separate instants. So depending upon the smaller of the two values t_n $(= x_o/v_n)$ and t_p $(= (d-x_o)/v_p)$, one of the charge carrier types will have been collected earlier than the other and the slope of the ramp will involve the contribution from the other charge carrier type which reaches later.

Therefore a kink will be observed in the rising edge of the charge waveform. Eventually all the charge collection will be complete and q will attain the final value equal to total charge generated($= n_o e$). The change in slope observed at the point of kink on the rising edge occurs at an instant equal to smaller of the two values :

$$t_n = x_n/v_n \qquad \ldots \ 3.32a$$

and $\qquad t_p = (d-x_o)/v_p$ $\qquad$ ... 3.32b

while the total collection time is larger of the two values. One of these two possibilities holds according to whether $t_n < t_p$ or $t_p < t_n$ i.e.,

$$x_o/(d-x_o) < v_n/v_p \qquad ...3.33a$$
or
$$x_o/(d-x_o) > v_n/v_p \qquad ... 3.33b$$

In either case, the presence of x_o, the point of incidence of radiation, means a cause of fluctuation in collection time from event to event of the same energy. Further, collection of both the charge carriers is to be allowed to be duly completed to develop the full charge strength ($n_o e$) generated by the incident radiation.

3.5 PULSE SHAPE OF SEMICONDUCTOR DETECTORS

Here too the pulse shape is determined by the motion of the carriers drifting under the influence of the electric field, upto the time in which carriers of both polarities have been collected. Most semiconductor detectors are operated as reverse biased diodes in which an applied electric field across the depleted region serves to sweep away the charge carriers created as hole-electron pairs. The interaction of an incident charged particle in the depleted region releases a large number of such hole-electron pairs whose initial spatial distribution depends on

the type and energy of the radiation. Subsequently, these pairs are separated and collected in a time which is a function of the initial location of pair formation point, electric field and the depletion region and on the mobility of the carriers at the operating temperature of the device. The charge transit time corresponds to the migration of electrons and holes formed by the incident radiation across the region of high electric field in the depletion region. The rise time of the output pulse is, therefore, limited by the time required for complete migration of these charges from their point of formation to the opposite extremes of the depletion region High electric fields and small depletion widths help to minimize this time.

In the simplest case of reverse biased diodes as detectors, the transition or depletion region is the active region because it is the region which can sustain an electric field necessary to sweep these charges. This depletion region is a PN junction having a space charge of immobile dopant ions of opposite polarities which exert this electric field. However, in general the electric field has a spatial variation in that it is maximum at the junction of discontinuity and tapers off to almost zero toward the bulk region of either P-type or N-type material.

Since on incidence of radiation, the hole-electron pairs are created generally within this depletion region, these charge carriers are treated like minority carriers to be swept away by the electric field as in the case of internal reverse current -- holes migrating towards the p-side and electrons towards the n-

side. Their behaviour can be analyzed like a minority carrier injection case in semiconductor physics. The velocities of holes (v_p) and of electrons (v_n) are drift velocities proportional to Electric field and through their respective mobilities. i.e.

$$v_p = \mu_p \in \qquad \qquad \dots 3.34a$$

and

$$v_n = \mu_n \in \qquad \qquad \dots 3.34b$$

where μ_p = mobility of hole,

μ_n = mobility of electron

$\in$ = electric field

As these charge carriers migrate towards the bulk regions, they move through regions of gradually decreasing electric field in the depletion region and hence their drift velocities are required to slow down. Thus charge carriers approach their destinations with diminising velocities, that is, virtually in a slowed down manner. This tendency works contrary to the requirement of prompt collection in short transit times. This can be observed from an inspection of the expressions listed in Table 2 appended to this chapter. Table 2 gives a listing of expressions pertaining to both holes and electrons, undergoing drift for collection within the depletion region of either only the P-side or only the N-side of one dimensional reverse biased P-N diode. Expressions are given for depletion region electric field, initial current

and final position on collection migration distance covered and migration time elapsed for collection at appropriate destinations for both electron and hole if irradiation and ionization occur in either side of the transition region alone.

The following noteworthy observations can be made from an inspection of the equations governing charge carrier transport in semiconductor diode depletion regions.

(1) On generation of charge-carriers following irradiation in the either segment of the depletion region, one type of charge carriers happens to be already in the native region where it is the majority carrier and the other type of charge carrier finds itself as a minority carrier in an "alien" region and therefore is speedily swept by electric field towards its own host region. e.g., in p-type segment of depletion region, holes are majority carriers and electrons are minority carriers, while vice versa is the case in N-type segment of depletion region.

(2) Majority carriers undergo migration in direction of diminishing electric field, and drift sluggishly approaching their destination asymptotically.

(3) Minority carriers undergo migration in direction of increasing electric fields and therefore drift faster and faster so as to reach their destination of peak electric field, in some finite time.

(4) Minority carrier migration yields lowest collection time provided it is prevented from encountering a tapering electric field in its own native segment depletion region. Assymetric doping produces depletion regions which are primarily in only one segment so as to exploit charge collection of minority carriers with smaller collectiontimes. Thus reverse biased type of semiconductor detectors are either P^+N type or NP^+ type.

In totally depleted detectors, the depletion width is fixed by the physical thickness of the silicon wafer, and, therefore, the transit time is decreased as the bias voltage is increased.

In partially depleted detectors, however, the depletion width increases with increasing bias, and therefore the effect of a larger bias voltage is to increase both the electric field and the distance over which charges must be collected. Moreover, because the electric field is not uniform, the drift velocity of electrons and holes changes as they move through the depletion region.

In literature, the principle of calculations for charge induced on electrodes by migration ion pairs within interelectrode space has been a matter of controversy. On the one hand application of Ramo's theorem [14-18] for planar electrodes has been universally extended by its proponents in European laboratories of nuclear physics for non-planar geometries and with space charge in interelectrode space.

The opponents of this view, particularly in laboratories in USA have used the principle of energy balance to derive the expression for charges induced on electrodes [19]. The latter has been adopted here. According to the energy balance approach, the terminal current (dq/dt) associated with time rate of change of induced charge is related to the migrating charge q, through its instantaneous velocity dx/dt and the electric field $\in(x)$ in space at the point in space of its motion by

(work done by   = (Work done on charge q_o to move
   external source)   through dx and potential difference
                            $\in (x) dx$)

$$V \, dq = q_o \in(x) \, dx \qquad \ldots 3.35$$

or

$$V \, \frac{dq}{dt} = q_o \in(x) \, \frac{dx}{dt} = q_o \in(x) \, v_d$$

$$\frac{dq}{dt} = \frac{q_o}{V} \frac{dx}{dt} \in(x)dx \qquad \ldots 3.36$$

Where V is the applied interelectrode potential difference and held constant for small values (incremental) charges induced and v_d = drift velocity of q_o.

Therefore expressions for pulse shape of charge due to single hole-electron pair created in different detector types are as follows:

(1) PN$^+$ diode detector (P region of high resistivity contains the depletion region to the maximum extent)

Induced charge contribution due to hole:

$$q_p(t) = (e/(\mu_p \tau_p))(1/2V)(L_p - x_o)^2 [1 - e^{-2t/\tau_p}] \qquad \ldots 3.37a$$

Induced charge contribution due to electron for $t < t_n$

$$q_n(t) = (e/(\mu_p \tau_p))(1/2V)(L_p - x_o)^2 [1 - e^{2\mu_n t/\mu_p \tau_p}] \qquad \ldots 3.37b$$

Total induced charge on positive electrode (N$^+$) is at any instant t given by

$$q(t) = q_p(t) + q_n(t)$$

V = applied d.c. voltage across detector

L_p = Depletion region width in P-region

x_o = Point of incidence of radiation measured from N$^+$ side of depletion region or from location of maximum electric field.(initial location of x_o).

μ_p = Mobility of hole

μ_n = Mobility of electron

τ_p = Dielectric relaxation time of p-type material

t_{cn} = electron collection time.

The time profiles of charge wave forms of Eq 3.37a and Eq 3.37b are shown in Fig.3.15a. Collection time of hole is
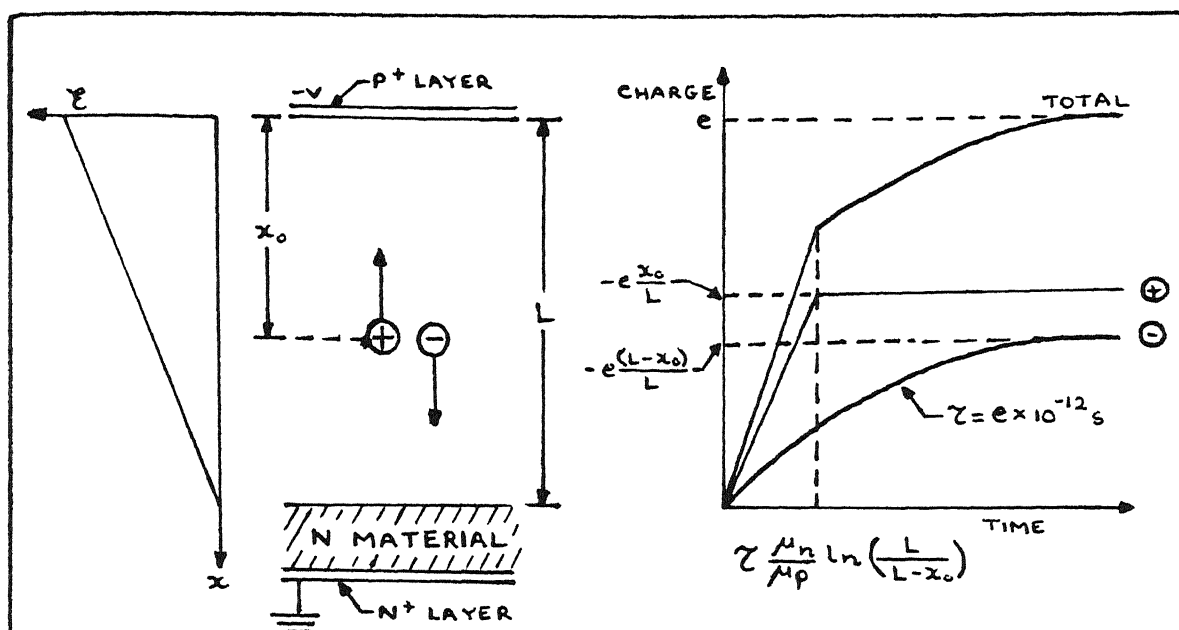
FIG. 3.15b. CHARGE WAVEFORMS DUE TO THE COLLECTION OF A SINGLE HOLE-ELECTRON PAIR IN A SILICON SURFACE-BARRIER DETECTOR

FIG. 3.15a CHARGE WAVEFORMS DUE TO THE COLLECTION OF A SINGLE HOLE-ELECTRON PAIR IN AN SILICON N-P JUNCTION DIODE.

infinity because of the asymptotic relation of Eq.3.37a. However collection time of electron in p-region is finite and is the time taken to reach the N-side (towards maximum electric field).

$$t_{cn} = \frac{\mu_p \tau_p}{\mu_n} \ln \frac{L_p}{L_p - x_o} \qquad \qquad \ldots 3.37c$$

However as $t \longrightarrow \alpha$, $q_p(\alpha) + q_n(\alpha) = e$ $\qquad \qquad \ldots 3.38$

that is eventually the total charge collected equals the charge generated (by irradiation)

(2) N^+P diode and Surface barrier diodes: The time profiles here are analogous to those for PN^+ diode except that the roles for holes and electrons are reversed (Fig.3.15b).

(3) P-1-N planar type detector (Fig.3.15c): The planar detector is analogous in geometry to a gaseous ionization chamber. Thus

a) Induced charge contribution due to hole for $t < t_{cp}$

$$q_p(t) = (V_o/L^2)\mu_p et = (ex_o/L)(t/t_{cp}) \qquad \ldots 3.39a$$

and for $t \geq t_{cp}$,

$$q_p(t) = (e\,x_o)/L \qquad \qquad \ldots 3.39b$$

(b) Induced charge contribution due to electron for $t < t_{cn}$,

$$q_n(t) = (V_o/L^2)\mu_n et = (e(L-x_o)/L)(t/t_{cn}) \qquad \ldots 3.39c$$
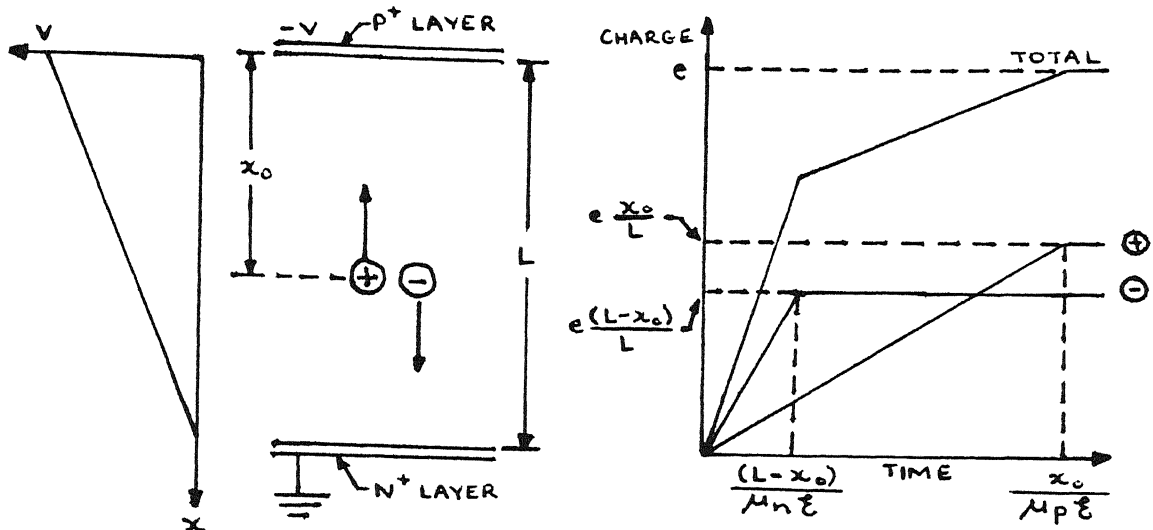
FIG. 3.15c CHARGE WAVEFORMS DUE TO THE COLLECTION OF A
SINGLE HOLE - ELECTRON PAIR IN A P-I-N
PLANAR DETECTOR.
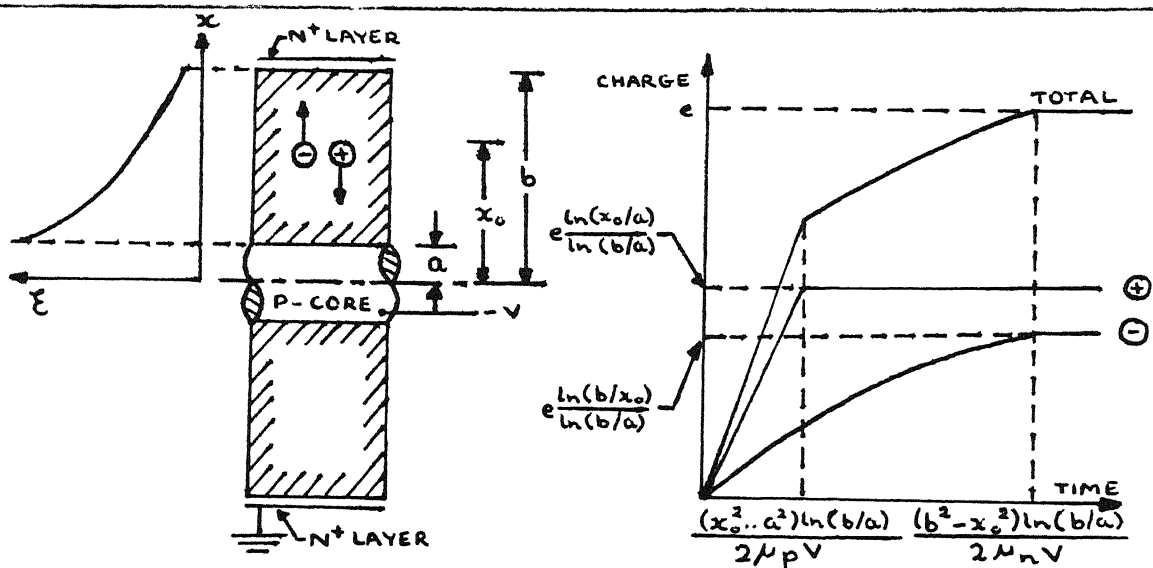
FIG. 3.15d CHARGE WAVEFORMS DUE TO THE COLLECTION OF A
SINGLE HOLE - ELECTRON PAIR IN A P-I-N DOUBLE-
ENDED CYLINDRICAL COAXIAL DETECTOR

for $t \geq t_{cn}$

$$q_n(t) = e(L-x_0)/L \qquad \ldots \text{3.39d}$$

where e = electron charge

   V_0 = applied d.c.voltage across the planar diode intrinsic
   region

   L = width of intrinsic region

   x_0 = Point of incidence of irradiation (also initial
   situation of hole and electron)

   μ_n = Mobility of electron

   μ_h = Mobility of hole.

   t_{cp} = collection time of hole = time of arrival of hole at
   negative electrode (p-side here)

$$= Lx_0/(\mu_p V_0) \qquad \ldots \text{3.39e}$$

   t_{cn} = collection time of electron = time of
   arrival of electron at positive electrode
   (n-side here)

$$= L(L-x_0)/(\mu_n V_0) \qquad \ldots \text{3.40f}$$

The same remarks concerning kink in slope and levelling off of
total profile as in case of gaseous ionization chamber apply
here. That is

$$q(\, t < \min(t_{cp}, t_{cn})) = q_p(t) + q_n(t) = \frac{e}{L^2}\left[\frac{x_0}{t_{cp}} + \frac{L-x_0}{t_{cn}}\right] \ldots \text{3.39g}$$

$$q(\, t > \max(t_{cp}, t_{cn})) = e \qquad \ldots \text{3.39h}$$

where $\min(t_{cp}, t_{cn})$ = lower of the two values : t_{cp}, t_{cn} and

$\max(t_{cp}, t_{cn})$ = higher of the two values: t_{cp}, t_{cn}

(3) P-i-N Coaxial Detector (Fig.3.15d). P-type at core of radius r = a and N-type at outer layer of radius = b

a) Induced charge contribution due to hole (proceeding to be collected at inner core)

$$q_p(t) = \frac{e_o}{2\ln(b/a)} \ln \frac{x^2}{x_o^2 - 2\mu_p kt} \qquad \ldots 3.40a$$

for $t < t_{cp}$ (collection time of hole)

$$q_p(t) = \frac{x_o^2 - a^2}{2V_o\mu_p} \ln(b/a)$$

for $t > t_{cp}$

$$q_p(t) = q(t=t_{cp}) = e_o \ln(x_o/a)/(\ln(b/a)) \qquad \ldots 3.40b$$

(b) Induced charge contribution due to electron (proceeding to be collected at outer layer)

$$q_n(t) = \frac{e_o}{2\ln(b/a)} \ln \frac{x^2}{x_o^2 + 2\mu_n kt} \qquad \ldots 3.40c$$

for $t < t_{cn}$ (collection time of electron)

$$t_{cn} = (b^2 - x_o^2)\ln(b/a)/2V_o\mu_n \qquad \ldots 3.40d$$

for $t > t_{cn}$, induced charge is

$$q(t>t_{cn}) = q(t=t_{cn}) = e \ln(b/x_o) / \ln(b/a) \qquad \ldots 3.40e$$

Practical forms of P I N detectors come as high purity Germanium (after referred to as HPGe and often called intrinsic Germanium detector) and Lithium-drifted Germanium detector (often referred to as Ge(Li) and pronounced as "jelly" detector). PIN detectors have an intrinsic region sandwiched between P and N regions. The intrinsic region can sustain a uniform electric field whose value is often adjusted by external supply to such a level that charge carriers are able to attain the maximum (saturation) drift velocities which remain uniform (10^7) cm/sec for both electrons and holes when cooled down to liquid nitrogen temperature (77^OK or -196^OC). Such a feature enables the shortest transit time for both charge carriers to be achieved and collection times can be extremely short and charge collection complete. Such detectors can have planar geometry or coaxial geometry. While planar geometry is preferred for thin detectors and timing spectroscopy, coaxial geometry is adopted for high-efficiency, high - energy gamma-ray spectroscopy using Ge(Li) material, because large volumes for interaction are essential [18,20,21]. The non uniform field distribution is obtained by this geometry(Fig.3.15d).

For a planar detector as shown in Fig.3.15e, the expression for pulse shape expected for an interaction occurring at a distance x_o from the n-type region of a planar detector of thickness d is
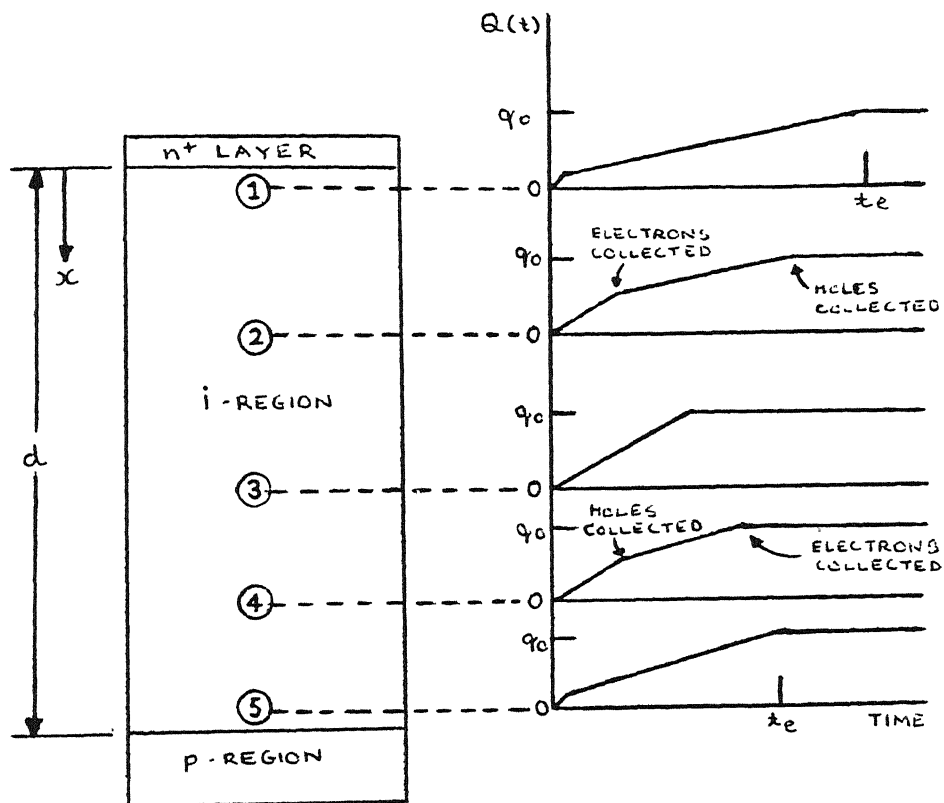
FIG. 3.15e SHAPE OF THE LEADING EDGE OF THE OUTPUT
PULSE Q(t) FOR VARIOUS INTERACTION
POINTS WITHIN THE i- REGION

$$Q(t) = n_o e \{(x_o/d)[(t-(t-t_e)u(t-t_e))/t_h]$$
$$+((d-x_o)/d)[(t-(t-t_h)u(t-t_h))/t_e]\} \qquad \ldots 3.41$$

where $n_o e$ = total charge (of either polarity) created on irradiation where n_o is the number of electron-hole pairs,

$u(t-t_e)$ = unit step function = 0 for $t < t_e$
$\qquad\qquad\qquad\qquad\qquad\quad$ = 1 for $t \geq t_e$

t_e = electron collection time
$\quad = x_o/v_e$ where v_e is the saturation drift velocity for electron
t_h = hole collection time

$\quad = (d-x_o)/v_h$, where v_h is the saturation drift velocity for hole.

$u(t-t_h)$ = 0 for $t < t_h$
$\qquad\qquad\;$ = 1 for $t > t_h$

This equation Eq.3.41 can be broken down into four possible time domains corresponding to a stage with both holes and electrons in motion, followed by a stage when either holes are collected but electrons are still drifting or electrons are collected but holes are still drifting, lastly a stage when both electrons and holes have been collected.

The intermediate stage when one carrier type has been collected and other still drifting has two possibilities and this depends on the relative magnitudes of hole and electron collection times t_h and t_e. These collection times get predetermined in this model by the value for x_o, distance of the location of the point of generation of charge carriers with

respect to one electrode (n-type region), given spacing d and saturation drift velocities.

Stage I: t such that $t < t_h$ and $t < t_e$: Both holes and electrons are drifting

$$Q(t) = (n_o e)\left[\frac{v_e}{d} + \frac{v_h}{d}\right]t$$

Stage II(a): $t_e < t < t_h$:Electrons have been collected but holes are still drifting (because x_o is such that $t_e < t_h$)

$$Q(t) = (n_o e)\left[\frac{x_o}{d} + \frac{v_h t}{d}\right]---$$

Stage II(b): $t_h < t < t_e$: Holes have been collected but electrons are still drifting(because x_o is such that $t_h < t_e$)

$$Q(t) = (n_o e)\left[\frac{d-x_o}{d} + \frac{v_e t}{d}\right]$$

Stage III: $t > t_e$ and $t > t_h$: Both holes and electrons have been collected

$$Q(t) = n_o e = \text{Charge initially generated and now finally collected}$$

Similarly, for coaxial detector with inner radius r_i and outer radius r_o and with a p-type case, the charge waveform (as pulse rise) can also be represented as also falling in 3 stages as in the case for planar geometry. Assuming that saturation velocities have been attained by holes and electrons, and

the point of radiation interaction with charge generation is situated at a radial distance x ($r_i < x < r_o$), then the charge waveform can be expressed as piecewise function of time as follows:

Stage I: $t < t_h$ and $t < t_e$: Both holes and electrons are drifting

$$Q(t) = [n_o e/\ln(r_o/r_i)]\left[\ln \left(1 + \frac{v_e t}{x}\right) - \ln \left(1 - \frac{v_h t}{x}\right)\right]$$

Stage II(a): $t_e < t_h$ i.e. Electrons have been collected and holes are drifting and for t such that $t_e < t < t_h$,

$$Q(t) = [n_o e/\ln(r_o/r_i)]\left[\ln \left(\frac{v_o}{x}\right) - \ln \left(1 - \frac{v_h t}{x}\right)\right]$$

Stage II(b): $t_h < t_e$ i.e. Holes have been collected and electrons are drifting and for t such that $t_h < t < t_e$

$$Q(t) = [n_o e/\ln(r_o/r_i)]\left[\ln \left(1 + \frac{v_e t}{x}\right) - \ln \left(\frac{r_i}{x}\right)\right]$$

Stage III: $t > t_h$ and $t > t_e$: Both holes and electrons have collected.

$$Q(t) = n_o e = \text{full charge generated}$$

Here,

Holes collection time $t_h = (x - r_i)/v_h$

Electron collection time $t_e = (r_o - x)/v_e$

The assumptions underlying the derivations of the above expressions for PIN type detectors are as follows :

(1) Electric field is high enough within the active volume to ensure saturation drift velocity for both electrons and holes.

(2) Ionization by radiation occurs entirely within the active volume

(3) Trapping and recombination of charge carriers are ignored so that all charge carriers generated are assumed to migrate completely.

(4) Point ionization is assumed so that all charge carriers are generated at the same coordinates within the active volume.

3.6 WAVE SHAPING AMPLIFIER CIRCUITS:

3.6.1. Introduction

The waveshaping amplifier is an integral part of the instrumentation chain following the detector-preamplifier combination. Besides providing gain, it performs waveshaping of the preamplified signal of the detector to obtain an optimum signal-to-noise ratio consistent with the counting rate and other experimental conditions. There are two principal reasons for introduction of waveshaping as follows :

(1) **Overlap Prevention:** Since the events of incident radiation are randomly spaced in time, the effect of each individual event in the detector must be completed in a time that is short compared to the average time interval separating successive events. Otherwise, response pulses to consecutive events overlap, with the

attendent consequences of waveform distortion and error in amplitude interpretation. Pulse shortening methods, called "clipping", are used for this purpose.

(2) Enhancement of Signal-to-Noise Ratio: The spectral bandwidth of the unavoidable noise sources in detector and preamplifier is much wider than that due to the significant components of the desired signal. Therefore pulse shaping techniques are resorted to in time domain to alter the waveforms in a controlled manner so as to equivalently perform in frequency domain an enhancement of spectral components of the signal while diminishing the noise components. Thus signal-to-noise ratio as well as resolution are improved.

The detector-preamplifier combination yields an output waveform whose magnitude is proportional to the charge collected by the detector. It has a shape of an essentially linear rising edge much like a ramp which after some time, equal to the collection time within the detector, levels off to a peak value proportional to the total charge finally collected, and representative of energy E of incident radiation. Since the order of magnitudes of the two collection times, each of radiation applicable to charge carriers of one type, is very small, the kink in the rising edge can be ignored and this edge be viewed as a single slope ramp until the peak value is attained. The temporal profile of the preamplifier, as suggested here, is shown in Fig.3.16a.

V_p = PEAK PREAMP OUTPUT

T_c = COLLECTION TIME
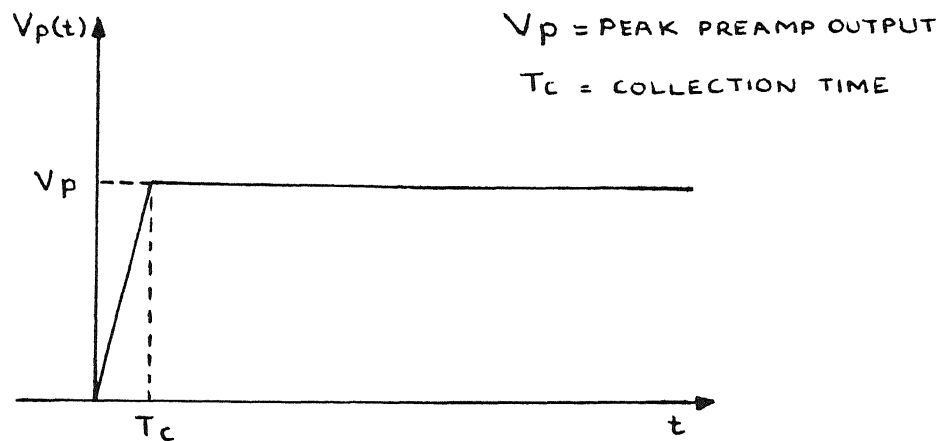
FIG. 3.16 (a) PREAMPLIFIER OUTPUT SIGNAL VOLTAGE
$V_p(t)$ WITH FLAT TOP

$V_p e^{-(t-T_c)/T_F}$
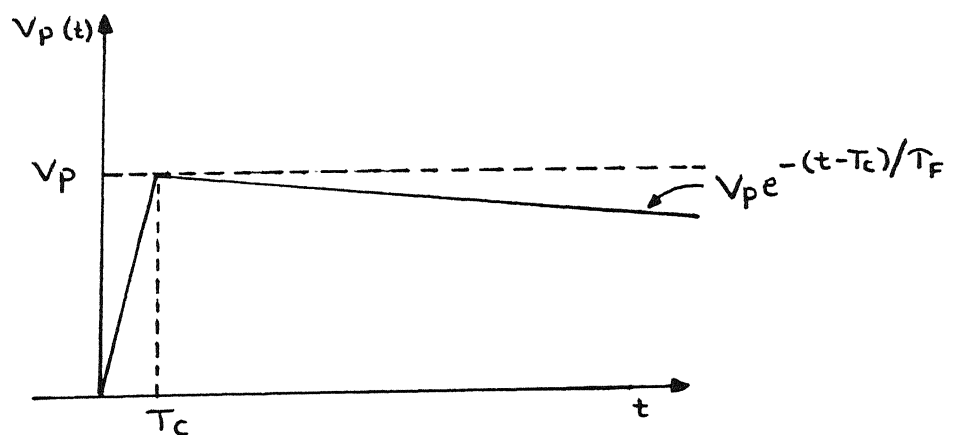
FIG. 3.16 (b) PREAMPLIFIER OUTPUT SIGNAL
VOLTAGE $V_p(t)$ WITH SLOW DECAY

The preamplifier output signal voltage $v_p(t)$ can be under these simplifications represented as

for $0 < t < T_c$

$$v_p(t) = (V_p/T_c)t \qquad \text{...3.41a}$$

for $T < t < \infty$

$$v_p(t) = V_p = AQ/C_T \qquad \text{...3.41b}$$

Where T_c = Collection time (due to charge carrier collected later than the other type).

V_p = Peak preamplifier output voltage

Q = Total charge collected (proportional to incident energy E)

A = Gain of preamplifier

C_T = Total effective capacitance at interface between detector output and preamplifier input.

Actually this idealized waveform is to be modified to account for the slow decay of charge on capacitance by the effective shunt resistance after the peak has been reached. This behaviour is evident from inspection of Fig.3.8. As a result, it seems proper to associate an exponential decay with time constant $T_F = R_T C_T$. The requirement $T_c \ll R_T C_T$ is necessary for consistency with the voltage mode or charge mode of detector operation. Moreover, such a modification is plausible also on the ground that if the decay were extremely slow, the voltage profile would resemble a step waveform for negligibly small collection times and successive events in detector would cause charge on feedback

capacitance of charge preamplifier to cumulatively build up causing output voltage to rise and eventually result in saturation of the preamplifier. Thereupon, the system would become inoperative. Therefore, it is imperative to introduce a certain finite decay time constant to allow the circuit to recover early enough before the next possible nuclear event. The modified temporal profile for preamplifier output voltage signal $v_p(t)$ is now represented as follows:

for $0 \leq t < T_c$

$$v_p(t) = (V_p/T_c)t$$

for $T_c \leq t < \infty$

$$v_p(t) = V_p \, e^{-(t-T_c)/\tau_F}$$

where $V_p = AQ/C_T$ and the terms have the same meaning as above.

T_F = decay time constant = $R_T C_T$

The profile is graphically shown in Fig.3.16(b)

3.6.2. Counting Rate-Resolution compromises

The waveshaping techniques which yield the optimum signal-to-noise ratio are always in conflict with the methods to achieve overlap prevention. This is explained below.

From the standpoint of accepting pulses spaced randomly in time, and particularly at a high mean recurrence rate, the slow exponential decay on the tail of each signal pulse becomes a nuisance as a substantial number of subsequent pulses will occur before the previous pulses have decayed to zero. This will

obviously cause errors in pulse amplitude measurement, because of
the pile-up of pulses on the tails of preceding pulses. The
random time spacing means each pulse can be superimposed on a
different residual tail. In such a situation the actually
measured amplitude is no longer a good measure of Q, the charge
deposited for an incident energy E. Similarly, errors in pulse
rate also occur due to the closely overlapping pulses being
recorded by the measuring instruments as a single pulse. To
minimize such an error, and for the distortion due to pile-up to
be small, the effective duration of the signal at the amplifier
output should be as short as possible. If the measurement of
individual signals is to be independent of previous ones, the
signals must be permitted to decay in a reasonable time which is
short compared with the average interval between pulses. At the
same time, it is desirable that the signal duration be longer
than the rise time, for the peak height to be truly indicative
of the total charge collected. Thus $\tau_F \gg T_c$ is a necessary
condition.

There are two reasons why the peak signal height (amplitude)
should represent the total collected charge:

(1) The accuracy with which the amplitude represents the
energy deposited by the incident radiation is limited by
the statistical uncertainty in the number of charge
carriers produced. Each signal pulse, in that sense,
represents a statistical sampling of some fraction of
these ion pairs and if larger is the efficiency of

3.6.3. Location of Pulse Shaping Circuits :

In the currently accepted practice of analog signal processing of nuclear detector signals, the circuits performing the primary pulse shaping functions are located in the main amplifier. The preamplifier carries out only RC differentiation of relatively long time constant to prevent pile-up. There are two main reasons for situation of primary waveshaping function in the main amplifier.

(1) When the shaping circuits have provisions for switch selection of pulse shape parameters, the main amplifier is a more preferable choice because it is within the reach of the operator whereas preamplifier could be in an inconvenient location or in a high radiation area.

(2) The preamplifier can be standardized to one specific design if it is not called upon to perform different waveshaping functions.

Most significant information in the preamplifier output signal is conveyed in the leading edge rise and in the peak value attained. The subsequent waveshaping amplifier operates with time constants much shorter than the decay of the preamplifier output signal and much longer than its rise time. Effectively this suppresses the slow component of the preamplifier signal, yielding narrow pulses whose amplitudes neverthless conveys the information of quantitative interest. Ideally the pulses out of the amplifier do not overlap but may do so if the count rate is high causing an error in amplitude(energy) interpretation.

3.6.4. Commonly Used Waveshaping Circuits:

There are four major categories of waveshaping approaches in prevalent use:

_____ RC pulse shaping

_____ Semigaussian pulse shaping

_____ Gated Integrator pulse shaping

_____ Delay Line pulse shaping

These are briefly described below:

(1) RC pulse shaping: This technique refers to the use of resistors and capacitors as shaping networks. Among several connections possible, CR-RC pulse shaping is the most useful pulse shaping method and is formed by cascading with suitable isolation a CR differentiator and an RC integrator. The connection is shown in Fig.3.17. The circuit attenuates both low frequency and high frequency signal as well as noise components but considerably enhances the signal-to-noise ratio. A majority of applications use equal CR differentiator and RC integrator time constants to optimize the result. This connection was adopted for simulation of amplified nuclear detector response. Other variations are also practiced. Step-response analyses have been extensively attempted in literature [15,19,22].

(2) Semigaussian Pulse Shaping [1,20,22]: A pulse shape that resembles the gaussian distribution function can be obtained if a large number of effective integrations follow a CR differentiation. This achieves theoretically
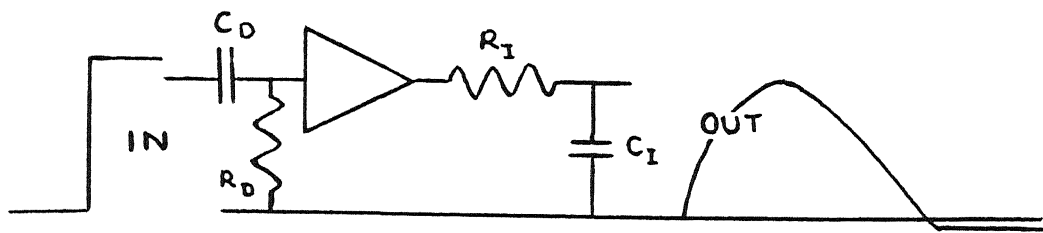
$$T = R_D C_D = R_I C_I$$

FIG. 3.17(a.) CR-RC PULSE SHAPING
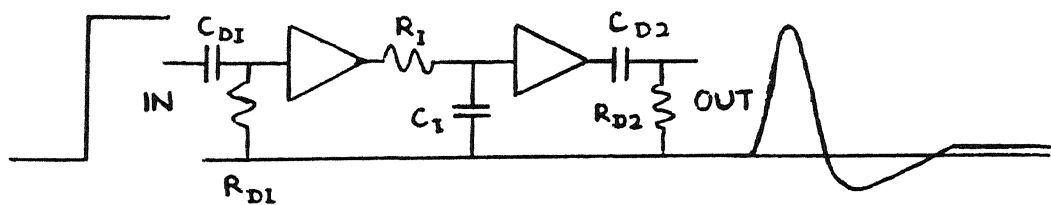
$$T = R_{DI} C_{DI} = R_I C_I = R_{D2} C_{D2}$$

FIG. 3.17 (b). DOUBLY - DIFFERENTIATED CR-RC-CR SHAPING.

18% improvement in relative signal-to-noise ratio with respect to CR-RC pulse shaper.

The step response is $R(t) = (t/\tau_o)^n \, e^{n(1-t/\tau_o)}$

where n = number of integrators.

τ_o = time constant of RC differentiator.

= time constant of integrator.

(3) **Gated Integrator Pulse Shaping:** The circuit of this type of shaper is shown in Fig.3.18. In the particular inplementation shown here, a gaussian shaped signal is given at the integrator. At the start of the signal, which is independently checked in a fast channel, switch S1 is closed and switch S2 opened simultaneously so that the feedback capacitor is invoked to act as an integrator for the signal. At the tail end of the signal, switch S1 is opened and thereby further signal integration is stopped. S2 is still held open for a short readout time interval just after S1 has been opened for the signal to be digitized or recorded. The switch operations are shown in the figure. Noise improvement indices are reported by Goulding and Landis[20]

(4) **Delay Line Pulse Shaping:** Using propagation delay of distributed or lumped delay lines combined into suitable configurations, essentially rectangular output pulses from each step input are obtained. This method is most
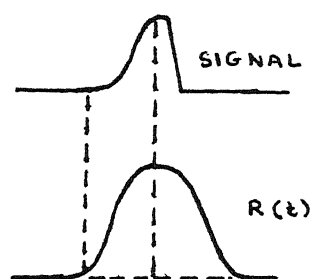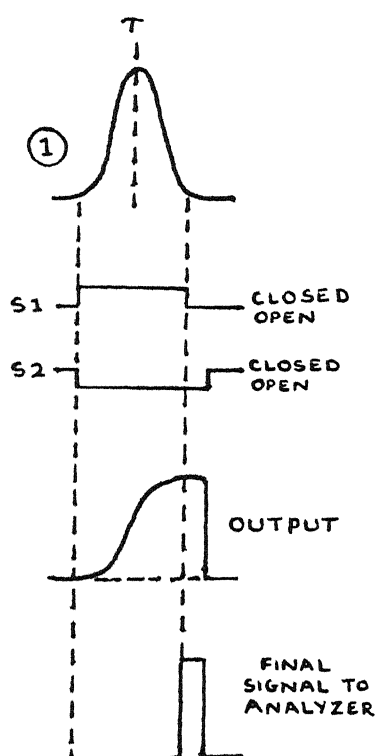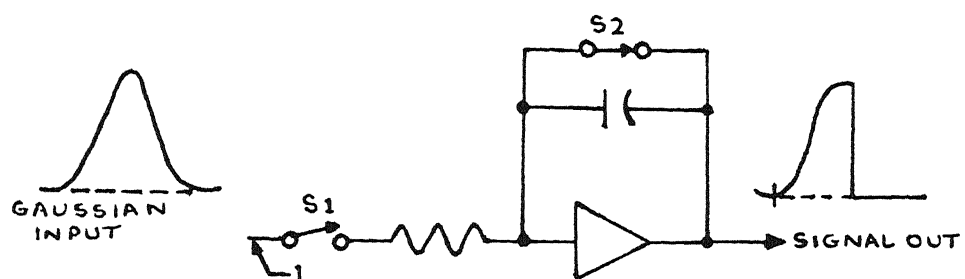
FIG. 3.18 GATED INTEGRATOR

effective in tackling pile-up but has a much poorer signal-to-noise ratio.

3.6.5. Performance Limitations of Wave Shaping Amplifiers:

There are two main factors that contribute to loss of amplitude resolution and are due to limitations in performance of amplifiers:

_____ Electronic Noise.

_____ Baseline shift

(1) Electronic Noise: The very early stages in the amplifier circuit have sources of noise that contribute to the overall noise level of a preamplifier-amplifier-analyzer system. Amplifier noise specification is given in terms of noise referred to input and depends on gain setup. It is of the order of 1 to $10\mu V$.

(2) Baseline Shift: In any radiation detector, pulses occur in a time sequence with other pulses. When the rate of input pulses is very high, the tendency of capacitors in a CR-RC network to block direct current manifests as a shift of baseline below zero so that equal areas are enclosed by the output waveform above and below the zero level axis or zero baseline. This shift becomes more severe as the average spacing between pulses is made smaller. In nuclear pulse analysis systems, basic information is conveyed by the amplitude which is measured relative to a true zero baseline. If any baseline shift occurs, the apparent pulse amplitude will

be reduced causing error in recurrence of signals. In case of perfectly periodic train of pulses, baseline shift is constant and can be compensated. But random time spacing is a characteristic of nuclear signals and therefore baseline shift is not constant but is variable. By making pulse shape bipolar which contains both positive and negative lobes, as opposed to unipolar pulse shapes which are restricted to voltages on only one side of the zero axis, and by ensuring the two lobes to be of equal area, the average or d.c. value is zero and can be coupled through capacitors without baseline distortion.

3.6.6 Shaping for Optimum S/N Ratio

Fig. 3.19 shows graphically how random noise components can degrade amplitude information carried by pulses from a radiation detector. The important sources of noise occur near the beginning of the signal chain where the signal level is minimum and is poised to undergo very high amplification (typically 10^4 times) to be registered by the MCA, for example. Noise generated at this point undergoes the same amplification as the signal, whereas noise generated elsewhere further along the chain is usually much smaller than the signal. Therefore, preamplifier and particularly its input stage, besides the detector are the main elements for noise analysis excercise.
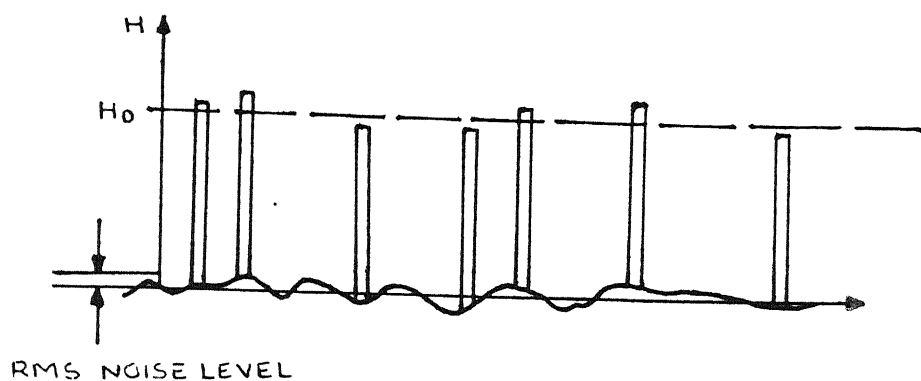
FIG. 3.19(a) SIGNAL PULSES OF CONSTANT AMPLITUDE SUPERIMPOSED ON A NOISY BASELINE
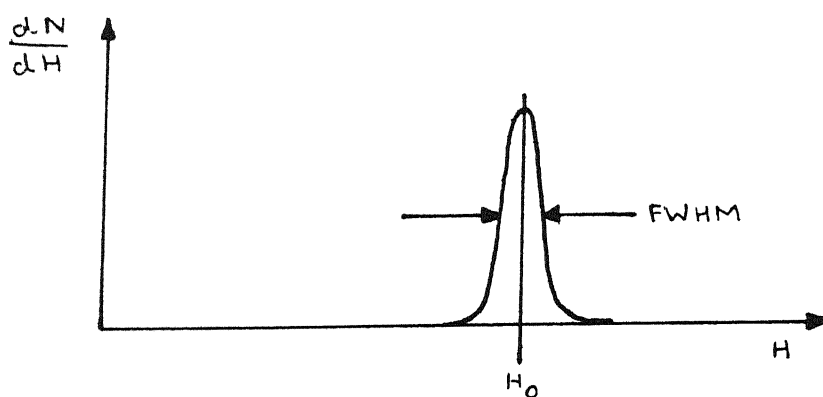
FIG. 3.19(b) BROADENED PEAK RECORDED IN PULSE HEIGHT SPECTRUM

Noise sources can be categorized conveniently into two classes: one, consisting of those that are effectively in parallel with the input and the other, comprising of those sources that are in series with the signal source. Sources of parallel noise comprise of detector leakage current fluctuations, and the fluctuations in the current drawn by the input stage of the preamplifier. Sources of series noise include the thermal noise in the field effect transistor (FET) of the preamplifier input. For analytical purposes, it is often assumed that a "white" noise or uniform distribution in frequency can represent their cumulative effect.

By contrast, the frequency spectrum of the signal is confined to a much narrower band. Therefore, waveshaping role assigned to the amplifier actually achieves selective filtering to remove as much broad spectrum noise as possible without severely attenuating the useful signal components. Waveshaping(i.e. pulse shaping) may be viewed as a combination of differentiating and integrating circuits but can be equivalently understood as high-pass and low-pass fitering respectively.

It has been shown in literature [4,20,22,23] that the best signal-to-noise ratio is achieved if the signal pulses are shaped to the form an infinite cusp as indicated in Fig 3.20. In practice a pulse has finite width and therefore the finite cusp has the best signal to noise properties if pulses of finite width are compared. It has also been established that no pulse shaping
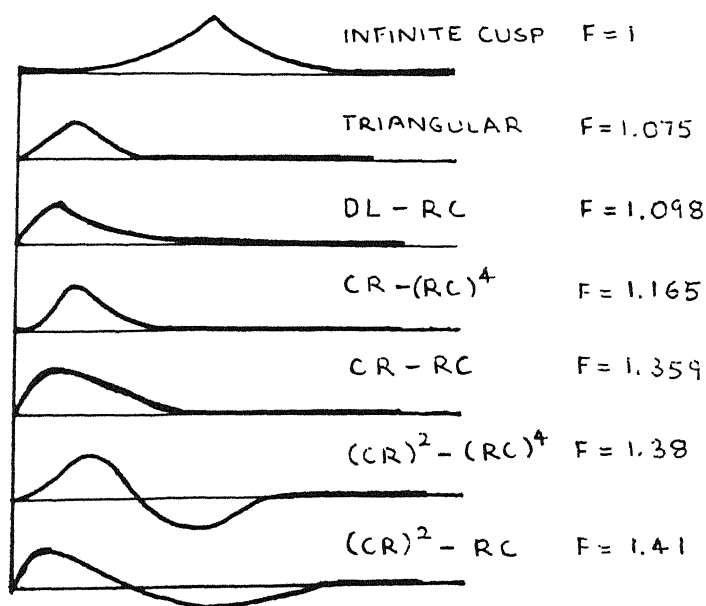
FIG. 3.20 VARIOUS PULSE SHAPES AND THEIR NOISE-TO-
SIGNAL RATIO F RELATIVE TO THE
INFINITE CUSP.
VARIOUS TIME CONSTANTS ARE CHOSEN TO
YIELD MINIMUM NOISE, AND PULSE SHAPES
ARE NORMALIZED TO CONSTANT HEIGHT.

can yield a pulse shape that can be superior to the cusp in its signal-to-noise properties. Hence this pulse shape has become a standard basis for judging the performance of several pulse shaping circuits.

The extent of noise injected into the preamplifier-amplifier combination is often expressed in terms of an equivalent noise charge (ENC). This is defined as the amount of charge, which if applied suddenly to the input terminals of the system, would give rise to an output voltage equal to the root mean square level of the output due only to noise, in absence of any incidence of radiation. For specific types of detectors, the ENC can sometimes be translated into the equivalent energy deposition by a charged particle in the detector.

If $\overline{v}_{rms}$ is the root mean square noise voltage observed at detector output and preamplifier input then it can be viewed as equivalent noise charge $\overline{q}$ which was collected and deposited on the capacitance C_T at detector. i.e.,

$$\overline{v}_{rms} = \frac{\overline{q}}{C_T} \qquad \qquad \ldots 3.42$$

Now $\overline{q}$ is the equivalent charge collected would

correspond to an energy $\overline{\sigma}_E$ so that

$$e\frac{\sigma_E}{\omega} = \overline{q} \qquad \qquad \ldots 3.43$$

ω = energy necessary to liberate one hole-electron pair.

$$\sigma_E = \frac{\omega}{e} \overline{q} = \frac{\omega}{e} C_T \overline{v}_{rms} \qquad \qquad \ldots 3.44$$

$$\text{or} \quad (FWHM)_{noise} = 2.35 \frac{W}{e} C_T \bar{v}_{rms} \qquad \ldots 3.45$$

3.6.7. Equivalent Input Circuit For Noise Analysis:

The equivalent input circuit for studying the energy resolution capabilities of the system is shown in Fig.(3.21). The various noise and signal elements are as follows.

(a) Input charge signal Q: It is usually assumed to be due to a pulse of current of very short duration compared with the time constants involved in the system.

(b) Detector Leakage Current Noise $(i_N)_D$: It is assumed to be pure shot noise which implies that it consists of individual holes and electrons crossing the depletion layer with no interaction occuring between individual carriers. It arises due to thermal generation of electron-hole pairs in the depletion layer. The mean square value of current fluctuations in a leakage current of this nature is given by

$$\bar{i}^2 = 2 q i df \qquad \ldots 3.46$$

where df is the frequency interval in which noise is measured.

(c) Detector series resistance noise $(e_n)_{R_s}$: It is due to the resistance in the connections to the sensitive volume of the detector. Generally it is negligible. This allows simplification of the equivalent circuit by

DETECTOR
SUPPLY VOLTAGE
+
LOAD
R_L

PREAMPLIFIER

C_c

MAIN AMPLIFIER

FREQUENCY
SENSITIVE
FILTER (SHAPER)

TO
PULSE-
HEIGHT
ANALYZER

N

DEPLETED

P

BLOCK DIAGRAM
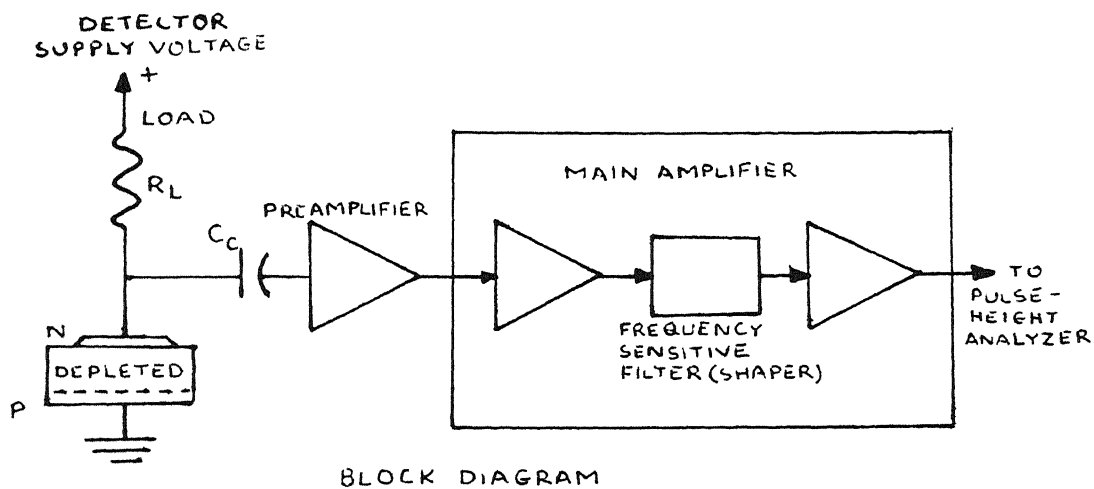
FIG. 3.21(a) TYPICAL ELECTRONICS FOR SPECTROSCOPY

C_F

SIGNAL
$\Omega + \frac{Q}{C_F}$

$(i_N)_D$

VOLTAGE GAIN
−A

SIGNAL
Q

C_D

C_{IN}

R_S $(e_n)_{R_S}$

R_{eq} $(e_n)_{R_{eq}}$ OUTPUT

R_L

$(e_n)_{R_L}$

$(i_N)_G$
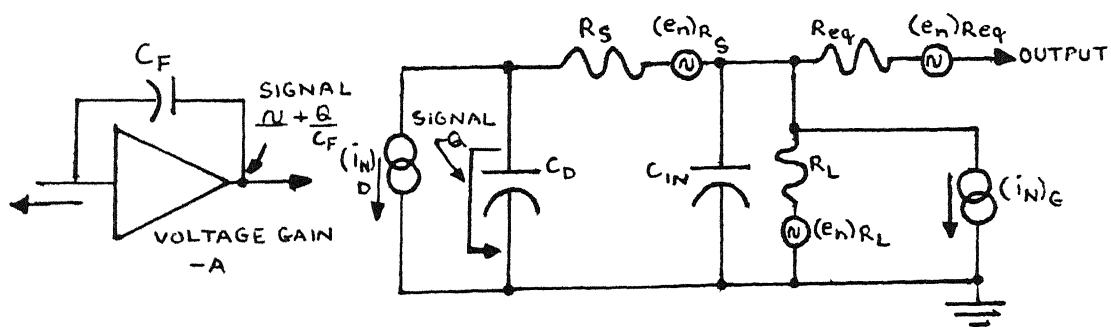
FIG. 3.21(b) EQUIVALENT INPUT CIRCUIT SHOWING
NOISE GENERATORS

considering the detector capacitance C_D to be in parallel with the input capacitance C_{IN} of the preamplifier and replace (C_D+C_{In}) by C_T.

(d) **Input current noise $(i_N)_G$:** It is due to fluctuations in the input current to the first amplifying device i.e., the FET preamplifier. These fluctuations in the current behave like those in detector leakage current.

(e) **Parallel resistance noise $(e_n)_{R_L}$:** This arises from resistors shunting the input circuit. This includes the detector load, any input biasing resistor in the first stage and any resistor included across C_F in a charge sensitive preamplifier. In practice very large values are used for these resistors and one can regard the voltage source $(e_n)_{R_L}$ in series with the large resistor R_L as a current source which must also be included in the value of the current generator $\overline{i}^2$ indicated above. The increase in $\overline{i}^2$ due to this is $4(KT/R_L)df$. For this to be negligible, it is necessary that $R_L \gg 2KT/qi$. If say $i=10^{-7}$Amps, $R_L \gg 5X10^5$ ohms meet this requirement.

(f) **Voltage Noise Source $(e_n)_{R_{eq}}$:** This noise produced by the first amplifying device This source of noise can be represented by Johnson noise in a resistor and has the value

$$\overline{e}_n^2 = 4\ KT\ R_{eq}df$$

... 3.47

The input circuit can be simplified for practical purposes to the one given in Fig.3.22a. This can be further simplified to contain only voltage generators as shown in Fig.3.22b.

Now the effect of amplifier frequency response upon the relative values of signal and noise at the amplifier output is considered next..

3.6.8. Noise Filtering Action of Waveshaping Amplifier Networks:

Besides boosting the signal strength to requisite level for finally actuating the data recording system(MCA), the noise and the signal are subjected to the frequency dependent transfer function of the waveshaping amplifier networks. In allowing only a certain band of frequencies through, the shaping network does minimize noise output power but also reduces the output signal. Therefore, the frequency selective characteristics have to be optimized and the optimum network will have to depend upon the relative values of the voltage noise components shown in Fig.3.22b. Examination of the noise generators indicates the following observations:

(a) Noise due to input current is predominantly low frequency noise.

(b) Shot noise input element is more important at high frequencies

(c) Flicker noise falls between these extremes.

To determine the actual contributions due to each of these terms, the effect over the full frequency response of amplifier must be evaluated.

$$\overline{e_n^2} = 4kTReq\,\Delta f \qquad \overline{e_F^2} = \frac{A}{f}\,\Delta f$$

$$\overline{i^2} = 2qi\,\Delta f$$

C_T

Q

(a)

$$\overline{e_i^2} = \frac{qi\,\Delta f}{2\pi^2 f^2 C_T^2} \qquad \overline{e_n^2} = 4kTReq\,\Delta f \qquad \overline{e_F^2} = \frac{A}{f}\,\Delta f$$

Q/C_T

C_T
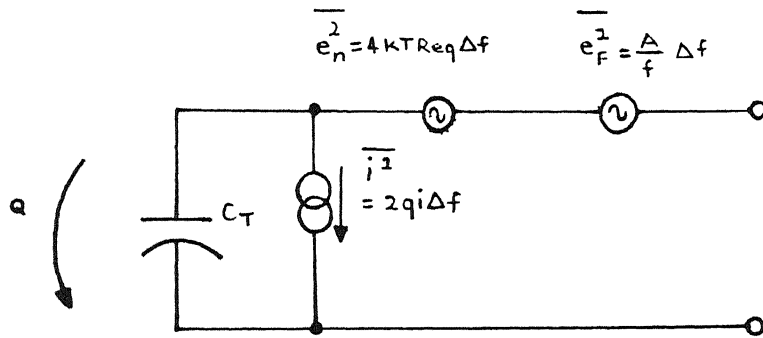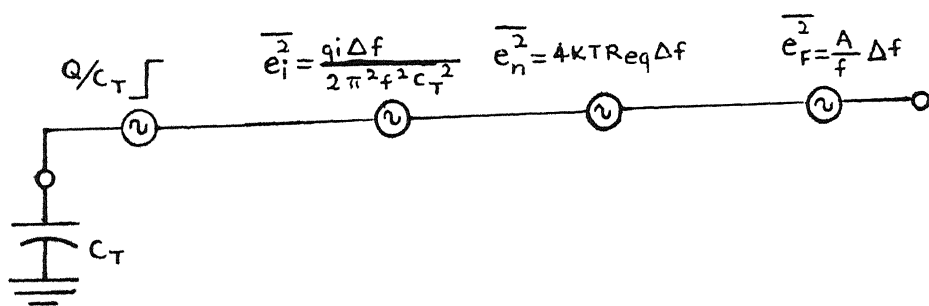
(b)

FIG. 3.22 SIMPLIFIED INPUT EQUIVALENT CIRCUITS

Let F(f)=frequency response of amplifier. Then the three contributions to output noise are

(a) Input Current Noise $\overline{E}_I^2 = \dfrac{qi}{2\pi^2 C^2} \displaystyle\int_0^\alpha \dfrac{[F(f)^2]}{f} df \quad - - \qquad \ldots 3.48$

(b) Shot Noise : $\overline{E}_N^2 = 4KTR_{eq} \displaystyle\int_0^\alpha [F(f)^2] df \qquad \ldots 3.49$

(c) Flicker Noise : $\overline{E}_F^2 = \dfrac{qi}{2\pi^2 C^2} \displaystyle\int_0^\alpha \dfrac{[F(f)^2]}{f^2} df \quad - - - \qquad \ldots 3.50$

Typical frequency selective networks are used to evaluate these integrators . In general the complete network will consist of at least one low-pass network (e.g.RC integrator) to reduce the shot noise, which would otherwise rapidly increase with frequency and at least one high-pass network (e.g. RC differentiator) which serves to reduce low frequency noise due to input circuit currents.

Goulding [20,22] has carried out analysis on a number of networks for the noise power indicated as above. The results are expressed as equivalent input signals quoted in ion-pairs or hole-electron pairs. The results are

(a) Shot Noise:

$$\overline{E}_N^2 = 2.08 \ T \ (R_{eq} C_T^2) f_o [I_1/P^2] X 10^{15} (\text{ion pairs})^2 \qquad \ldots 3.51$$

(2) Flicker Noise

$$\overline{E_F^2} = 3.9 \ (AC_T^2)(I_2/P^2)\text{X}10^{37}(\text{ion pairs})^2 \qquad \ldots 3.52$$

(c) Input Current Noise

$$\overline{E_I^2} = 3.15 \ i \ (1/f_o)(I_3/P^2)\text{X}10^{17}(\text{ion pairs})^2 \qquad \ldots 3.53$$

where I_1, I_2, I_3 are values of integrals whose numerical values are given in Table 3.3 for various networks.

P = output peak pulse height for unity amplitude for the network

f_o = $1/2\pi\tau_o$ and τ_o = time constant of a RC network given in Table 3.3

T = Absolute Temperature

A = Flicker effect Noise constant (usually about 10^{-13})

i = Detector leakage current.

The dependence of noise on the input circuit and on the input amplifying element is contained in the first terms in parenthesis. The equivalent shot noise squared and flicker noise squared are each proportional to the total input capacity squared. On the other hand, the equivalent input current noise squared is independent of the capacity. The nature or type of frequency dependence of the three types of noise is shown in the terms containing f_o.

3.7 SUMMARY OF THE MAIN PARAMETERS AFFECTING PERFORMANCE CHARACTERISTICS OF A SEMICONDUCTOR DETECTOR

(A) Sensitive Area: This parameters affects both sensitivity and signal resolution. A smaller detector gives much better resolution. Selecting the right detector area requires a compromise between sensitivity and resolution.

(B) Sensitive Depth: For energy spectroscopy the sensitive depth must be sufficient to completely absorb all the particle energy. If the sensitive depth increases, the capacitance will decrease and so will be the noise of preamplifier. But sensitive volume increase will increase the current and therefore the noise of detector will also increase.

(C) Capacitance : The major effect of detector capacitance is its influence on the noise contribution and rise time. It is necessary to minimize the capacitance by restricting the active area or optimizing the sensitive depth. If S is area and W is the thickness then the Capacitance of the Detector is given by

$$C(pF) \cong 1.05 \ S(cm^2)/W(cm)$$

(D) Reverse Current : 3 main components

      ____ saturation current (due to minority carriers)

      ____ Generation current (due to impurities)

      ____ Surface leakage current

(E) Detector Noise : Noise source in the detector and the preamplifier introduce a dispersion that broadens the pulse height spectrum.

(F) **Energy Resolution** : Noise factors such as statistical effects incomplete charge collection causes additional broadening of the peak.

(G) **Window** : The layer of P-N junction constitutes a window which must be crossed by the particles before they reach the depletion layer. Window thickness is equal to dead layer.

(H) **Rise Time** : The measurement of time intervals is important in basic nuclear physics (decay scheme, lifetime studies etc.,). The rise time of the pulse generated by a semiconductor detector is mainly determined by charge collection time(nano seconds for Silicon detectors).

TABLE 3.2

EQUATIONS GOVERNING CHARGE TRANSPORT IN REVERSE-BIASED P-N SEMICONDUCTOR ABRUPT JUNCTIONS (ONE DIMENSION & PLANAR)

PARAMETER	P-REGION	N-REGION
1.* DEPTH OF TRANSITION REGION	d_p	d_n
2.* DOPANT CONCENTRATION	N_A=Number of acceptor atoms per unit volume	N_D=Number of Donor atoms per unit volume
3.* MOBILITY a)ELECTRON b)HOLE	μ_e μ_p	μ_e μ_p
4.* DIELECTRIC RELAXATION TIME *due to majority of carriers*	τ_p	τ_n
5. Maximum Magnitude of Electric Field *(occurs at x=0 i.e the abrupt junction)* ϵ = Dielectric Constant ; e = Electronic Charge	$\lvert E_{max} \rvert = d_p/\mu_p \tau_p$ $= eN_A d_p/\epsilon$	$\lvert E_{max} \rvert = d_p/\mu_n \tau_n$ $= eN_D d_n/\epsilon$
6. Spatial Profile Of Electric Field	$E(x) = E_{max}(1 - \dfrac{x}{d_p})$ for $0 \le x \le d_p$	$E_{max}(1 - \dfrac{x}{d_n})$ for $0 \le x \le d_n$
7.* INSTANTANEOUS POSITION a)Hole b)Electron	$x_{hp}(t)$ $x_{ep}(t)$	$x_{hn}(t)$ $x_{en}(t)$
8.* INITIAL POSITION OF OF HOLE/ELECTRON *at t =0 on Ionization*	$x_{hp}(0)=x_{ep}(0)=x_o$ for $0 \le x \le d_p$	$x_{hn}(0)=x_{en}(0)=x_o$ for $0 \le x_o \le d_n$

TABLE 3.2   (Continued)

9. INSTANTANEOUS POSITION AS FUNCTION OF TIME	$x_{hp}(t)$	$x_{hn}(t)$
a) HOLE	$=d_p-(d_p-x_o)\exp(-t/\tau_p)$	$=d_n-(d_n-x_o)\exp(\dfrac{\mu_p t}{\mu_e \tau_n})$
b) ELECTRON	$x_{ep}(t)$	$x_{en}(t)$
	$=d_p-(d_p-x_o)\exp(\dfrac{\mu_e t}{\mu_p \tau_p})$	$=d_n-(d_n-x_o)\exp(-t/\tau_n)$

10.* FINAL ARRIVAL TIME INSTANT		
a) HOLE	t_{fhp}	t_{fhn}
b) ELECTRON	t_{fep}	t_{fen}

11. DESTINATION POSITION ON COLLECTION		
a) HOLE	$x_{hp}(t_{fhp})=d_p$	$x_{hn}(t_{fhn})=0$
b) ELECTRON	$x_{ep}(t_{fep})=0$.	$x_{en}(t_{fen})=d_n$

12. DESTINATION TRAVERSED UNTIL COLLECTION		
a) HOLE	d_p-x_o	x_o
b) ELECTRON	x_o	d_n-x_o

13. COLLECTION OR MIGRATION TIME		
a) HOLE	INFINITE	$\dfrac{\mu_e \tau_n}{\mu_p}\ln[d_n/(d_n-x_o)]$
b) ELECTRON	$\dfrac{\mu_p \tau_p}{\mu_e}\ln[d_p/(d_p-x_o)]$	INFINITE

<div align="center">

TABLE 3.3

Noise integral and peak response of several networks

</div>

Network description		Peak output (P) (unity input)	I_1	P^2/I_1	I_2	P^2/I_2	I_3	P^2/I_3
1. RC integ + RC diff	(τ_0) (τ_0)	0.365	0.784	0.172	0.500	0.270	0.785	0.172
2. Two RC integ + RC diff	(τ_0) (τ_0)	0.271	0.196	0.372	0.250	0.292	0.589	0.124
3. Three RC integ + RC diff	$(\frac{1}{3}\tau_0)$ (τ_0)	0.356	0.407	0.310	0.421	0.300	0.771	0.163
4. RC integ two RC integ RC diff	(τ_0) $(\frac{1}{2}\tau_0)$ (τ_0)	0.295	0.233	0.373	0.373	0.290	0.640	0.136
5. RC integ DL diff	(τ_0) (τ_0)	0.628	1.98	0.200	1.05	0.376	1.16	0.341
6. Two RC integ DL diff	$(\frac{1}{2}\tau_0)$ (τ_0)	0.631	1.87	0.214	1.20	0.333	1.32	0.303
7. RC integ two RC integ DL diff	(τ_0) $(\frac{1}{2}\tau_0)$	0.388	0.494	0.303	0.481	0.312	0.823	0.182
8. Two FB integ two DL diff two DL diff	(τ_0) (τ_0) $(2\tau_0)$	1.000	4.19	0.239	3.61	0.277	4.82	0.208
9. RC integ DL diff	$(0.4\,\tau_0)$ $(1.6\,\tau_0)$	0.981	7.70	0.125	3.77	0.254	3.79	0.253
10. RC integ two DL diff	$(0.4\,\tau_0)$ $(1.6\,\tau_0)$	0.981	23.0	0.042	9.82	0.098	6.37	0.151

4 SIMULATION PACKAGE DESIGN AND DEVELOPMENT

In this chapter, the steps involved in the design and development of a software package for computer simulation of the nuclear detector and its ancilliary electronics are reported.

This presentation begins with a discussion of the rationale underlying the strategy adopted in the package construction. Next the requisite mathematical expressions are identified. Also cognizance is made of the appropriate random processes involved in the nuclear detector behaviour. These tools are then consolidated into the software development in conformity with the strategy. Programs that allow testing and visualization of spectra for evaluation are also included as adjuncts to the main functional segments of the package. FORTRAN 77 has been adopted as the vehicular high-level language for this software development.

4.1 STRATEGY OF APPROACH

In order that the computer simulation model may mimic the actual process of nuclear detection and signal generation with a high degree of fidelity, it seemed logical to review the architectural configuration of a real-life' nuclear spectrometer and look for clues and analogies needed in formulation of the

software specifications. Fig.4.1 depicts schematically the configurations of two routinely used nuclear spectrometers:

(i) Energy Spectroscopy System

(ii) Time Spectroscopy System

The energy spectroscopy system involves a single path for flow of signal generation and processing. The time spectroscopy system involves two such paths in parallel, which work simultaneously in time. Since simulation of time spectroscopy system would require the feature of two independent processing activities, it has not been pursued further in the present context. Instead, the energy spectroscopy system has been adopted for consideration because its characteristic feature of a single path for sequential signal flow makes it more feasible for simulation studies and software development than the time spectroscopy counterpart. This choice was also motivated by the fact that since the scope of the current thesis is of an exploratory nature, an experience in a more tractable case is necessary to be acquired first.

Accordingly a simplified block diagram of the energy spectrometer is presented in fig.4.2. The purpose of such an analysis is to identify the functions involved in the operation of such an instrument and the functional blocks that constitute it. In a corresponding simulation model, the same functions would have to be duplicated by specific routines. The strategy here has been to identify the functions in the actual spectrometer and associate an analogous program 'module' with each function in

a. ENERGY SPECTROSCOPY SYSTEM

b. TIME SPECTROSCOPY SYSTEM
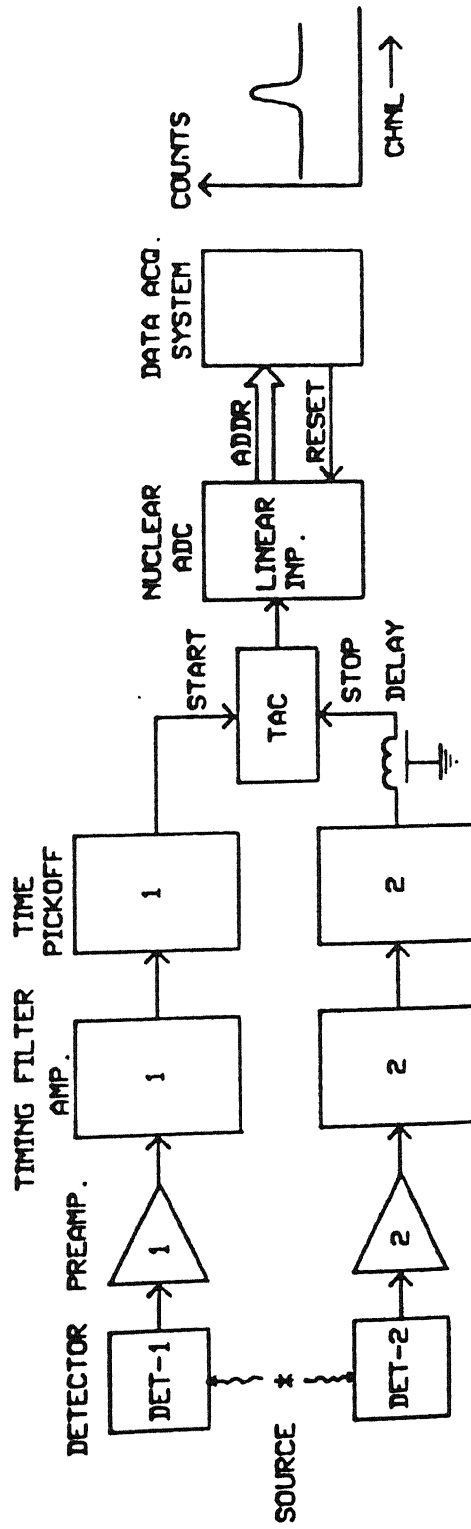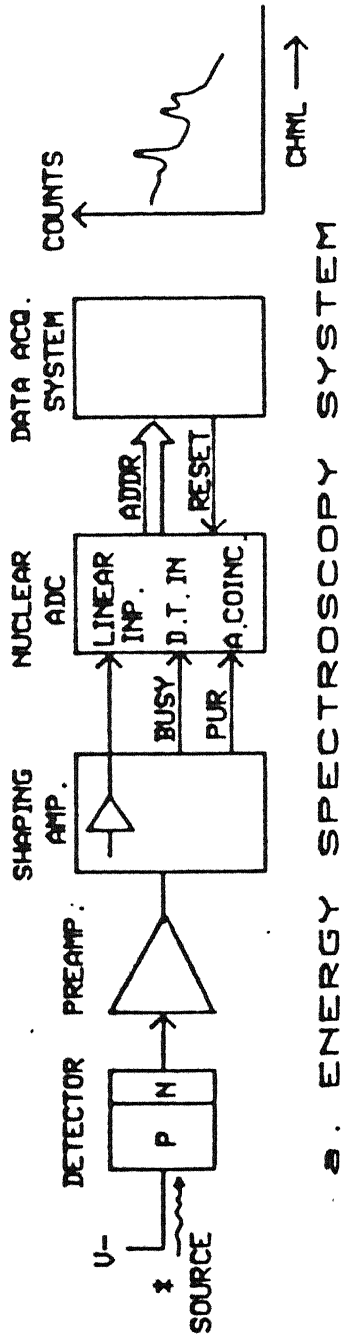
FIG.4.1 TYPICAL NUCLEAR SPECTROMETERS
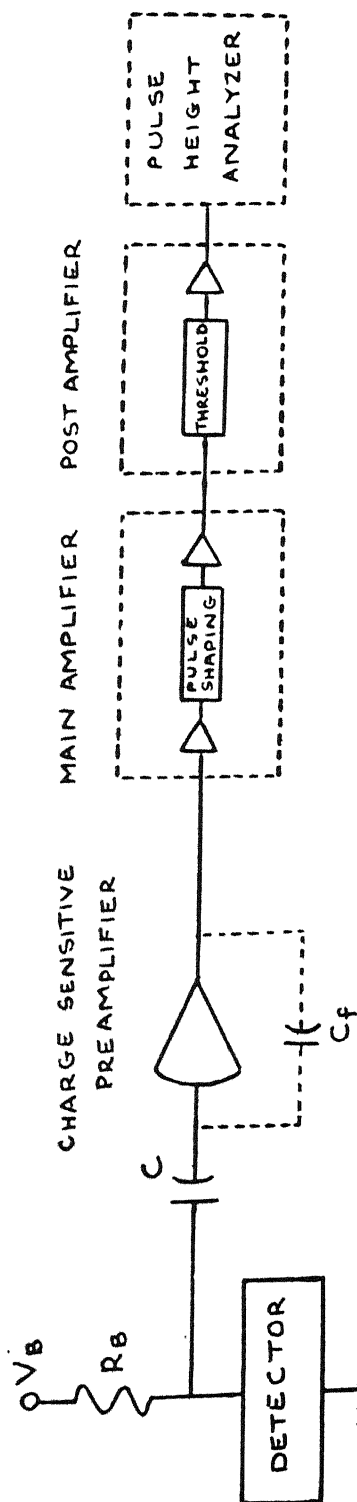
FIG. 4.2 SIMPLIFIED BLOCK DIAGRAM OF ENERGY SPECTROMETER
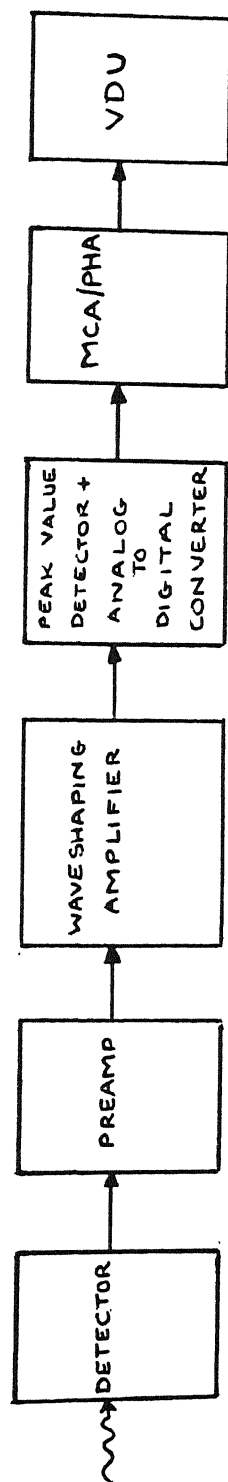
FIG. 4.3 FUNCTIONAL BLOCK DIAGRAM OF SPECTROMETER CONFIGURATION

hardware on a one-to-one correspondence basis. Experimenters in nuclear laboratories are accustomed to using instrumentaion modules as universal blocks in their experimental apparatuses which they freely insert/remove by wiring and patching to setup various configurations for different experiments. Likewise program modules, if so created on a functional basis, are such software entities that can be used flexibly to configure or reconfigure different experiments for simulation. As a result of this strategy, the following considerations emerged.

(1) Identification of functions in hardware of the instrumentation configuration.

(2) Input-Output specifications of various functional modules in hardware.

(3) Formulation of input-output specifications of corresponding functional modules in software. These modules are essentially subroutines or software function.

(4) Heirarchy in configuration of software modules. Certain modules can be connected only as inputs to other modules and no other.

4.1.1. Program Module Identification.

The following functional software modules were identified on the basis of a hardware-software equivalence (Fig 4.3). The functionality is considered by proceeding along the signal chain backwards from the data-acquisition system towards the detector and a one-to-one correspondence is evolved.

(1) Multichannel Analyzer (MCA)

This is a hardware module which stores cumulative counts in its memory for different channel numbers. The range of these channel numbers is adjustable depending upon user's choice of resolution. On encountering a command from the Analog to Digital Converter(ADC), it retrieves the channel number from the ADC itself, interprets it as address, reads form its memory the contents of this location, adds one to the number, writes it back as incremented count at the same location in the memory.

Similarly the 'read-add one -write ' is implemented in an equivalent software module MCANL. Essentially this is a histogram generating program but is tailored to correspond to the hardware MCA. It operates on a predefined one dimensional matrix of fixed size corresponding to the range of channels(in hardware MCA, this range is selectable from among 128, 256, 512, 1024, 2048, 4096 and 8192 channels). As the matrix is indexed, the index corresponds to channel numbers and the variable referred to by the matrix represents counts as contents at the location specified by this index. So whenever any index number within the span or range of matrix dimensions is specified the corresponding contents as counts is incremented by one.

(2) Visual Display Unit(VDU)

In case of MCA, the spectrum can be visually displayed simultaneously as it works in real-time on an appropriately provided display unit which essentially is x-y plotter. The

channel number goes to the x-axis display circuit and counts to the y-axis display circuit.

However, here the software graph plotting routine can display the histogram plot in only 'off-line' modeof the MCANL routine. i.e. when histogram matrix is not being operated upon. The graph plotting routine, neverthless, corresponds to the visual display unit.

(3) Analog to Digital Converter(ADC).

The hardware version of ADC receives as input the signal from the amplifier and monitors the waveform for the peak. When the peak is encountered, its magnitude is sensed and converted to a unique integer which represent the channel number and is therefore the slot or bin number whose contents are to be handled by the MCA. Also the ADC monitors to see whether the magnitude of peak falls within the permitted range(selected by user as between two specified levels, the upper level and lower level) with the help of its internal upper level and lower level discriminators so as to consider it valid to be accepted by the MCA and rejected otherwise.

A peak detector routine and a sorter routine have been incoorporated in the corresponding software module. The peak detector routine continuously monitors the temporal profile coming as a sequence of discrete numerical values, from the simulated amplifier output routine and is able to detect the peak when all the incoming numbers have been scanned over a specified

software logic switch to determine whether it is within a window of permitted values. If found valid, it is scaled within this window by an integer mode operation on its magnitude so as to obtain the index number of the histogram matrix which is the software analog of the channel number.

(4) Waveshaping Amplifier

This functional unit interfaces with the preamplifier. Its output is a temporal waveform in response to excitation by the preamplifier. The amplifier provides both gain and frequency filtering action in the form of waveshaping. As there are several choices of waveshaping circuits possible, for the case of RC shapers, different time constants can be selected from the front panel.

Similarly a pulse processing software routine has been developed which can for a particular choice of circuit, accept different parameter values for various time constants. Gain is of course, a simple scalar multiplication. However, if the hardware pulse shaper circuit is changed then correspondingly, the complete software routine has to be substantial. In the current thesis, the most commonly used CR-RC differentiator-cum-integrator circuit has been represented for both equal and unequal time constants. The step response of this circuit, shown in Fig.4.4 as well as response to the particular preamplifier signal were theoretically derived in closed form leaving only parametric values for circuit time constants to be specified by user.
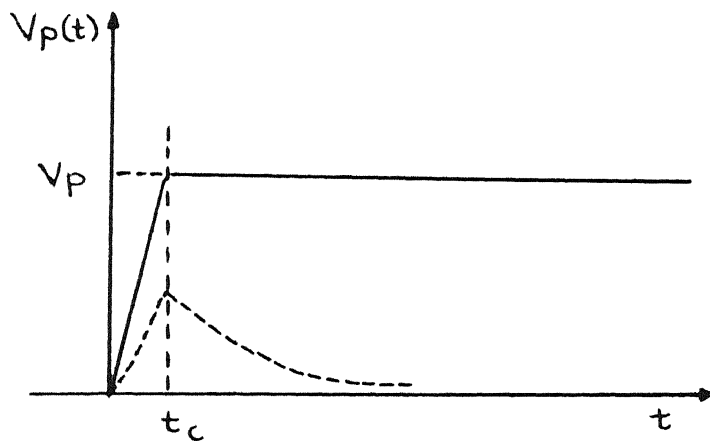
FIG. 4.4 (a) PREAMPLIFIER OUTPUT SIGNAL VOLTAGE
$V_P(t)$ WITH FLAT TOP. DASHED CURVE
DENOTES A TYPICAL RESPONSE PROFILE
OF CR - RC TYPE AMPLIFIER TO THE
PREAMPLIFIER SIGNAL
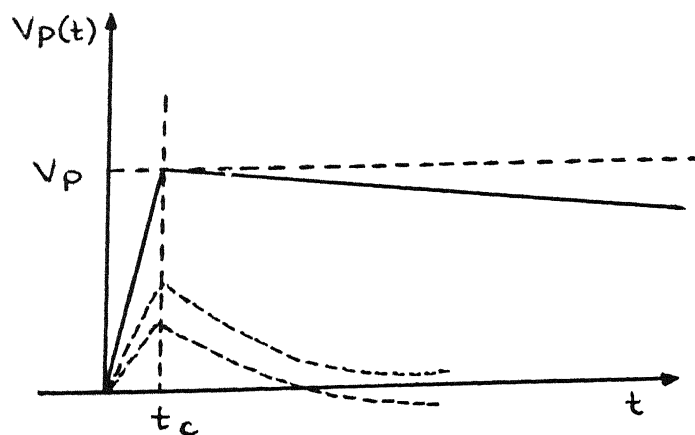
FIG. 4.4 (b) PREAMPLIFIER OUTPUT SIGNAL VOLTAGE
$V_P(t)$ WITH SLOW DECAY. DASHED CURVE
DENOTE TYPICAL RESPONSE PROFILES OF
CR-RC TYPE AMPLIFIER FOR TWO DIFFERENT
PAIRS OF TIME CONSTANTS T_1 AND T_2.

(5) Preamplifier

The preamplifier is an entity which is distinct from the detector and buffers it from the waveshaping amplifier. It responds to detector signal by following the rise time of the detector charge waveform due to collection. Once the peak value is reached, after collection time is over, there occurs on onset of exponential decay. Its peak voltage is proportional to charge value and inversely proportional to the composite detector capacitance of specified magnitude. Its decay profile is determined by a specified time constant.

Therefore its software counterpart is a piecewise waveform generator which provides a ramp for a duration equal to collection time and attains the height equal to the ratio of specified charge value specified by detector output and the specified capacitance. For the subsequent phase it provides an exponentially decaying profile of numerical values, based on the peak value and the decay time constant. Hence the software module receives values of charge and collection time, from the detector routine while the capacitance value and fall time constant values are specified by the user in advance.

(6) Detector

As a physical device, the detector converts the information of incident energy to a charge signal. Its own parameters, determine the magnitude and shape of the profile of this signal. Additional factors that are important from the stand point of simulation are:

(a) position of point of incidence with respect to electrodes- this determines collection times. Since ion pairs are created, there are two collection times, one for each charge carrier type. However, for simulation only the larger of the two values is adopted as the only value of collection time, because it predominantly determines the total collection time.

(b) Geometric dimensional & physical parameters such as material type, temparature of operation etc..

For the software counterpart, the detector is viewed as a series of computations on certain input values to provide as results, the quantities required by the preamplifier. The dimension of the active volume of the detector, and the ionization coefficient, are given as constants. The variable inputs are energy, and the point of incidence. These are statistically fluctuating inputs in the actual detector and so are implemented using random process generator algorithms.

4.2 OVERALL SIMULATION FLOW CHART

The various software modules were merged by suitable calling commands to pass requisite parameters. The overall simulation flow chart is shown in Fig.4.5

Two uniform random number generator routines (each labelled UPRNG), which are really Pseudo Random Number Generator routines as implemented on a computer, are used. One UPRNG determines x_o, the position of incidence of radiation with respect to D, the
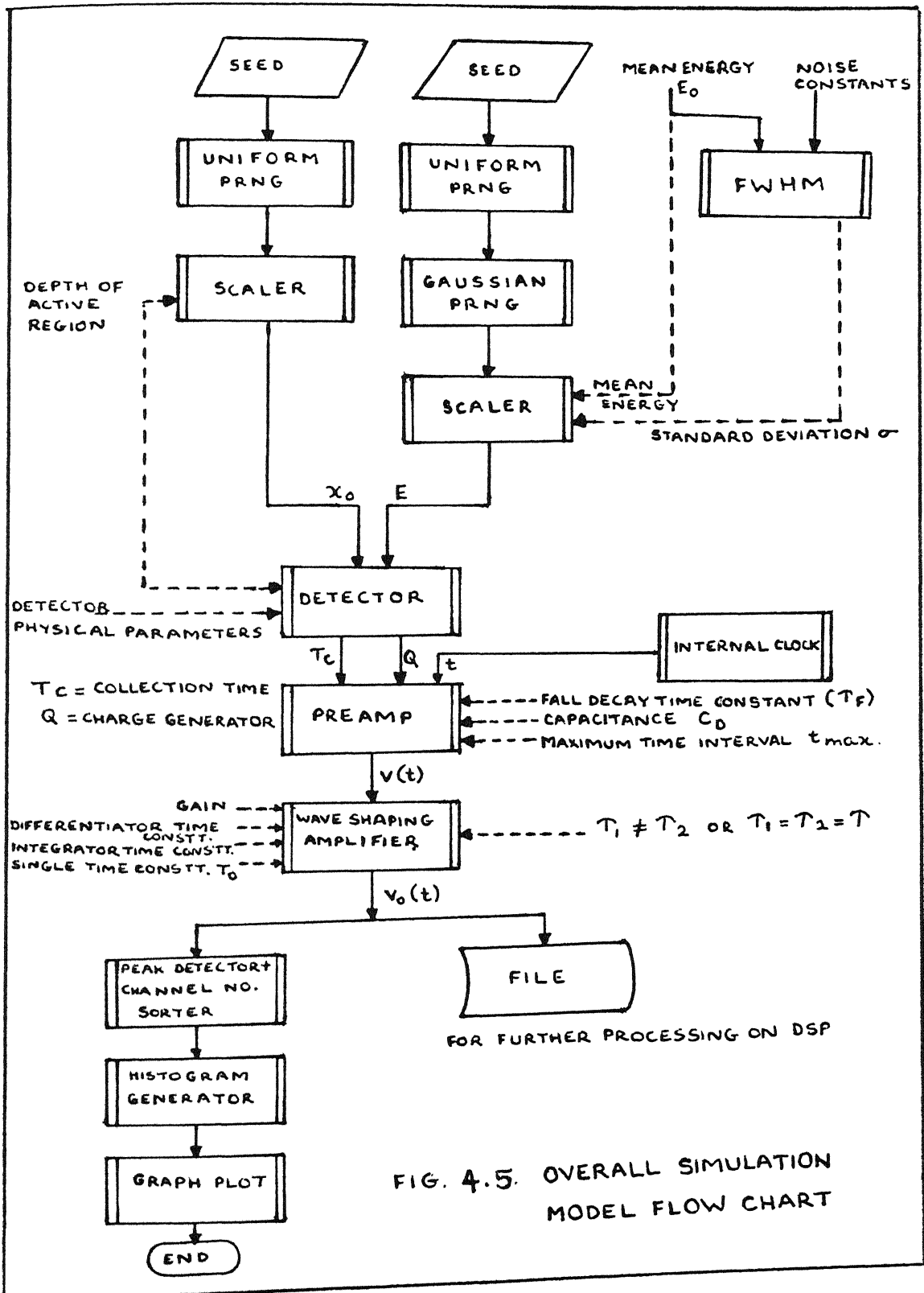
FIG. 4.5. OVERALL SIMULATION MODEL FLOW CHART

detector depth. Scalar routine effectively translates UPRNG output values, which lie between 0 and 1, to values between 0 and D. The other UPRNG is used as a set of seed values to the Gaussian Random Number Generator (GPRNG) routine. The GPRNG routine is used to simulate statistical fluctuations in energy of incidence. All causes of fluctuations can be represented as a lumped fluctuation referred to input after quadrature summation by the FWHM routine which computes the effective standard deviation. Statistical fluctuations inherent in ionization process and the Fano factor. F are already accounted for in the FWHM routine to define the minimum standard deviation. Since Gaussian PRNG generates numbers with statistical parameters of zero mean and unity standard deviation, the use of scalar routine attached to it translates the energy given by user as mean E_o into a different value in a distributed set of numbers having E_o as mean and the standard deviation as computed to produce the requisite FWHM if several simulation program runs with the same E_o are made. The modules are shown receiving parameters passed to them as inputs and delivering outputs. These inputs and output flow lines are shown as continuous lines, to signify passing of parameters during calls. The constants for each module are specified once by the user. The relevant constants are shown with symbols at the head of dashed lines touching module boxes at the sides for distinguishing these constants from proper variables.

The waveshaping amplifier output $v_o(t)$ is a sequence of numbers which can be routed to both a file for further processing by DSP algorithms as well as a histogram generator routine to obtain a locally generated spectral distribution which can be graphically plotted.

Since only one value of energy is used at a time it represents a monoenergetic incidence for a given detector type. Several runs for several counts can be performed iteratively. As a result over large runs, there will be variations in Energy values and also fluctuations in collection times. Consequently broadening of peak occurs in the spectral distribution at the histogram stage which thus corresponds to the simulated spectrum. The file storage of $v_o(t)$ provides a facility for this signal to be used as a simulated stimulus to DSP algorithms.

4.3   WAVESHAPING AMPLIFIER TRANSIENT RESPONSE EQUATIONS

The transient response of the waveshaping amplifier for CR-RC waveshaping amplifierwas derived to obtain a closed form representation for use in the simulator model. The circuit schematic is shown in Fig. 4.6. The two RC sections are buffered by an intermediate unity gain amplifier to provide isolation so that the differentiator and integrator time constants are as per expressions

$$\tau_1 = R_1 C_1$$
$$\text{and} \quad \tau_2 = R_2 C_2$$

4.1

4.2

Final gain is provided at the last stage as indicated by symbol G. Here G is assumed as unity without loss of generality.

The input stimulus is the preamplifier output(Fig. 4.4)

For $t < t_c$, $\qquad v_p(t) = \dfrac{V_p}{t_c} t$ $\qquad$ (4.1a)

For $t \geq t_c$ $\qquad v_p(t) = V_p\, e^{-(t-t_c)/\tau_F}$ $\qquad$ (4.1b)

where $v_p(t)$ = preamplifier signal voltage

$\qquad V_p$ = peak voltage

$\qquad t_c$ = collection time

Denote amplifier output by $v_o(t)$

The corresponding expressions are

<u>Case 1</u> $\qquad \tau_1 = \tau_2$

$\qquad$ For $t < t_c$: $\qquad v(t) = p(t)$ $\qquad$ 4.2(a)

$\qquad$ For $t \geq t_c$: $\qquad v(t) = p(t)+q(t)$ $\qquad$ 4.2(b)

where $p(t) = a_o + a_1 \exp(-\alpha_1 t) + a_2 \exp(-\alpha_2 t)$ $\qquad$ 4.3(a)

and for $x > 0$

$$q(t) = (V_p \theta)\left[b_o + b_F \exp(-\alpha_F x) + b_1 \exp(-\alpha_1 x) + b_2 \exp(-\alpha_2 x) \right] \quad 4.3(b)$$

where $x = t - t_c$ $\qquad$ 4.4

$\qquad\qquad\qquad\qquad\qquad\qquad\qquad\qquad\qquad\qquad$ 4.5

and $a_o = k/\alpha_1$

$\qquad a_1 = (k/\alpha_1)\left[\dfrac{\alpha_2}{\alpha_1 - \alpha_2}\right] = a_o\left(\dfrac{\alpha_2}{\alpha_1 - \alpha_2}\right)$ $\qquad$ 4.6

$$a_2 = - \left[\frac{k}{\alpha_1 - \alpha_2} \right] \qquad 4.7$$

$$b_o = - \frac{\alpha_c}{(\alpha_c + \alpha_F)\alpha_1\alpha_2} \qquad 4.8$$

$$b_F = \frac{\alpha_F}{(\alpha_F - \alpha_1)(\alpha_2 - \alpha_F)(\alpha_F + \alpha_c)} \qquad 4.9$$

$$b_1 = \frac{\alpha_{FC} - \alpha_1}{\alpha_1(\alpha_F - \alpha_1)(\alpha_2 - \alpha_1)} \qquad 4.10$$

$$b_2 = \frac{\alpha_{FC} - \alpha_2}{\alpha_2(\alpha_F - \alpha_2)(\alpha_1 - \alpha_2)} \qquad 4.11$$

$$k = V_p / t_c \qquad 4.12$$

$$\alpha_c = 1/t_c \qquad 4.13$$

$$\alpha_F = 1/\tau_F \qquad 4.14$$

$$\alpha_1 = 1/\tau_1 \qquad 4.15$$

$$\alpha_2 = 1/\tau_2 \qquad 4.16$$

$$\alpha_{FC} = \frac{\alpha_F \alpha_C}{\alpha_F + \alpha_C} \qquad 4.17$$

$$\theta = - \alpha_2(\alpha_C + \alpha_F) \qquad 4.18$$

Case 2: $\tau_1 = \tau_2 = \tau$ $\qquad$ 4.19

For $t < t_c$: $\qquad v_p(t) = p(t)$ $\qquad$ 4.20(a)

For $t > t_c$: $\qquad v_p(t) = p(t) + q(t)$ $\qquad$ 4.20(b)

where $p(t) = a_o + a_1 \exp(-\alpha t) + a_2 t \exp(-\alpha t)$

$\qquad = a_o + (a_1 + a_2 t) \exp(-\alpha t)$ $\qquad$ 4.21

and

for x > 0, $q(t) = V_p(b_0 + b_1 \exp(-\alpha_F x) + b_2 \exp(-\alpha x) + b_3 x \exp(-\alpha x)$

$$4.22$$

where $x = t - t_c$

$$4.23$$

$$k = V_p / t_c$$

$$4.24$$

$$\alpha_c = 1/\tau_c$$

$$4.25$$

$$\alpha_F = 1/\tau_F$$

$$4.26$$

$$\alpha = 1/\tau$$

$$4.27$$

$$\alpha_{FC} = \frac{\alpha_F + \alpha_c}{\alpha_F + \alpha_c}$$

$$4.28$$

$$a_0 = k/\alpha$$

$$4.29$$

$$a_1 = -(k/\alpha)$$

$$4.30$$

$$a_2 = -k$$

$$4.31$$

$$b_0 = -\alpha_c/\alpha$$

$$4.32$$

$$b_1 = -\frac{\alpha \alpha_F}{(\alpha - \alpha_F)^2}$$

$$4.33$$

$$b_2 = \frac{(\alpha^2 - \alpha_{FC}(2\alpha - \alpha_F))(\alpha_F + \alpha_c)}{\alpha(\alpha_F - \alpha)^2}$$

$$4.34$$

$$b_3 = \frac{(\alpha_2 + \alpha_F)(\alpha - \alpha_{FC})}{\alpha_F - \alpha}$$

$$4.35$$

4.4 GAUSSIAN RANDOM PROCESS GENERATOR

A rule is needed for picking a random number η from an infinite set of numbers having a Gaussian distribution for the probability of each number being selected. The selection is implemented as an arithmatic computation. The underlying principle is that if random numbers η with a nonuniform

distribution are required, with the probability density $f(\eta)$, then such numbers can be generated from an uniform distribution of random numbers ζ by equating the cumulative distributions[17,18].i.e.,

$$\int_{0}^{\zeta} 1.d\zeta = \int_{0}^{\eta} f(\eta)d\eta \qquad 4.36$$

$$\text{or} \qquad \zeta = \int_{0}^{\eta} f(\eta)d\eta \qquad 4.37$$

$$\text{where } f(\eta) = \frac{1}{\sigma(2\pi)^{1/2}} \exp\left[-(\eta - \mu)^2/(2\sigma^2) \right] \qquad 4.38$$

and

μ = mean in distribution of η values

σ = standard deviation in distribution of η values

Thus the procedure for generating the random number with Gaussian probability distribution function involves a selection of ζ from a uniform distribution between 0 and 1. This is followed by a substitution in eq 4.37 and solve for η to obtain the required Gaussian random number. The closed form solution for η is given by eq 4.39 below [23-26]

$$\eta = (3/n)^{1/2}\sigma \sum_{i=1}^{n} (2\zeta_i - 1) + \mu \qquad 4.39$$

where n is an arbitrarily chosen large positive integer.

This process depends upon the fact that the sum of several uniformly distributed random numbers is closed to Gaussian distribution.

4.5 Simulation Results: An Appraisal

The simulation software was used to simulate waveforms of a nuclear detector response as obtainable at the output of a CR-RC waveshaping amplifier stage following the composite detector and preamplifier subsystem. Various combinations of parametric values of differentiator (t1) and integrator (t2) time constants were chosen with a purpose to portray their effects on the shape and size of the temporal profiles of these waveforms. These waveforms, so simulated, are shown as plotted in Figs. 4.7.1 to 4.7.14. Here it was arranged to study these effects for the case of inputs having constant peak height and free from statistical perturbations. To facilitate a more precise scrutiny of these profiles, certain standard attributes, such as peak pulse amplitude (Vpk), instant of occurrence of peak (tpk), rise time (tr), delay time (td), fall time (tfall), and effective pulse width (tpw) were extracted, by suitable programs, from these simulated waveform data and have been tabulated in tables 4.1 to 4.14. On examining these tables, certain qualitative conclusions about the salient features have emerged and these are presented in table 4.15. This table also indicates the recommended range of combinations of t1 and t2 which enable meaningful data to be obtained. They can be broadly summarized as follows:

* For energy spectroscopy, it is necessary to have as little attenuation as possible and also it is desirable to have a linear or proportional relationship between peak pulse

amplitude and the input energy of incident radiation.

* The case of t1 < t2 is not at all suitable as it leads to suchy a severe attenuation that the output signal will be too feeble and inextricably swamped in noise for any meaningful measurement to be possible. Such is a situation is to be avoided.

* the case of t1 > t2 is generally favourable for energy spectroscopy experiments since attenuation is not serious and as long as t2 is constrained to be less than 1000 nsec, peak pulse height improves as t1 is increased. But this leads to a broadening of pulse shape and causes pile up errors especially at higher count rates with resultant loss of resolution. Since lowering t1 improves the temporal characteristics such as sharper rise and fall, a proper choice of t1 value can be empirically made for a suitable tradeoff between good energy resolution (pulse height-wise) and count rate (pile-up error-wise) provided t1 > t2 and t2 < 1000 nsec.

For the case of t1 = t2, it is observed that output peak height is alwlays (1/e) times input step height and so actual values of t1 (=t2) will have a more noticeable effect on the temporal attributes (rise-time, fall-time etc.) than on peak amplitude. These attributes are more significant in time-spectroscopy measurements where a sharp pulse fixes the time of occurrences of events more precisely.

Of course, in general, it would be desirable to have both a high peak amplitude and sharp pulse widths (small rise-time, fall-time and pulse-width) but here in simulation it is noticed that t1 has opposing effects on these two features, making tradeoff an inevitable reality.

Furthermore, it is observed that whereas step input stimulus (i.e. zero collection and infinite decay time) of the detector signal to the waveshaping amplifier is a simplistic representation, it does bring out the prominence of roles of t1 and t2 (as well as their relative values). Moreover, the introduction of nonzero collection times and decay times of increasing magnitudes in simulation runs reinforces the conclusion taht sluggish detector signals yield correspondingly sluggish waveshaper output responses which are also attenuated in height. This is attributable, evidently, to the fact that a waveshaping amplifier exhibits frequency dependent transfer characteristics since it is essentially a band-pass amplifier.

VOLTAGE VARIANCE

tf Infinite; tc = 0.0 s; t1<t2 ; t1= 1.000E-09s ; t2= 1.000E-08s ;

tf Infinite; tc = 0.0 s; t1<t2 ; t1= 1.000E-08s ; t2= 1.000E-07s ;

tf Infinite; tc = 0.0 s; t1<t2 ; t1= 1.000E-07s ; t2= 1.000E-06s ;

tf Infinite; tc = 0.0 s; t1<t2 ; t1= 1.000E-06s ; t2= 1.000E-05s ;

Time (nanoseconds)

Voltage Output
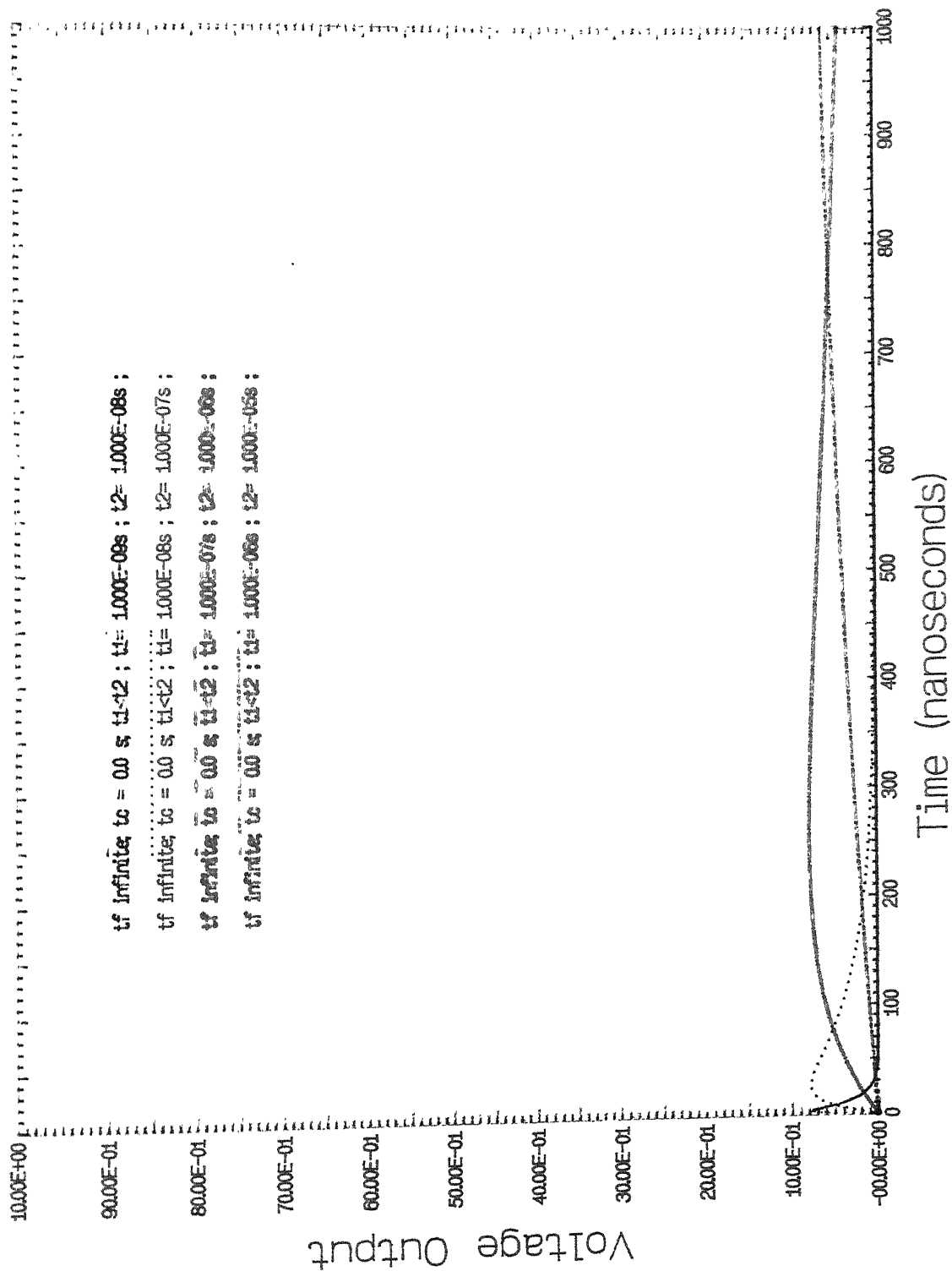
Figure 4.7. 1 : Step Response curves for (t1/t2)=0.1

VOLTAGE VARIANCE

tf infinite; to = 0.0 s; t1<t2 ; t1= 1.000E-09s ; t2= 1.000E-07s ;

tf infinite; to = 0.0 s; t1<t2 ; t1= 1.000E-08s ; t2= 1.000E-06s ;

tf infinite; to = 0.0 s; t1<t2 ; t1= 1.000E-07s ; t2= 1.000E-05s ;

tf infinite; to = 0.0 s; t1<t2 ; t1= 1.000E-06s ; t2= 1.000E-04s ;

Voltage Output

Time (nanoseconds)
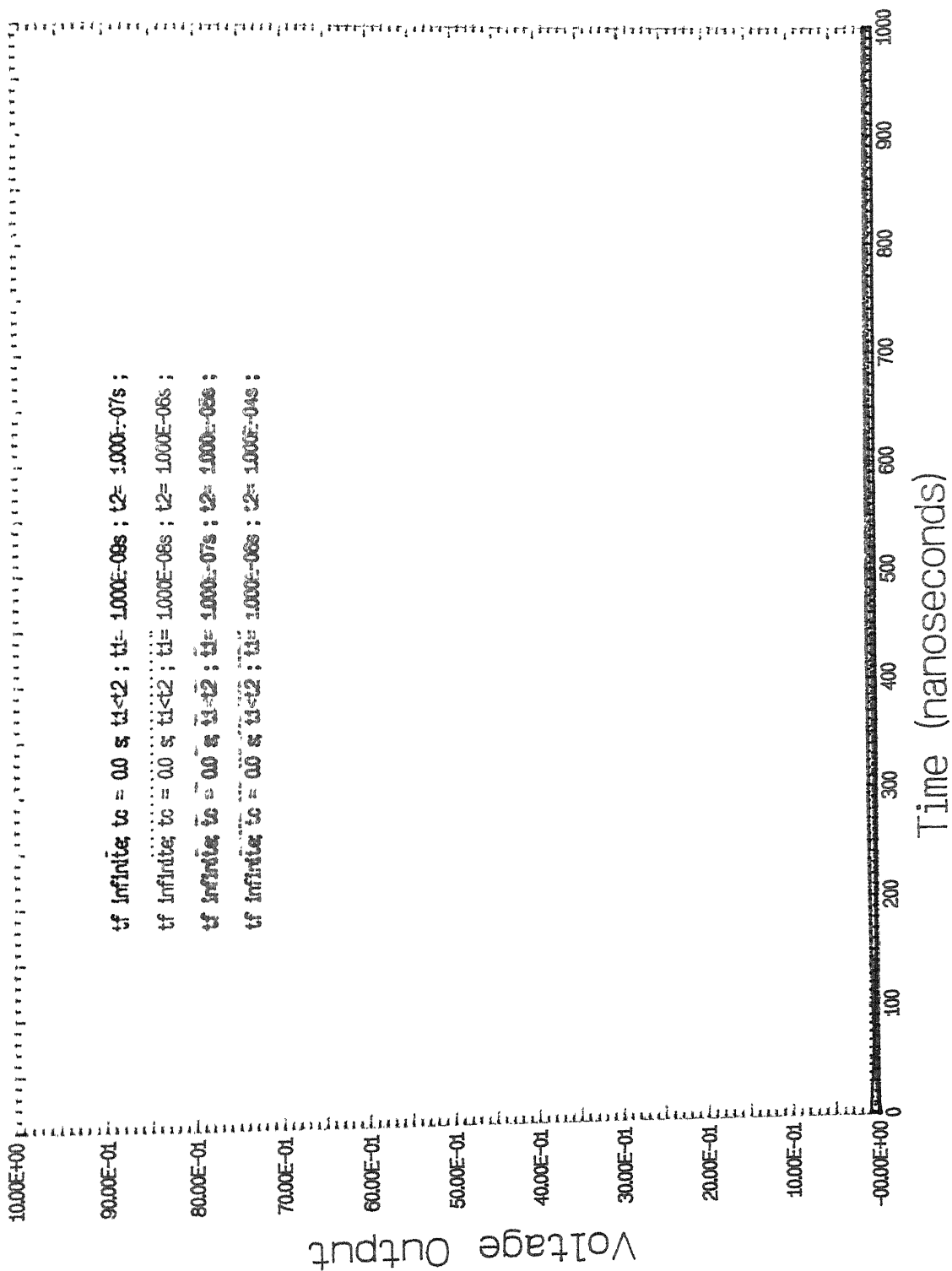
Figure 4.7. 2 : Step Response curves for (t1/t2)=.01
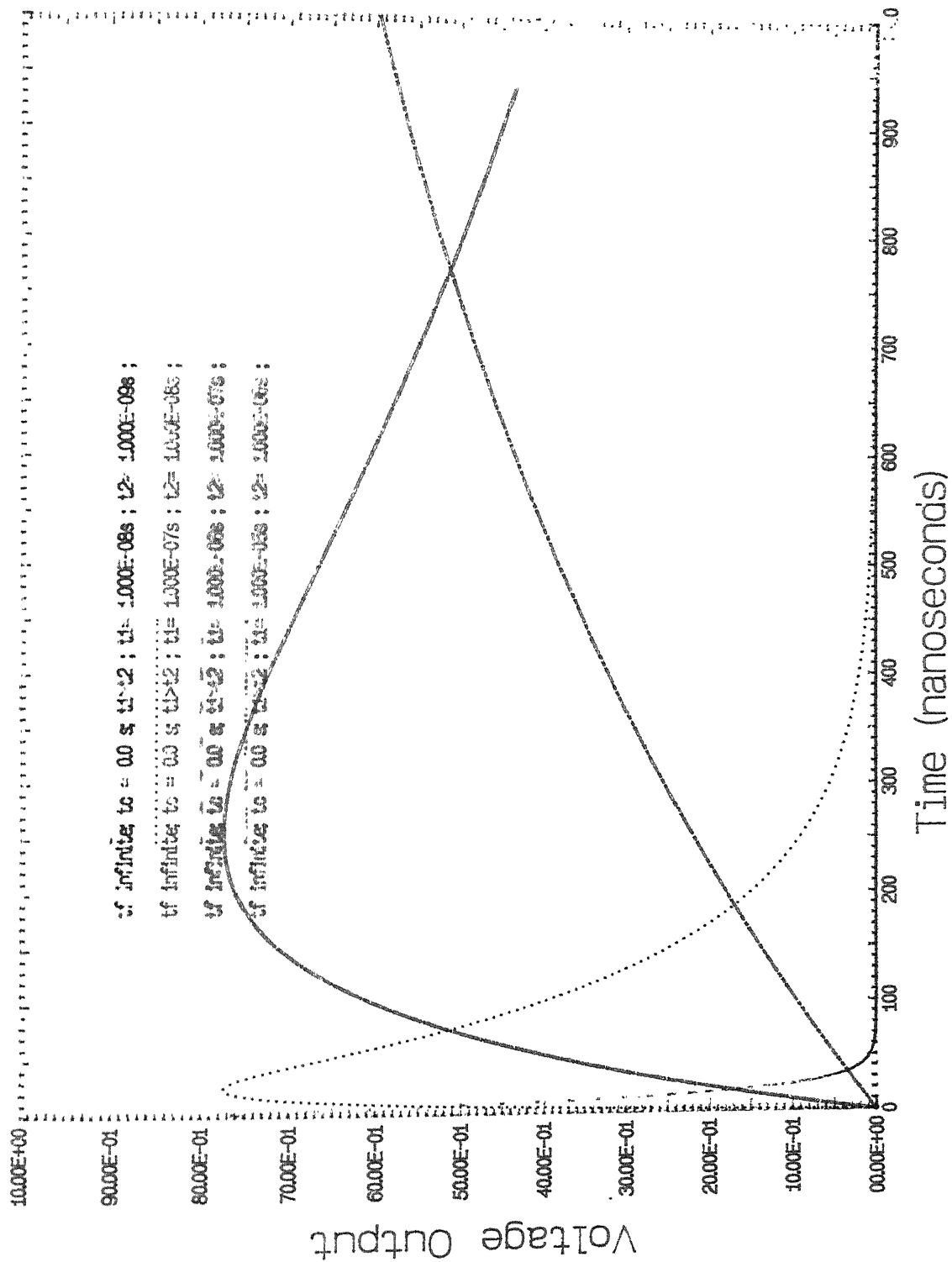
VOLTAGE VARIANCE

Figure 4.7. 3 : Step Response curves for (t1/t2=10)

VOLTAGE VARIANCE
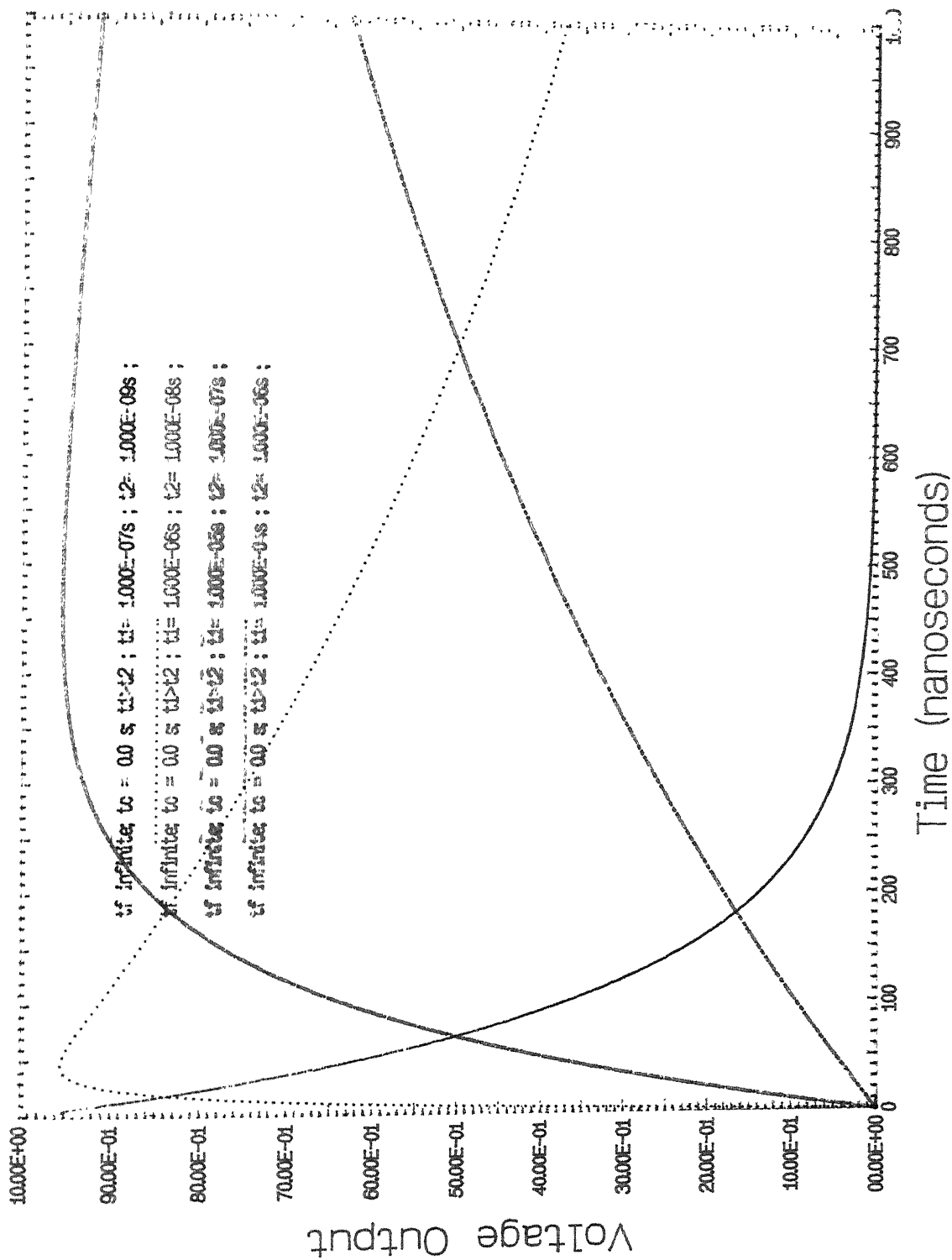
Figure 4.7. 4 : Step Response curves for (t1/t2)=1.00

tf infinite to = 0.0 s; t1=t2 ; t1= 1.00E-07s ; t2= 1.00E-09s ;
tf infinite to = 0.0 s; t1>t2 ; t1= 1.00E-06s ; t2= 1.00E-08s ;
tf infinite to = 0.0 s; t1=t2 ; t1= 1.00E-05s ; t2= 1.00E-07s ;
tf infinite to = 0.0 s; t1>t2 ; t1= 1.00E-04s ; t2= 1.00E-06s ;

Time (nanoseconds)

Voltage Output

VOLTAGE VARIANCE

tf infinite tc = 0.0 s t1=t2 ; t1= 1.000E-06s ; t2= 1.000E-07s ;

tf infinite tc = 0.0 s t1>t2 ; t1= 1.000E-06s ; t2= 1.000E-08s ;

tf infinite tc = 0.0 s t1>t2 ; t1= 1.000E-06s ; t2= 1.000E-09s ;

tf infinite tc = 0.0 s t1>t2 ; t1= 1.000E-07s ; t2= 1.000E-09s ;

Time (nanoseconds)

Voltage Output

Figure 4.7. 5 : Step Response curves for (t1/t2) >1 & variable'

VOLTAGE VARIANCE

tf infinite; tc = 0.0 s; t1 = t2 = 1.000E-05s ;

tf infinite; tc = 0.0 s; t1 = t2 = 1.000E-06s ;

tf infinite; tc = 0.0 s; t1 = t2 = 1.000E-07s ;

tf infinite; tc = 0.0 s; t1 = t2 = 1.000E-08s ;

tf infinite; tc = 0.0 s; t1 = t2 = 1.000E-09s ;

Time (nanoseconds)

Voltage Output

Figure 4.7. 6 : Step Response curves for (t1/t2)=1
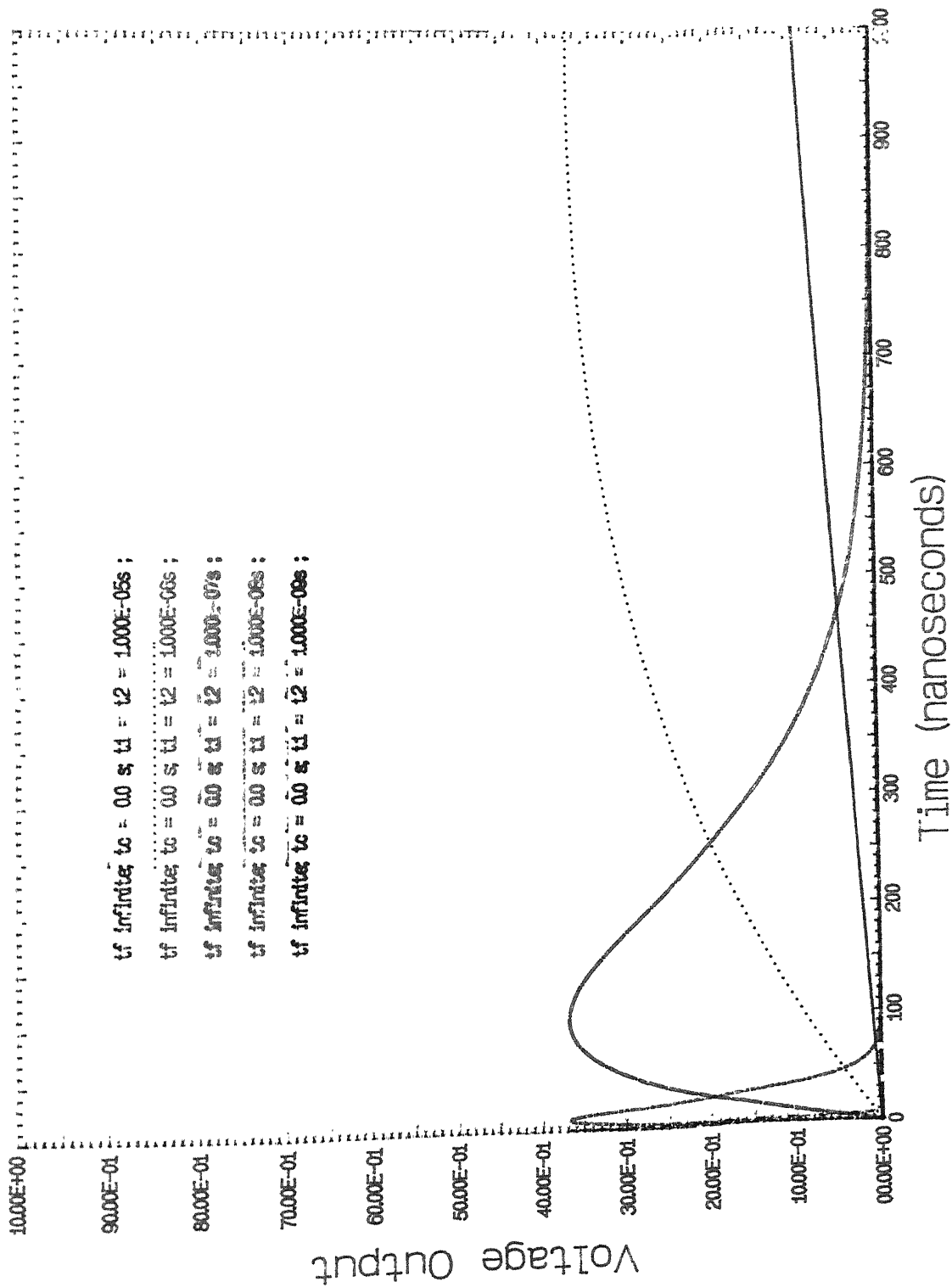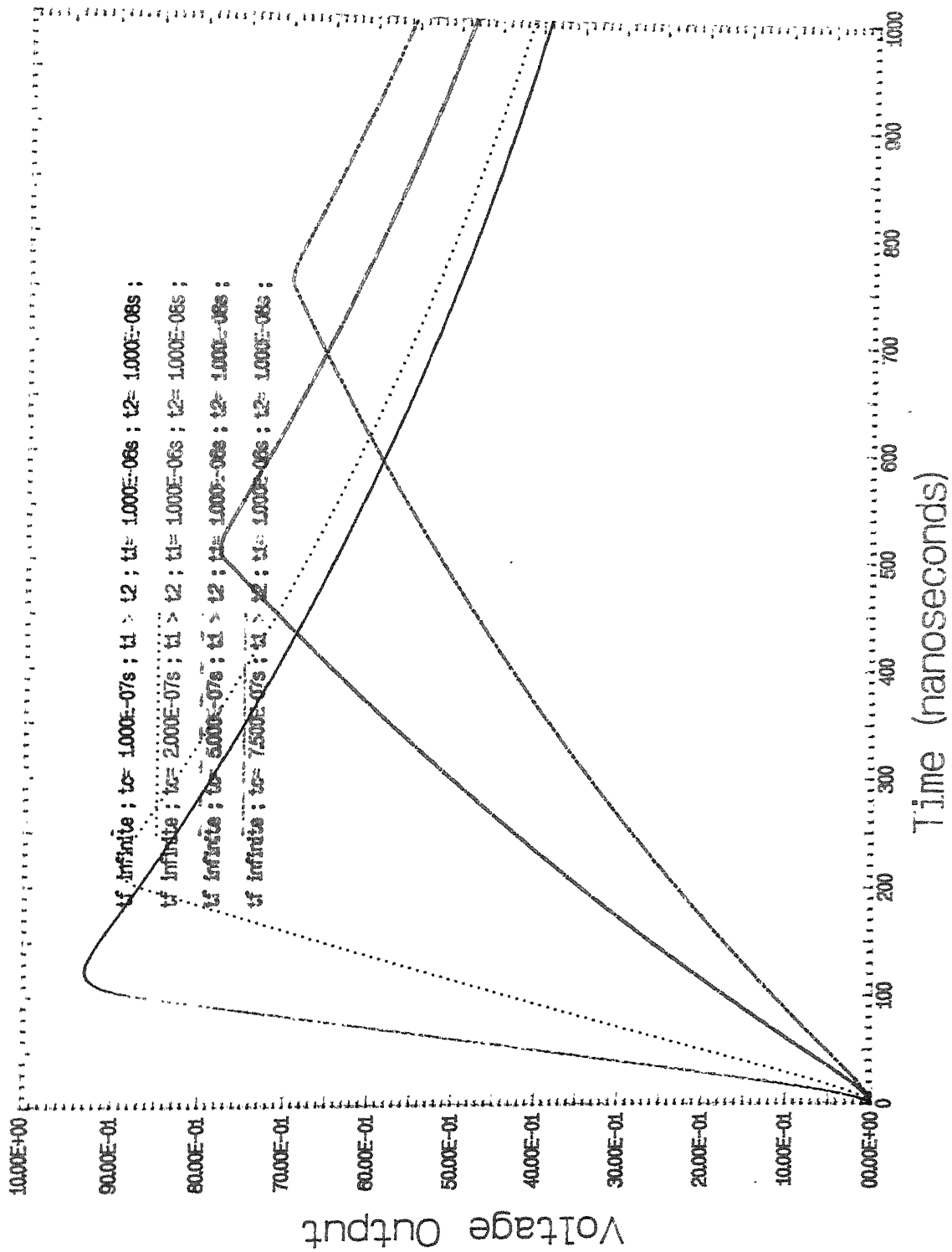
VOLTAGE VARIANCE

Figure 4.7. 7 : Response curves for (t1/t2=.01 & variable tc

VOLTAGE VARIANCE

tf infinite ; tc= 1.000E-07s ; t1 > t2 ; t1= 1.000E-07s ; t2= 1.000E-08s ;

tf infinite ; tc= 2.000E-07s ; t1 > t2 ; t1= 1.000E-07s ; t2= 1.000E-08s ;

tf infinite ; tc= 5.000E-07s ; t1 > t2 ; t1= 1.000E-07s ; t2= 1.000E-08s ;

tf infinite ; tc= 7.500E-07s ; t1 > t2 ; t1= 1.000E-07s ; t2= 1.000E-08s ;
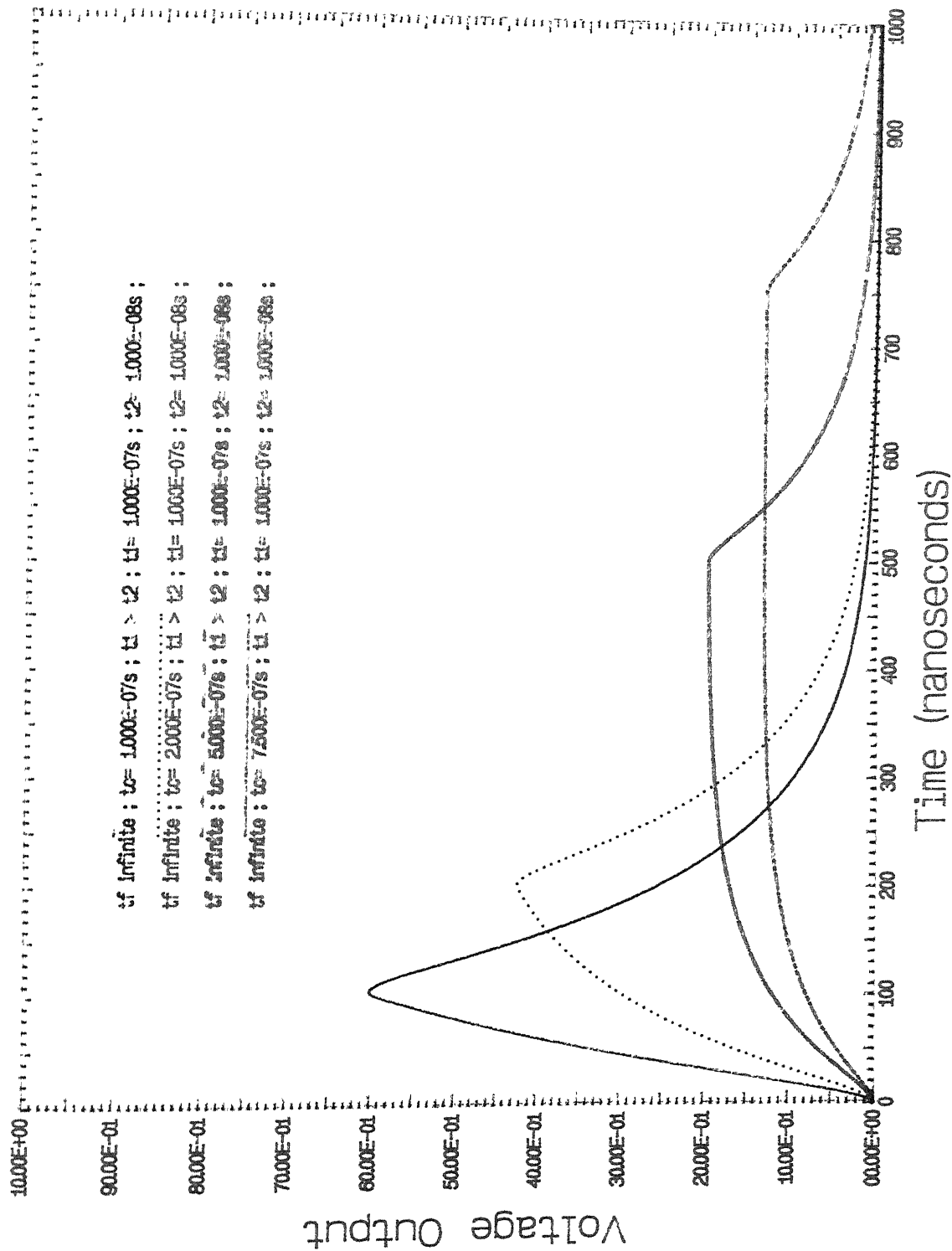
Figure 4.7. 8 : Response curves for variable tc & fixed (t1/t2)=1

Time (nanoseconds)

Voltage Output

VOLTAGE VARIANCE

tf infinite ; tc= 1.000E-07s ; t1 = t2 = 1.000E-06s ;

tf infinite ; tc= 1.000E-07s ; t1 = t2 = 1.000E-07s ;

tf infinite ; tc= 1.000E-07s ; t1 = t2 = 1.000E-08s ;

tf infinite ; tc= 1.000E-07s ; t1 = t2 = 1.000E-09s ;

Time (nanoseconds)

Voltage Output
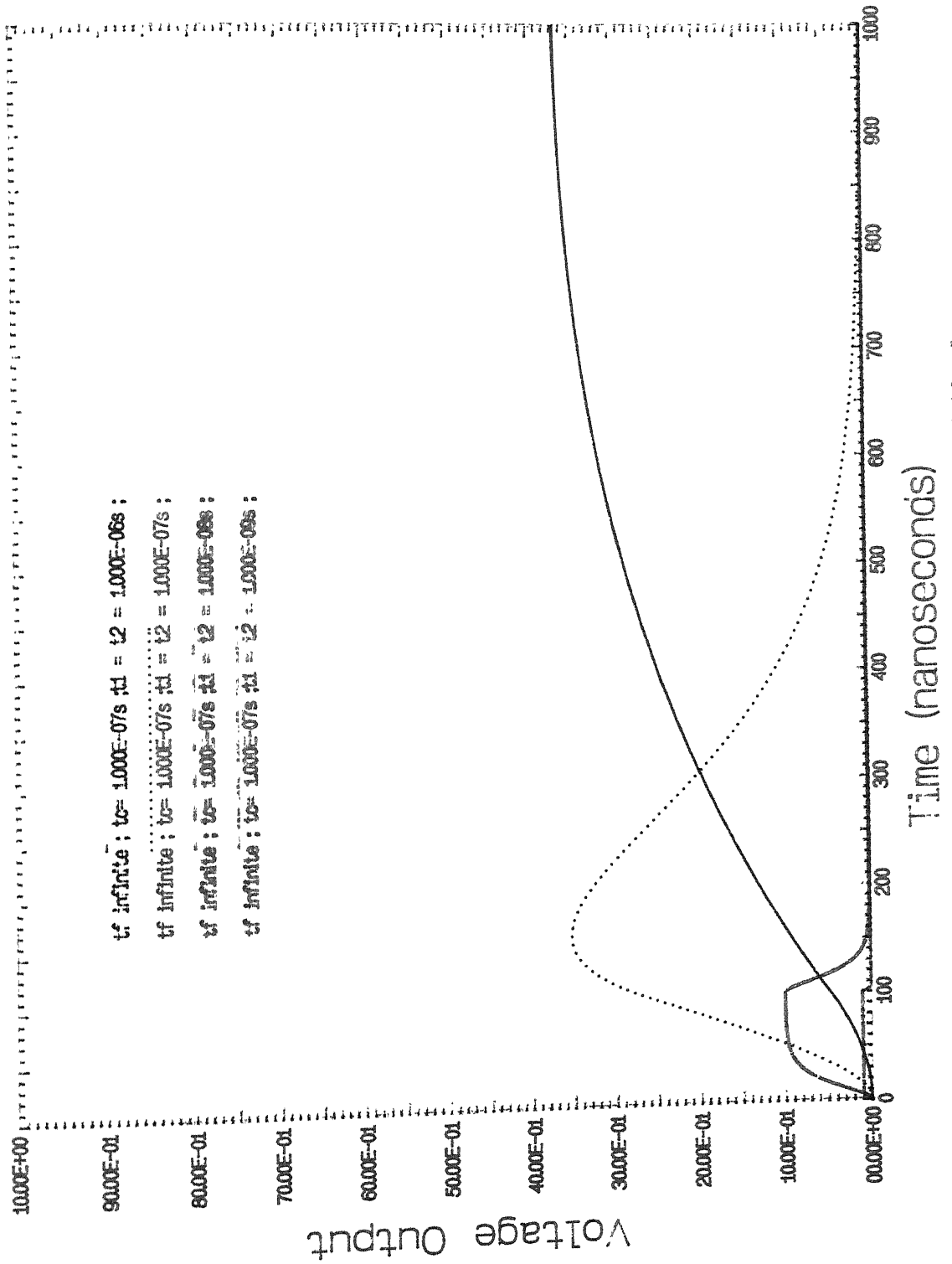
Figure 47. 9 : Response curves for fixed tc & variable t1=t2 values

VOLTAGE VARIANCE
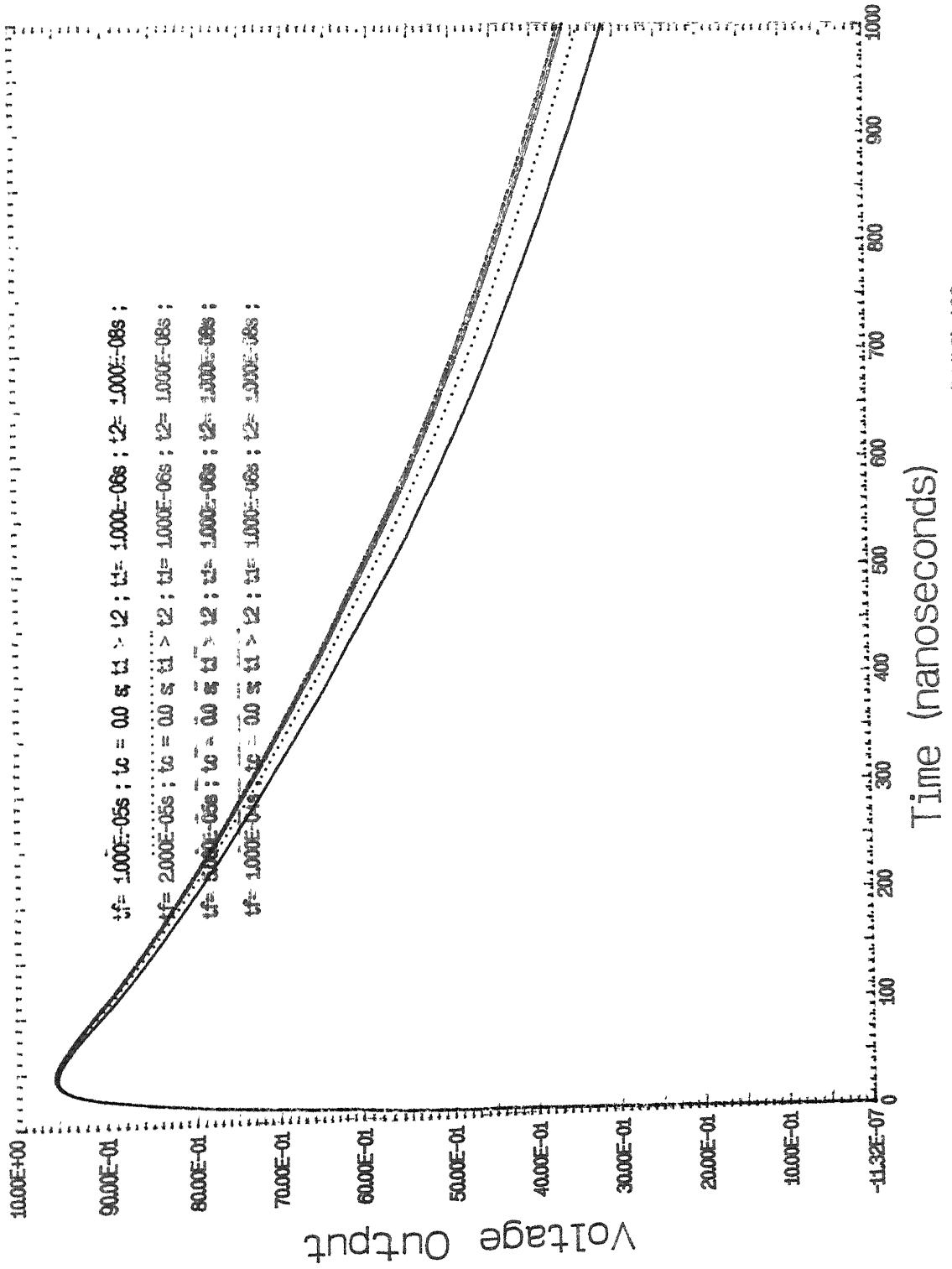
Figure 4.7.10 : Responses for tc=0.0 & variable input decay/t1/t2=100

VOLTAGE VARIANCE
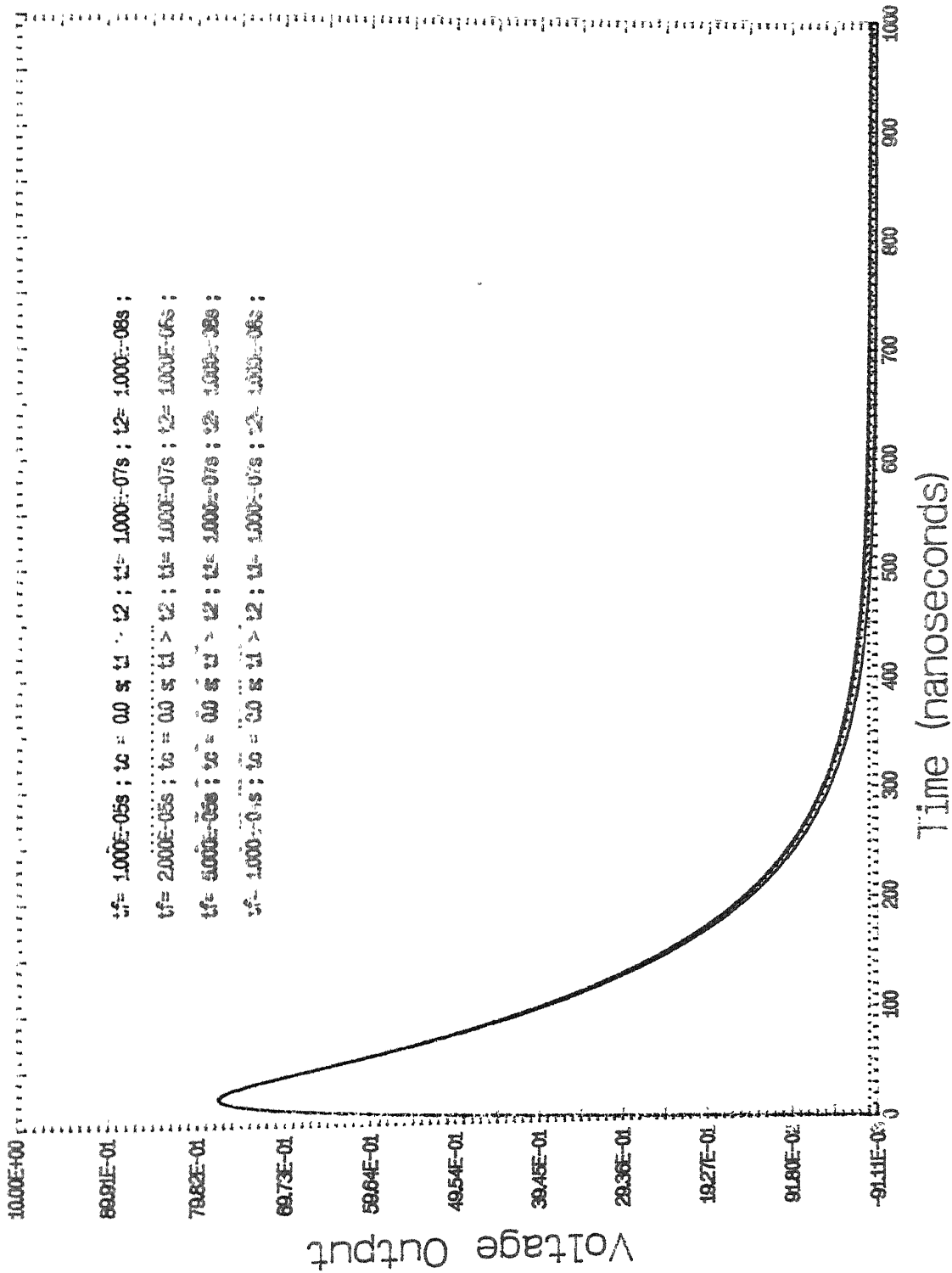
Figure 4.7.11 : Responses for tc=0.0, variable input decay; (t1/t2)=10
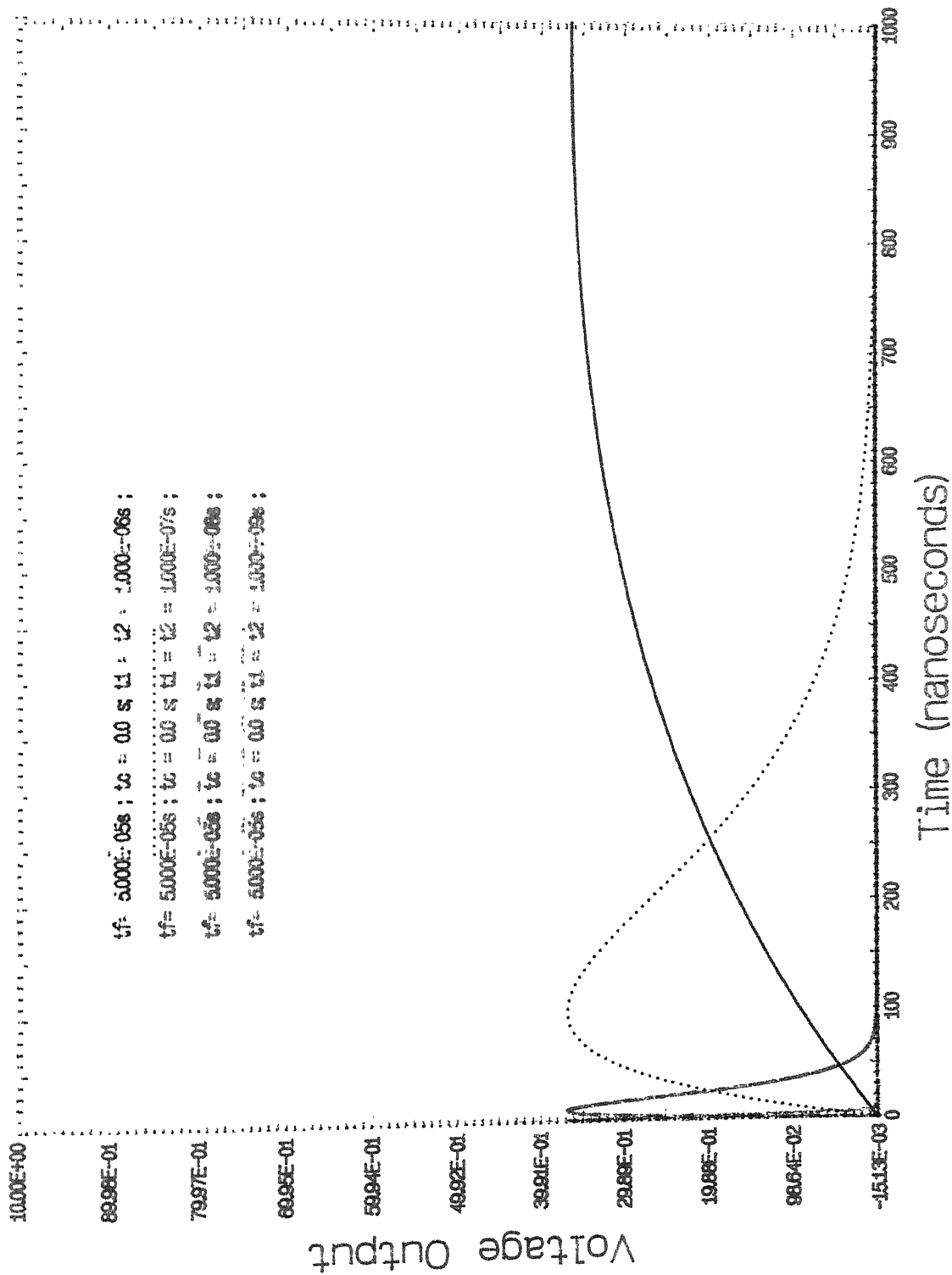
Figure 4.7.12 : Responses at tc=0.0,fixed input decay rate,variable t1(=t2)

VOLTAGE VARIANCE
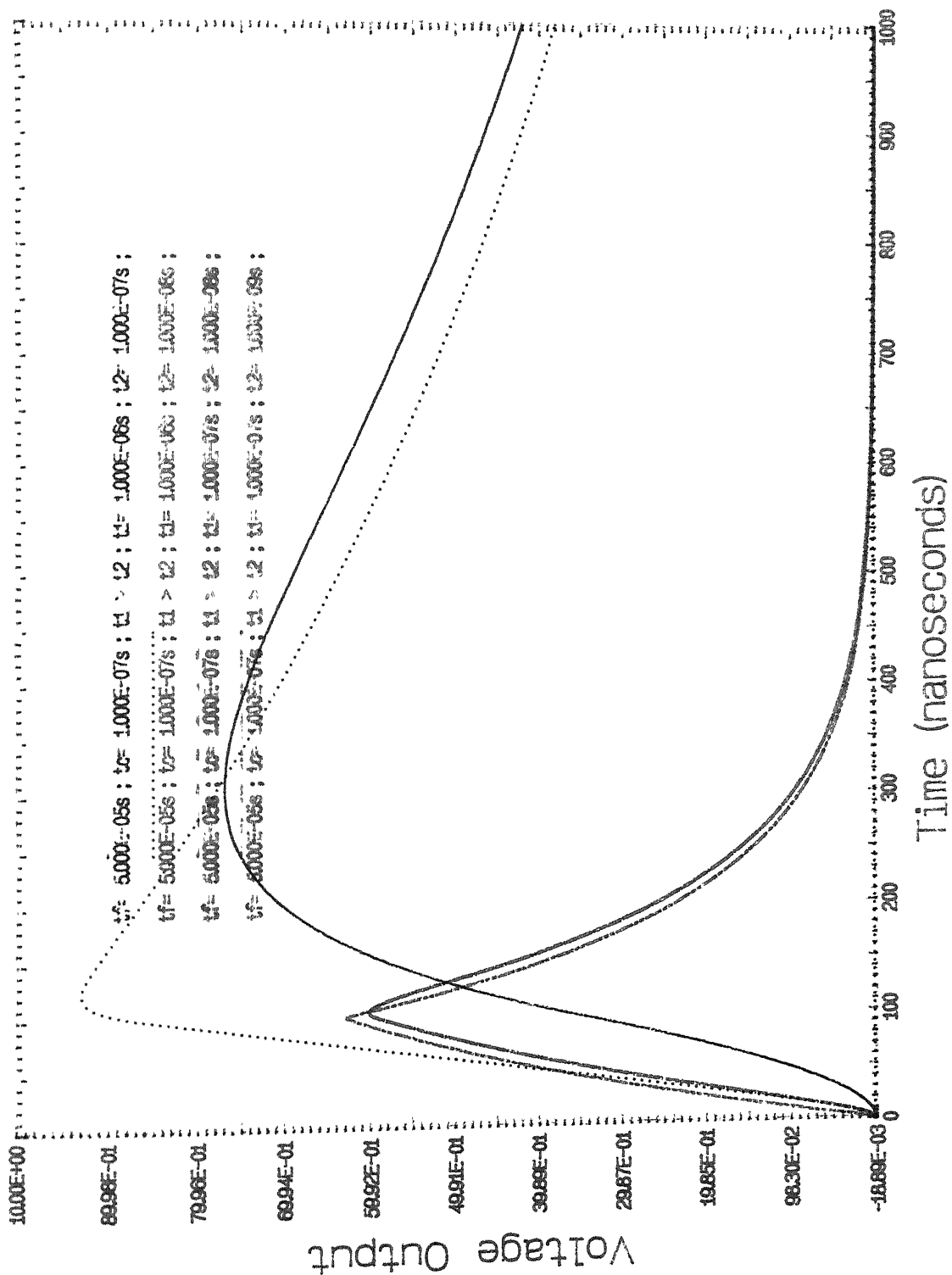
Figure 4.7.13 : Responses for fixed decay rate & tc valuesvariable t1&t2
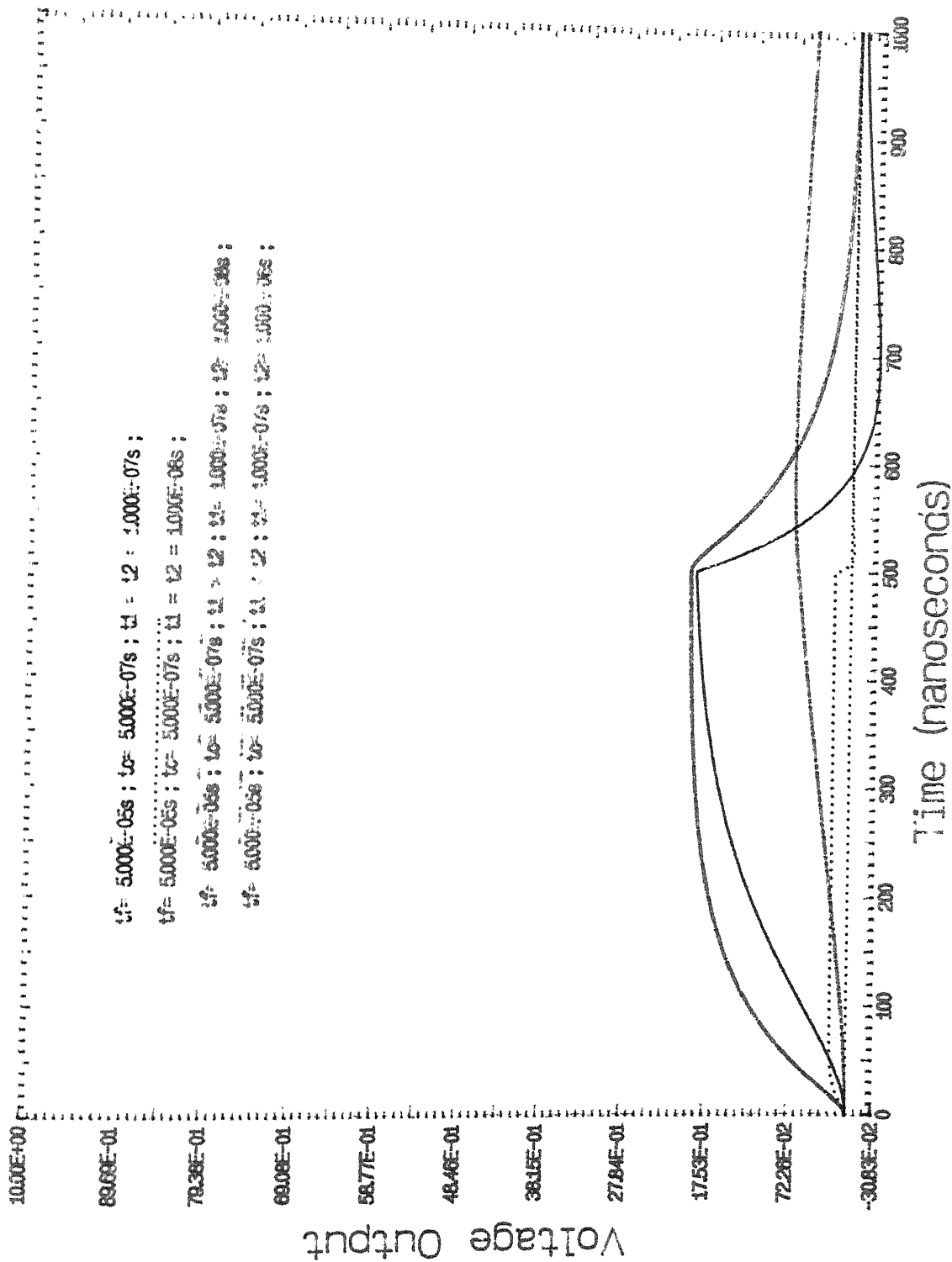
Figure 4.7.14 : Responses for all parameters changed generally

Table 4 1: Table of the parameters of waveforms displayed in the plots

figure reference	lgnd	decay time constt τf (us)	collection time constt τc (ns)	diff. time constt τl (ns)	integr time constt τ2 (ns)	peak o/p (% of 1/p)	peak location τpk (ns)	delay time τd (ns)	rise time τr (ns)	fall time τfall (ns)	pulse width τpw (ns)
Fig4.7.1	1	inf.	0.	1	10	7 68	3 00	1 00	2 00	22 00	10 00
Fig4.7.1	2	inf.	0	10	100	7 74	26 00	5 00	13 00	221.00	100.00
Fig4.7.1	3	inf	0	100	1000	7.74	256 00	51 00	135 00	550 99	948 99
Fig4.7.1	4	inf	0	1000	10000	5 97	999 99	363 00	764 99	.00	636 99
Fig4.7.2	1	inf.	0	1	100.	95	5 00	1 00	2.00	220.00	74.00
Fig4.7.2	2	inf.	0	10	1000	95	47 00	7 00	19 00	837.99	742 99
Fig4.7.2	3	inf	0.	100	10000	.95	465 00	65 00	195 00	.00	934.99
Fig4.7.2	4	.inf	0	1000.	100000	63	999 99	378 00	774.99	.00	621.99
Fig4.7.3	1	inf	0	10	1	76 78	3 00	1 00	2.00	22.00	10.00
Fig4.7.3	2	inf	0	100.	10	77 42	26 00	5 00	13.00	221.00	100.00
Fig4.7.3	3	inf	0	1000.	100	77 43	256 00	51 00	135 00	550.99	948 99
Fig4.7.3	4	inf	0.	10000	1000	59 66	999 99	363 00	764 99	.00	636 99
Fig4.7.4	1	inf.	0	100.	1.	95 40	5 00	1 00	2.00	220.00	74 00
Fig4.7.4	2	inf	0	1000	10	95.45	47 00	7.00	19.00	837.99	742 99
Fig4.7.4	3	inf	0	10000	100	95 45	465 00	65 00	195 00	.00	934 99
Fig4.7.4	4	inf	0.	100000.	1000	62 85	999 99	378 00	774.99	.00	621.99
Fig4.7.5	1	inf	0	1000	100	77 43	256 00	51 00	135 00	550.99	948 99
Fig4.7.5	2	inf	0	1000	10	95 45	47 00	7 00	19.00	837.99	742.99
Fig4.7.5	3	inf	0	1000	1	99 31	7 00	1 00	2 00	886.99	700.00
Fig4.7.5	4	inf.	0	100.	1.	95 40	5 00	1 00	2 00	220.00	74 00
Fig4.7.6	1	inf	0.	10000	10000	9 05	999 99	474 00	798.99	00	525.99
Fig4.7.6	2	inf	0.	1000.	1000.	36 79	999 99	232 00	570.00	.00	767 99
Fig4.7.6	3	inf	0	100	100	36 79	100 00	23 00	57 00	336.00	245 00
Fig4.7.6	4	inf	0	10	10	36 79	10 00	2 00	6 00	34 00	25.00
Fig4.7.6	5	inf	0	1	1	36 79	1 00	00	1 00	4.00	3 00
Fig4.7.7	1	inf	100	1000	10	92 93	124 00	58 00	79.00	760.99	768 99
Fig4.7.7	2	inf.	200	1000.	10.	89 08	217 00	103 00	158.00	666.99	816.99
Fig4.7.7	3	inf	500.	1000	10	77 96	509 00	227 00	392 00	375.00	772 99
Fig4.7.7	4	inf	750	1000	10	69 90	755 99	314 00	584 00	128 00	685 99
Fig4.7.8	1	inf	100	100	10	60 07	105 00	46 00	74 00	222.00	139 00
Fig4.7.8	2	inf	200	100	10	42 54	202 00	66 00	139.00	221 00	215 00
Fig4.7.8	3	inf	500	100	10	19 85	500 00	79 00	215 00	222.00	501.00
Fig4.7.8	4	inf	750	100	10	13 33	749 99	80 00	221 00	222 00	749 99
Fig4.7.9	1	inf	100	1000.	1000	36 72	999 99	282 00	569.00	00	717 99
Fig4.7.9	2	inf	100	100	100	35 32	158 00	76.00	90.00	336.00	250 00
Fig4.7.9	3	inf	100	10	10	10 00	100 00	17 00	34 00	34 00	100 00
Fig4.7.9	4	inf	100	1	1	1 00	49 00	2 00	4 00	55.00	100.00
Fig4.7.10	1	10	100	1000.	10	95 10	46 00	7.00	19 00	848 99	654.00
Fig4.7.10	2	20	100	1000	10	95 28	46 00	7 00	19.00	843 99	694 00
Fig4.7.10	3	50.	100.	1000	10	95 38	46 00	7 00	19.00	840 99	722 00
Fig4.7.10	4	100.	100	1000.	10	95 42	46 00	7 00	19 00	838 99	731.99
Fig4.7.11	1	10.	100	100	10	77 27	25 00	5 00	13.00	211.00	99.00
Fig4.7.11	2	20.	100	100	10	77 34	25 00	5.00	13.00	216 00	100.00
Fig4.7.11	3	50.	100.	100.	10	77 39	26 00	5 00	13.00	219 00	100.00
Fig4.7.11	4	100.	100	100.	10	77 40	26 00	5 00	13.00	220 00	100.00
Fig4.7.12	1	50	100.	1000.	1000	36 27	980 99	228 00	560.00	00	771.99
Fig4.7.12	2	50.	100.	100.	100.	36 74	100 00	23 00	57.00	330.00	244.00
Fig4.7.12	3	50.	100.	10.	10.	36 78	10 00	2 00	6.00	34.00	25 00
Fig4.7.12	4	50.	100.	1.	1.	36 79	1 00	00	1.00	4 00	3.00
Fig4.7.13	1	50.	100.	1000.	100	76 88	308 00	105 00	155.00	501 99	894 99
Fig4.7.13	2	50.	100.	1000.	10.	92 90	124 00	58 00	79 00	762 99	747.99
Fig4.7.13	3	50.	100.	100.	10.	60 07	105.00	46 00	74.00	217 00	132.00
Fig4.7.13	4	50.	100.	100.	1.	62 84	101 00	39.00	77 00	217 00	132.00
Fig4.7.14	1	50	500.	100.	100	2 00	202 00	17.00	34.00	7.00	486.00
Fig4.7.14	2	50	500.	10.	10.	19 85	500 00	79.00	215.00	213.00	500.00
Fig4.7.14	3	50.	500.	100.	10.	62 84	101 00	39.00		217.00	132.00
Fig4.7.14	4	50.	500.	100.	1000.	7.09	601 00	293 00	389.00	209.00	706.99

Table 4 2: Effects on waveform characteristics of t1 being less than t2

sn.	figure reference	lgnd decay time constt. tf (us)	collection time constt. tc (ns)	diff time constt t1 (ns)	integr time const t2 (ns)	peak o/p (% of 1/D)	peak location tpk (ns.)	delay time td (ns.)	rise time tr (ns.)	fall time tfall (ns.)	pulse width tpw (ns.)
1	Fig4 7 1 1	inf	0	1	10	7.68	3.00	1.00	2.00	22.00	10.00
2	Fig4 7 1 2	inf	0	10	100	7.74	26.00	5.00	13.00	221.00	100.00
3	Fig4 7 1 3	inf	0	100	1000	7.74	256.00	51.00	135.00	550.99	948.99
4	Fig4 7 1 4	inf	0	1000	10000	5.97	999.99	363.00	764.99		636.99
5	Fig4 7 2 1	inf	0	1	100	.95	5.00	1.00	2.00	220.00	74.00
6	Fig4 7 2 2	inf	0	10	1000	.95	47.00	7.00	19.00	837.99	742.99
7	Fig4 7 2 3	inf	0	100	10000	.95	465.00	65.00	195.00	.00	934.99
8	Fig4 7 2 4	inf	0	1000	100000	.63	999.99	378.00	774.99		621.99

Table 4.3: Effects on response waveform characteristics due to variation in t1 at fixed t2(=1ns.) at infinite tf, zero tc.

sn.	figure reference	lgnd decay time constt. tf us.	collection time constt. tc ns	diff. time constt. t1 ns.	integr. time constt. t2 ns.	peak o/p (% of i/p)	peak location tpk ns.	delay time td ns.	rise time tr ns.	fall time tfall ns.	pulse width tpw ns.
25	Fig4.7.6 5	inf	0.	1.	1	36.79	1.00	.00	1.00	4.00	3.00
9	Fig4.7.3 1	inf	0.	10.	1	76.78	3.00	1.00	2.00	22.00	10.00
13	Fig4.7.4 1	inf	0.	100.	1	95.40	5.00	1.00	2.00	220.00	74.00
19	Fig4.7.5 3	inf	0.	1000.	1	99.31	7.00	1.00	2.00	886.99	700.00

ble 4.4: Effects on response waveform characteristics due to variation in t1 at fixed t2(=10ns.)
at infinite tf, zero tc.

figure reference	lgnd decay time constt. tf us.		collection time constt. tc ns.	diff. time constt. t1 ns.	integr. time constt. t2 ns.	peak o/p (% of i/p)	peak location tpk ns.	delay time td ns.	rise time tr ns.	fall time tfall ns.	pulse width tpw ns.
Fig4.7.6	4	inf.	0.	10.	10.	36.79	10.00	2.00	6.00	34.00	25.00
Fig4.7.3	2	inf.	0.	100	10.	77.42	26.00	5.00	13.00	221.00	100.00
Fig4.7.4	2	inf.	0.	1000.	10.	95.45	47.00	7.00	19.00	837.99	742.99

Table 4.5. Effects on response waveform characteristics due to variation in t1 at fixed t2(=100ns.) at infinite tf, zero tc.

| sn. | figure reference | lgnd | decay time constt. tf | collection time constt. tc | diff. time constt. t1 | integr. time constt. t2 | peak o/p (% of i/p) | peak location tpk | delay time td | rise time tr | fall time tfall | pulse width tpw |
			us.	ns.	ns.	ns.	ns.	ns.	ns.	ns.	ns.	ns.
23	Fig4.7.6	3	inf	0.	100.	100.	36.79	100.00	23.00	57.00	336.00	245.00
17	Fig4.7.5	1	inf	0.	1000.	100.	77.43	256.00	51.00	135.00	550.99	948.99
15	Fig4.7.4	3	inf	0.	10000.	100.	95.45	465.00	65.00	195.00	.00	934.99

Table 4.6. Effect on response waveform characteristics due to variation in t1 at fixed t2(=1000ns.) at infinite tf, zero tc

Sr.	figure reference	long decay time constt. tf us.	collection time constt. tc ns	diff time constt. t1 ns.	integr. time constt. t2 ns.	peak o/p (% of i/p)	peak location tpk ns.	delay time td ns.	rise time tr ns.	fall time tfall ns.	pulse width tpw ns
12	Fig 4.7.6	inf	0.	1000	1000	36.79	999.99	232.00	570.00	.00	767.99
13	Fig 4.7.3	inf	0.	15000	1000	59.66	999.99	363.00	764.99	.00	636.99
16	Fig 4.7.4	inf	0.	100000	1000	62.85	999.99	378.00	774.99	.00	621.99

Table 4.7: Effects on waveform characteristics at different magnitudes of equal t1/t2

sn.	figure reference	lgnd decay time constt. tf	collection time constt. tc	diff. time constt. t1	integr. time constt. t2	peak o/p (% of i/p)	peak location tpk	delay time td	rise time tr	fall time tFall	pulse width tpw
		ns.	ns.	ns.	ns.		ns.	ns.	ns.	ns.	ns.
25	Fig4.7.6 5	inf	0.	1.	1.	36.79	1.00	.00	1.00	4.00	3.00
24	Fig4.7.6 4	inf	0.	10.	10.	36.79	10.00	2.00	6.00	34.00	25.00
23	Fig4.7.6 3	inf	0.	100.	100.	36.79	100.00	23.00	57.00	336.00	245.00
22	Fig4.7.6 2	inf	0.	1000.	1000.	36.79	999.99	232.00	570.00	.00	767.99
21	Fig4.7.6 1	inf	0.	10000.	10000.	9.05	999.99	474.00	793.99	.00	525.99

Table 4.8: Effects on waveform characteristics of varying t2 at fixed t1(=1 ns.), tf infinite, tc zero

sn.	figure reference	lgnd decay time constt. tf	collection time constt. tc	diff. time constt. t1	integr. time constt. t2	peak o/p (% of 1/p)	peak location tpk	delay time td	rise time tr	fall time tfall	pulse width tpw
		us.	ns.	ns.	ns.		ns.	ns.	ns.	ns.	ns.
25	Fig4.7.6	5 inf.	0.	1.	1.	36.79	1.00	.00	1.00	4.00	3.00
1	Fig4.7.1	1 inf.	0.	1.	10.	7.68	3.00	1.00	2.00	22.00	10.00
5	Fig4.7.2	1 inf.	0.	1	100.	.95	5.00	1.00	2.00	220.00	74.00

Table 4.9: Effects on waveform characteristics of varying t2 at fixed t1(=10 ns.), tf infinite, tc zero

sn.	figure reference	lgnd decay time constt. tf us.	collection time constt. tc ns.	diff. time constt. t1 ns.	integr. time constt. t2 ns.	peak o/p (% of i/p)	peak location tpk ns.	delay time td ns.	rise time tr ns.	fall time tfall ns.	pulse width tpw ns.
9	Fig4.7.3 1	inf.	0	10.	1.	76.78	3.00	1.00	2.00	22.00	10.00
24	Fig4.7.6 4	inf.	0	10.	10.	36.79	10.00	2.00	6.00	34.00	25.00
2	Fig4.7.1 2	inf.	0	10.	100.	7.74	26.00	5.00	13.00	221.00	100.00
6	Fig4.7.2 2	inf.	0	10.	1000.	.95	47.00	7.00	19.00	837.99	742.99

Table 4.10: Effects on waveform characteristics of varying t2 at fixed t1(=100 ns.),
tf infinite, tc zero

sn.	figure reference	lgnd decay time constt. tf	collection time constt. tc	diff. time constt. t1	integr. time constt. t2	peak o/p (% of 1/p)	peak location tpk	delay time td	rise time tr	fall time tfall	pulse width tpw
		us.	ns.	ns.	ns.		ns.	ns.	ns.	ns.	ns.
20	Fig4.7.5 4	inf.	0.	100.	1.	95.40	5.00	1.00	2.00	220.00	74.00
10	Fig4.7.3 2	inf.	0.	100.	10.	77.42	26.00	5.00	13.00	221.00	100.00
3	Fig4.7.1 3	inf.	0.	100.	1000.	7.74	256.00	51.00	135.00	550.99	948.99
7	Fig4.7.2 3	inf.	0.	100.	10000.	.95	465.00	65.00	195.00	.00	934.99

Table 4.11: Effects on waveform characteristics of varying t2 at fixed t1(=1000 ns.),
tf infinite, tc zero

sn.	figure reference	lgnd	decay time constt. tf us.	collection time constt. tc ns.	diff. time constt. t1 ns.	integr. time constt. t2 ns.	peak o/p (% of i/p)	peak location tpk ns.	delay time td ns.	rise time tr ns.	fall time tfall ns.	pulse width tpw ns.
19	Fig4.7.5	3	inf.	0.	1000.	1.	99.31	7.00	1.00	2.00	886.99	700.00
18	Fig4.7.5	2	inf.	0.	1000.	10.	95.45	47.00	7.00	19.00	837.99	742.99
17	Fig4.7.5	1	inf.	0.	1000.	100.	77.43	256.00	51.00	135.00	550.99	948.99
22	Fig4.7.6	2	inf.	0.	1000.	10000.	36.79	999.99	232.00	570.00	.00	767.99
4	Fig4.7.1	4	inf.	0.	1000.	100000.	5.97	999.99	363.00	764.99	.00	636.99
8	Fig4.7.2	4	inf.	0.	1000.	100000.	.63	999.99	378.00	774.99	.00	621.99

Table 4.12: Effects on waveform characteristics of varying tc at tf infinite i.e. flat top

sn.	figure reference	lgnd decay time constt. tf (us)	collection time constt. tc (ns)	diff. time constt. t1 (ns)	integr. time constt. t2 (ns)	peak o/p (% of i/p)	peak location tpk (ns)	delay time td (ns)	rise time tr (ns)	fall time tfall (ns)	pulse width tpw (ns)
26	Fig4.7.7 1	inf.	100	1000.	10.	92.93	124.00	58.00	79.00	760.99	768.99
27	Fig4.7.7 2	inf.	200	1000.	10.	89.08	217.00	103.00	158.00	666.99	816.99
28	Fig4.7.7 3	inf.	500	1000.	10.	77.96	509.00	227.00	392.00	375.00	772.99
29	Fig4.7.7 4	inf.	750	1000.	10.	69.90	755.99	314.00	584.00	128.00	685.99
30	Fig4.7.8 1	inf.	100	100.	10.	60.07	105.00	46.00	74.00	222.00	139.00
31	Fig4.7.8 2	inf.	200	100.	10.	42.54	202.00	66.00	139.00	221.00	215.00
32	Fig4.7.8 3	inf.	500	100.	10.	19.85	500.00	79.00	215.00	222.00	501.00
33	Fig4.7.8 4	inf.	750	100.	10.	13.33	749.99	80.00	221.00	222.00	749.99
34	Fig4.7.9 1	inf	100.	1000.	1000.	36.72	999.99	282.00	569.00	.00	717.99
22	Fig4.7.6 2	inf	0.	1000.	1000.	36.79	999.99	232.00	570.00	.00	767.99
35	Fig4.7.9 2	inf	100.	100.	100.	35.32	158.00	76.00	90.00	336.00	250.00
23	Fig4.7.6 3	inf	0.	100.	100.	36.79	100.00	23.00	57.00	336.00	245.00
36	Fig4.7.9 3	inf.	100.	10.	10.	10.00	100.00	17.00	34.00	34.00	100.00
24	Fig4.7.6 4	inf.	0.	10.	10.	36.79	10.00	2.00	6.00	34.00	25.00
37	Fig4.7.9 4	inf	100.	1.	1.	1.00	49.00	2.00	4.00	55.00	100.00
25	Fig4.7.6 5	inf	0.	1.	1.	36.79	1.00	.00	1.00	4.00	3.00

Table ... Details of results of waveform characteristics of varying tf at tc fixed i.e drooping toc

sr	reference	collection time const. tc (ns)	diff time const. t1 (ns)	integr time const. t2 (ns)	peak o/p (% of i/p)	peak location tpk (ns)	delay time td (ns)	rise time tr (ns)	fall time tfall (ns)	pulse width tpw (ns)
35	Fig4.7.10	100.	1000	10.	95.10	46.00	7.00	19.00	845.99	654.00
34	Fig4.7.10	100.	1000	10.	95.28	46.00	7.00	19.00	843.99	694.00
49	Fig4.7.10	100.	1000	10.	95.38	46.00	7.00	19.00	840.99	722.00
41	Fig4.7.10	100.	1000.	10.	95.42	46.00	7.00	19.00	838.99	731.99
26	Fig4.7.9	100	1000.	10.	92.93	124.00	58.00	79.00	760.99	768.99
42	Fig4.7.11	100.	100	10	77.27	25.00	5.00	13.00	211.00	99.00
43	Fig4.7.11	100.	100	10.	77.34	26.00	5.00	13.00	216.00	100.00
44	Fig4.7.11	100.	100	10.	77.39	26.00	5.00	13.00	219.00	100.00
45	Fig4.7.11	100.	100	10.	77.40	26.00	5.00	13.00	220.00	100.00
30	Fig4.7.8	100	100	10	40.07	105.00	46.00	74.00	222.00	139.00
46	Fig4.7.12	100.	1000	1000.	36.27	930.99	228.00	560.00	.00	771.99
34	Fig4.7.9	100.	1000	1000.	36.72	999.99	232.00	569.00	.00	717.99
47	Fig4.7.12	100.	100	100.	36.74	100.00	23.00	57.00	330.00	244.00
35	Fig4.7.9	100.	100	100.	35.32	158.00	76.00	90.00	336.00	250.00
48	Fig4.7.13	100.	10	10	36.78	100.00	2.00	6.00	34.00	25.00
36	Fig4.7.9	100.	10	10	10.00	100.00	17.00	34.00	34.00	100.00
49	Fig4.7.13	100.	1	1	36.79	1.00	.00	1.00	4.00	3.00
37	Fig4.7.9	100.	1	1	1.00	49.00	2.00	4.00	55.00	100.00
51	Fig4.7.13	100.	1000	10.	92.90	124.00	58.00	79.00	762.99	747.99
26	Fig4.7.1	100.	1000	10.	92.93	124.00	58.00	79.00	760.99	768.99
52	Fig4.7.13	100.	100	10	60.07	105.00	46.00	74.00	219.00	139.00
30	Fig4.7.8	100.	100	10	60.07	105.00	46.00	74.00	222.00	139.00
56	Fig4.7.14	500	100	10.	19.85	500.00	79.00	215.00	213.00	500.00
32	Fig4.7.8	500	100	10.	19.85	500.00	79.00	215.00	222.00	501.00

14· Effects on waveform characteristics of varying tf,tc at
  a) t1=t2 (variable magnitudes)
  b) t1 fixed, variable t2 (for different fixed values of t1)
  c) t2 fixed, variable t1 (for different fixed values of t2)

ase: t1 = t2

refe rence#	lgnd decay time constt. tf	collection time constt tc	diff time constt t1	integr time constt t2	peak o/p (% of i/p)	peak location tpk	delay time td	rise time tr	fall time tfall	pulse width tpw
	us	ns	ns	ns		ns	ns	ns.	ns.	ns
7 12 4	50	100	1	1	36 79	1 00	00	1 00	4.00	3 00
7 9 4	inf	100	1	1	1 00	49 00	2 00	4 00	55 00	100 00
7.6 5	inf	0	1	1	36 79	1 00	00	1 00	4 00	3 00
7.12 3	50.	100	10	10	36 78	10 00	2 00	6 00	34 00	25.00
7 9 3	inf.	100	10	10	10 00	100 00	17 00	34 00	34 00	100.00
7.6 4	inf	0.	10	10	36 79	10 00	2 00	6 00	34 00	25 00
7.14 2	50.	500.	10	10.	2 00	202 00	17 00	34 00	7 00	486.00
7.12 2	50.	100.	100.	100	36 74	100 00	23 00	57 00	330 00	244 00
7.9 2	inf.	100.	100	100	35 32	158 00	76 00	90 00	336 00	250.00
7.6 3	inf	0.	100	100	36 79	100 00	23 00	57 00	336 00	245 00
7 14 1	50.	500.	100	100	62 84	101 00	39 00	77 00	217 00	132 00

• t1 fixed;tc variable

refe rence	lgnd decay time constt tf	collection time constt tc	diff time constt. t1	integr time constt t2	peak o/p (% of i/p)	peak location tpk	delay time td	rise time tr	fall time tfall	pulse width tpw
	us	ns	ns	ns		ns	ns	ns.	ns	ns
7 13 4	50	100	100	1	62 84	101 00	39 00	77 00	217 00	132 0
7.5 4	inf	0	100	1	95 40	5 00	1 00	2 00	220 00	74 0
7 13 3	50	100	100	10	60 07	105 00	46 00	74 00	219 00	139 0
7.3 2	inf	0.	100	10	77 42	26 00	5 00	13 00	221 00	100 0
7.14 3	50	500.	100	10	19 85	500 00	79 00	215 00	213.00	500 0
7.13 2	50	100.	1000	10	92 90	124 00	58 00	79 00	762 99	747 9
7.4 2	inf	0.	1000	10	95 45	47 00	7 00	19 00	837 99	742 9
7.3 3	inf.	0	1000	100	77 43	256 00	51 00	135 00	550 99	948 9
7 13 1	50.	100.	1000	100	76 89	308 00	105 00	155 00	501 99	894 9
7.12 2	50	100.	100	100.	36 74	100 00	23 00	57 00	330.00	244 0
7.6 3	inf	0	100	100	36 79	100 00	23 00	57.00	336.00	245 0

•: t1 variable; t2 fixed.

refe rence#	lgnd decay time constt. tf	collection time constt. tc	diff time constt t1	integr time constt. t2	peak o/p (% of i/p)	peak location tpk	delay time td	rise time tr	fall time tfall	pulse width tpw
	us.	ns.	ns.	ns		ns	ns.	ns	ns	ns
7.12 3	50.	100.	10.	10	36 78	10 00	2 00	6 00	34.00	25.0
7.6 4	inf.	0.	10	10.	36 79	10 00	2 00	6 00	34.00	25 0
7.13 3	50	100	100.	10	60 07	105 00	46 00	74 00	219 00	139.0
7.3 2	inf.	0.	100	10	77 42	26 00	5 00	13 00	221.00	100 0
7.13 2	50.	100.	1000.	10	92 90	124 00	58 00	79 00	762.99	747.9
7.4 2	inf.	0.	1000	10.	95 45	47 00	7 00	19.00	837 99	742.9

Sl. No.	Parameter Variation	Effect on peak height vpk	Effect on characteristics of the rising part of waveform (tpk, t2, tr)	Effect on fall time of the profile tfall	Effect on pulse width tpw	Ref. to Table No.	Remarks
1.	t1 < t2	Severely attenuated	Irrelevant because of attenuation of peak height			4.2	Mode of operation not recommended
2.	t1 < t2, t1 rises at t2 = 1 nsec	Improved height at larger t1	Marginally alters	Prolongs significantly at larger t1	Increases significantly at larger t1	4.3	Lower t1 preferable to avoid pile-up errors
3.	t1 ≥ t2, t1 rises at t2 = 10 nsec	do	do	do	do	4.4	do
4.	t1 ≥ t2, t1 rises at t2 = 100 nsec	do	Relative alteration same as in (2) & (3) above but since absolute magnitudes change we observe significant protraction of leading edge of profile	do	do	4.5	do
5.	t1 = t2, t1 rises at t2 = 1000 nsec	Peak Height improves as t1 increases	Extremely sluggish rising profile	Extremely sluggish falling profile	Data in table 4.6 meaningless for duration of observation	4.6	Unacceptable mode of operation; t2 must be smaller
6.	t1 = t2	Independent of magnitude from 1 nsec to 1000 nsec Diminishes severely at 10,000 nsec.	Rising profile deteriorates (prolonged) as magnitude increases	Trailing edge profile also deteriorates	Pulse width also increases	4.7	Smaller magnitudes of t1, t2 preferred
7.	t2 varies at t1 = 1 nsec.	Diminishes as t2 increases	Marginally altered	Significantly prolongs as t2 increases	Significantly increases	4.8	Smaller t2 preferred

Sl. No.	Parameter Variation	Effect on peak height vpk	Effect on characteristics of the rising part of waveform (tpk, td, tr)	Effect on fall time of the profile tfall	Effect on pulse width tpw	Ref. to Table No.	Remarks
8.	t2 varies at t1 = 10 nsec.	do	Becomes marginally more sluggish as t2 increases	do	do	4.9	do
9.	t2 increases at t1 = 100 nsec.	do	Relative variation in rise time characteristics same as in (7) and (8) but since magnitudes change, increased sluggishness in rise time characteristics is more noticeable.	do	do	4.10	do
10.	t2 varies at t1 = 1000 nsec.	do	do	Very poor profile time	Very poor pulse width	4.11	Unacceptable
11.	tc varies at tf = infinite	In general, there is a decrease in height with increasing tc	Becomes more sluggish with increasing tc	Characteristics depend on absolute magnitudes of t1 and t2.	Same tendency as in case of fall time.	4.12	Smaller tc preferred in general.
12.	tf varies as tc is fixed	Peak Height sensitive to tf only for low values of t1 and t2.	Peak location and rise time sensitive only at low t1, t2 values	Fall time sensitive only at very low values of t1, t2.	Sensitive only at low t1, t2	4.13	tf matters only at t1,t2

Simulated outputs can be used for stimulating the DSP algorithms and evaluate various aspects of their performance so as to help evolve a technique for on-line processing of real life nuclear by efficient digital signal processing.

Investigations into various detector parameters and types can also be carried out with the assistance of such simulation tools. Also instrumention in the area of time spectroscopy also merits similar investigative treatment and furtherance of experience in simulation tool development of the type carried out here can of relevance in this direction also.

REFERENCES

1. R.E.Chrien and R.J.Sutter, *Noise and Pile-up Suppression by Digital Signal Processing*, Nuclear Instruments and Methods A 249 (1986) p421-425.

2. M.Moszynski and J.Jastrzebski, *Reduction of Pile-up Effects in time and energy measurements,* Nuclear Instruments and Methods 47(1967) p61-70,

3. R.D.Evans, *The Atomic Nucleus*, McGraw Hill Book Co. N.Y. 1968.

4. Glenn F.Knoll, *Radiation Detection and Measurement,* John Wiley and Sons, N.Y. 1979.

5. Yu.M.Shirokov and N.P.Yudin, *Nuclear Physics,* Vol.2. Mir Publishers Moscow 1982 (English transalation by Mark Samookhvalov.

6. R.M.Singru, *Introduction to Experimental Nuclear Physics,* Wiley Eastern Pvt. Ltd, N.D., 1972.

7. Bruno B.Rossi and Hans H.Staub, *Ionization chambers and counters:Experimental Techniques,* Mc.Graw-Hill Book Co., Inc., N.Y., 1964.

8. Jack Sharpe, *Nuclear Radiation Detectors,* John Wiley and Sons, Inc. and Methuen and Co.Ltd. London, 1964

9. G.Dearnaley, D.C.Northrop, *Semiconductor Counters for Nuclear Radiations,* John Wiley and Sons, N.Y. 1966.

10. J.M.Taylor, *Semiconductor Particle Detectors*, Butterworths Inc., Washington 1963.

11. J.Sharpe, *Nuclear Radiation Measurement*, Temple Press Limited, London. 1960.

12. Eds.G.Bertolini and A.Coche, *Semiconductor Detectors*, North-Holland Publishing Co. Amsterdam 1968.

13. William J.Price, *Nuclear Radiation Detection*, McGraw-Hill Book Co., Inc., N.Y., 1958.

14. Robert L.Chase, *Nuclear Pulse Spectroscopy*, McGraw-Hill Book Co., INC., N.Y., 1961.

15. Gillespie, *Signal, Noise and Resolution in Nuclear Counter Amplifiers*, Pergamon Press Ltd, London, 1953.

16. A.Alberigi Quaranta, M.Martini, G.Ottaviani, *The Pulse shape and the Timing problem in solid state detectors-A review Paper*, IEEE Trans. on Nucl. Science NS-16 Vol.1 No.2 April. 1969 p 35-61

17. M.Moszynski and W.Przyborski, *The Shape of Pulses Generated by Alpha-particles in Silicon drifted Detectors*, Nuclear Experiments and Methods, 64(1968) p244-250.

18. H.Spieler, *Fast Timing Methods for Semiconductor detectors*, IEEE Trans. on Nucl. Science , NS-29, No. 3, June 1982, p 1142-1158.

19. F.S.Goulding, *Semiconductor detectors for nuclear spectrometry*, I, Nuclear Instruments and Methods, 43(1966) p1-54.

20. F.S.Goulding and Landis, *Signal Processing for Semiconductor Detectors*, IEEE Trans on Nucl.Science NS-29 vol 3 June 1982, p1125-1141.

21. Ed: F.J.M.Farley, *Progress in Nuclear Techniques and Instrumentation* vol.3. North-Holland Publishing Co. Amsterdam 1968.

22. F.S.Goulding, *Pulse Shaping in low-noise nuclear amplifiers: A Physical Approach to noise Analysis*, Nuclear Instruments and Methods 100(1972) p 493-504

23. Jozef Cacko, Matej Bily and Juraj Bukoveczky, *Random Processes:Measurement, Analysis and Simulation*, Elsevier Amsterdam-1988.

24. John M.Smith, *Mathematicall Modelling and Digital Simulation for Engineers and Scientists*, John Wiley and Sons N.Y., 1978.

25. Donald E.Knuth , *The Art of Computer Programming, Vol.2: Seminumerical Algorithms*, Addison-Wessley Publishing Co. 1969.

26. Maurice F.Aburdence, *Computer Simulation of Dynamic Systems*, Wm.C.Brown Publishing Dubuque, IOWA 1988.

A130783